Department of Chemical Engineering

A Study of Erosion Phenomena in Coal Fired Furnace using CFD modeling

Mikilkumar Bansilal Gandhi

This thesis is presented for the Degree of
Master of Engineering
of
Curtin University of Technology

June 2010

Declaration

To the best of my knowledge and belief this thesis contains no material previously published by any other person except where due acknowledgment has been made.

This thesis contains no material which has been accepted for the award of any other degree or diploma in any university.

Signature:

Date:

Abstract

In pulverised coal fired boilers, entrained fly ash particles in the flue gas often leads to erosive wear on metal surfaces along the flow field. This can have a significant effect on the operational life of various sections of boiler (in particular regenerative heat exchanger tubes). In this work, CFD based code FLUENT is used in conjunction with erosion model developed by other researchers for a large-scale furnace to identify the areas likely to be subjected to erosion under various operating conditions. Eulerian- Lagrangian approach is considered to analyse continuum phase and particle tracking for the coal particle. Flow field has been thoroughly examined in terms of velocity, particle and temperature profiles along the gas flow path. The data obtained on particle velocities and trajectories have been utilised to predict the extent of erosion in selected areas of boiler components. Predictions have been found to be in good agreement with the published data as well as plant observations for velocities ranging from 15 to 32 m/s showing a deviation of approximately 4.9 % with 20° impact angle.The results obtained from the present work for understanding erosion pattern in boilers are not only of practical significance but also provides platform for the development of an erosion tool which could assist power utilities in avoiding unnecessary shutdowns and penalties associated with the replacement of boiler components.

Acknowledgements

I would like to thank a number of people who have provided me with a great deal of help to complete this project. I am thankful to my project supervisors A/Professor Hari Vuthaluru and Dr Rupa Vuthaluru for giving an opportunity to pursue master degree under their supervision. I am very grateful to them for their enormous time and effort spent guiding and assisting me throughout my dissertation period. I would like to thank Dr Hon Lye (Pacific West) for providing technical assistance in this project. I express my sincere gratitude to the Chairman of Thesis Committee Professor Moses Tadé and Head of the Chemical Engineering Department Professor Ming H. Ang for their constant support and advice. I would like to thank all members of the administrations at Chemical Engineering Department as well as library staff for their help during this course. I would also like to acknowledge the support of my friends. Foremost I would like to thank Mr. Nilesh Kotadiya for his friendship, unfailing support and confidence in my capacity to complete this study. I am also thankful to my colleagues, Kalpit Shah, Pradip Shukla, Tejas Bhatelia, Milin Shah, Deepak Jagannatha, and Chirayu Shukla at Curtin University of Technology for their outstanding assistance in technical and non-technical matters during this project. I am also thankful to Er Bhavesh Patel, Dr Ravish Shah, Mitul Rafalia, Aakash Patel, for their motivation and best of support during my academic period.

Finally, all the credentials of this degree go to my beloved parents. This journey would not have been possible without their love and support. I am deeply indebted to my parents, and my Family, who have been with me at every step before and during this project completion. I would like to thank every hand that helped me directly or indirectly in completion of this project work.

Brief Biography of Author

Author of this thesis Mr. Mikil Gandhi has completed his bachelor in chemical engineering from AISSMS' College of engineering, pune, India with first class. In february'07 he joined Curtin University of Technology, WA,Perth, to opt Master of chemical engineering by course work. After first semester he transferred to Master of Engineering by research.

He has written paper in support of thesis:

"**CFD based prediction of erosion rate in opposite wall fired large scale boiler**", a paper to be submitted to Fuel Processing Technology, 2010

Thesis Contents

Chapter 3

Chapter 6

List of Figures

List of Tables

Nomenclature

Symbol	Definition
β	Thermal expansion coefficient
C_p	Specific heat at constant pressure (kJ/kg)
d_p	Diameter of the particle (m^2)
D_{eff}	Effective diffusivity
E	Total energy (kJ)
ε	Turbulence dissipation rate (m^2/s^3)
ε	Erosion rate (mg/kg)
$\overline{f^2}$	Mixture fraction variance
f	Mixture fraction
G_k	Turbulence kinetic energy due to mean velocity radiant (m^2/s^2)
G_b	Turbulence kinetic energy due to buoyancy force
$H_{i,j}$	Diffusion flux of species i, j
H_v	Vickers hardness
h	Enthalpy (kJ/kg)
I_e	Erosion index
k	Turbulence kinetic energy (m^2/s^2)
K_e	Erosion constant
K	Overall constant for erosion
K_{eff}	Effective conductivity
L	Turbulent length
m_i	Local mass fraction of each species
$M_{i'}$	Mass rate of removal or formation by chemical reaction
p	Static pressure (kg/m^2)
ρ	Density of the fluid (kg/m^3)
ρ_m	Density of material
ρ_p	Density of the particle

q_r	Radiation flux (kJ/s)
S_{mi}	Momentum in particular direction
S_i	Mass source
s	Path length
T	Local temperature (K)
t	Time (s)
τ_{ij}	Stress tensor
$(\tau_{ij})_{eff}$	Effective stress tensor
V	Turbulent velocity scale (m^2/s)
v_i	Velocity component in i direction
Z_k	Mass fraction
Ω_ϕ	Transport coefficient for variable ϕ
Ω_t	Transport coefficient for mean variable $\bar{\phi}$
ϕ	General scalar variable
$\bar{\phi}$	Mean scalar variable
ϕ'	Fluctuating scalar variable
ω	Intensity gradient
μ_t	Turbulent viscosity (kg/ms)
μ_{eff}	Effective viscosity
σ_s	Scattering coefficient
σ	Stefan Boltzmann constant
Φ	Phase function
σ_y	Yield stress (kgf/m^2)

Chapter 1

Introduction

1.1 Background

In the modern increasing competitive environment, an efficient operating criterion for pulverised coal fired furnace is vital for the future of thermal power station. In worldwide energy sector, total 37% of electricity is produced by combusting raw coal. Different grade of raw coals are used as fuel in thermal power stations.

In the thermal power station, the boiler performance is a backbone for power production. Growing problem of global warming makes efficient operation of furnace as main interest of research in the energy sector. Process design parameters of coal combustion inside the furnace are precisely decided to achieve long life of boiler and boiler tubes, to attain maximum thermal efficiency, to minimise NO_x emission and for maximum power generation. Furnace is highly heterogeneous and highly non-predictive part of the power industry. Various influencing parameters make the coal combustion process less controllable inside the furnace (Belosevic et al., 2008). Further more, during coal combustion the inorganic mineral matter undergoes different mechanisms, including char oxidation, decomposition, coalescence, fragmentation and vaporization, generating ash particle of different shape and size with different composition from those of mineral matters in coal. However, ash and minerals are completely opposite to each other. The ash formed in coal combustion is major constrain in power generating utility boiler. It becomes difficult to predict the problem related to ash formation and behaviour of ash during coal combustion (Hurley and Schobert, 1993). It has been observed that around 20% of ash produced during combustion has erosive effect on the wall surface of burner and tubes (Das et al., 2007).

Ash produced after combustion flows through the system along with hot combustion gas and impacts on wall surfaces on its way out. Some of the ash particles will separate from this flow and impact at certain angle with relatively high velocity damaging the target surface. The tendency of ash to impact or to stick to the boiler

surface is a function of ash particle size, shape and its composition. Mineral form and its occurrence dictate the abrasive nature of mineral. Included minerals are not as abrasive as excluded minerals which exist as individual entities within the coal matrix. Thus, it is not alumina (Al_2O_3) which occurs in a softer form, but the minerals of which is a major constituent. Similarly it is not silica (SiO_2) which is abrasive, but the mineral form quartz which can be abrasive depending upon size and shape of the grains (Raask, 1969). Repeated collisions of these particles on target surface reduce the strength of the metal structure and deformed the surface layer. In other case due to irregular shape of particles, their impact velocity at different impingement angle, material is removed by the cutting action (Bitter, 1963).

Erosion of material also depends upon mechanical properties of target surface such as material of construction, thickness of the material, tensile strength of the material to resist the impact of solid ash particles. Also erosion, together with the process of blocking, fouling and corrosion, reduce life of boiler and boiler tubes. These results in reduced thermal efficiency or immediate shut down or unwanted maintenances and penalty of millions of dollars production lost. Thus everlasting demand of clean coal technology and its implementation has accelerated the requirement of more precise information on particle erosion behaviour in coal combustion system. However various tests or experimental work can not describe the complexity of the physical and chemical phenomena that happen in a large scale boiler significantly, resulting in under prediction of erosion due to flue gas flow. It becomes expensive and time consuming to analyse this behaviour using different grade of coal for different operating conditions, not at industrial scale but also in small experimental work. Computational Fluid dynamics (CFD) technique is an effective tool to study and analyse complex process occurring inside the furnace. It provides very precise numerical values for velocity, temperature, species concentration and heat transfer distribution for combustion process. CFD codes help us to visualise different parametric effects inside the boiler, to understand flue gas flow pattern and its effect in various boiler section during the combustion (Vuthaluru and Vuthaluru, 2006).

In this work, an attempt has been made to identify different areas inside the furnace which are more prone to erosive behaviour. Computational study of furnace geometry is carried out by providing different parameters to visualise the effect of particle

velocity, particle residence time, and its impact on plates and wall surface. Study is carried out to evaluate wear effect, high velocity zones, temperature distribution at cross over pass, and oxygen concentration at the exit. This study provides necessary plat form for design engineer to mitigate issues related to erosion on the basis of flue gas behaviour inside the boiler for various combustible, and operating parameters without expensive and complex trials on actual boiler. Thus it is essential to understand the fundamentals of erosion phenomena which is described in detailed in next chapter.

1.2 Objectives

Ash formed during combustion of inorganic mineral matters in coal can lead to problems causing erosion, slagging and fouling; this study is aimed to investigate the flue gas behaviour and predicting the erosive effect of fly ash particles along the flue gas flow during direct combustion in pulverised coal plant. The knowledge gained from the literature is used as tool for better understanding of coal combustion process and ash behaviour, paving a way towards optimisation of efficient boiler operation. The scope of this research includes the study of erosion phenomena in conjunction with numerical modelling approach, will be useful to enhance the understanding of the characterised flow inside the furnace during combustion.

The goals of this work can be summarized into following sequence:

- Develop furnace geometry with different mesh scheme, using Gambit 2.3.16 with general arrangement drawing available from industry;
- Numerical simulation using CFD code Fluent 6.3.26 under different operating condition considering different case scenario;
- Evaluating temperature distribution along different cross section and identify temperature zones;
- Evaluating velocity distribution and particle trajectories along the furnace height;
- Calculate erosion rate with obtained numerical values from simulations and compare with experimental and available literature data;
- Identifying popping furnace zones from the particle trajectories of simulation cases, which are likely to be under, wear influence.

1.3 Thesis Outline:

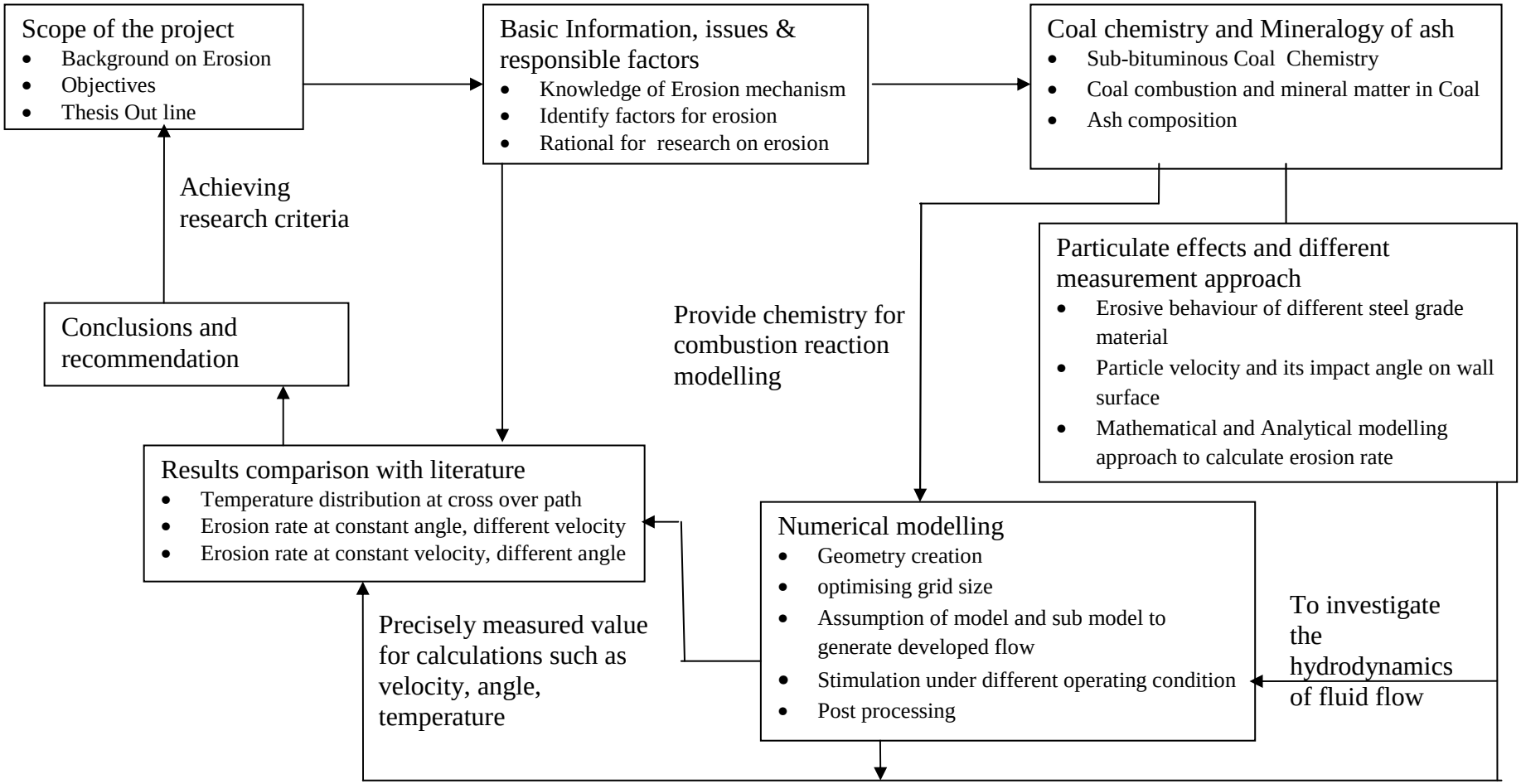

Chapter 2

Literature Review

The literature review provides insight in to the background information and research that has been carried in relation to solid particle erosion in pulverised coal fired furnace. The first section will discuss the coal combustion and problem arises from coal combustion. The second section will describe the behaviour of mineral matters included in coal and formation of ash during combustion process. The following section will review erosion phenomena and effect of diverse parameter causes erosive wear such as solid particle impact, effect of impact velocity, particle rotation and effect of temperature on target surface. This section will describe all the detailed information on how all these parameters are responsible to cause mechanical damage to the furnace wall surface and tube surface. Final section will look into summarising available literature review and identify the necessary additional research required to optimise the erosion behaviour of solid particle inside the furnace.

2.1 Coal and coal combustion

Pulverised coal combustion is one of the most efficient techniques for power generation industry over several decades, with high performance and high technical designed for large scale utility boiler. In combustion systems, raw coal chunks are grounded in pulverised mill to small particles. These particles range between 5 to 400 μm in diameter (Z.Wu, 2005). The grounded particles are then mixed with the air to combustion chamber for combustion process. As per coal rank, combustion temperature varies from 1300° C to 1700° C. A mixing of fuel (coal) and oxidiser (air) gives high temperature flame end up in high intensity of combustion. An additional secondary air is added after the primary combustion zone to complete the burn out of the coal. Usually the area of burner is much smaller as compared to combustion chamber. Coal solid particles are dispersed in gas phase, injected through small area of burner (primary burner) with different velocity then the gas phase. The inertia force, effects the flame pattern due to change in direction of gas flow. In the process of coal combustion coal particle goes through following steps.

- Drying of coal particle, attain pyrolysis temperature by heating up;
- Pyrolysis of coal particle to produce non condensable volatiles, condensable volatiles and carbonaceous char;
- Oxidation and char oxidation.

Investigation of coal particle combustion in industrial conditions is not an easy task; therefore, most of the present knowledge was gained through experiments with single coal particles. In such cases, the numbers of parameters influencing the process are limited to the type of coal, size of coal particle, rate of heating, gaseous atmosphere surrounding the coal particle. The rate of surface temperature increase and the profile of temperature within the particle is a function of heat flux to the particle surface by radiation and convection, particle size, thermal properties of the particle, and thermal effects within the particle (Tomeczek, 1994).

Combustion process starts with drying and heating of particles when they approach a flame. Drying and heating results in physical change to coal particles. Volume of coal particle reduces due to change in moisture content in coal particle and type of coal. As moisture converts to steam phase, it migrates to exterior part of particle and break the particle due to pressure build up inside. This fragmentation will increase with increase in heat rate. As heat drives through the particle, it reaches a reaction temperature where thermal decomposition starts and coal is converted into volatiles and char. Thus heat along with the volatile gases is carried out of particle, continuing the heating process. At the particle surface devolatilisation starts and proceeds towards the centre. Here particle temperature varies from 450° C to 500° C (Tillman, 1991). As coal is heated, disruption of hydrogen bonds, vaporisation and transport of molecular phase and low temperature linking occurs. Generalised bonding structure of coal particle is shown in Figure 2.1. After weak bonds break up, the functional groups decompose to release gases mainly CO_2, CH_4 and H_2O. Primary devolatilisation produces different non condensable gases and condensable volatiles or tars. Finally it leaves solid carbonaceous residue which is called as char (Glarborg et al., 2003). Generally coal combustion process is rarely completed in large scaled furnaces. A small amount of unburned carbon is emitted from boiler. This will limits the overall combustion efficiency of the plant.

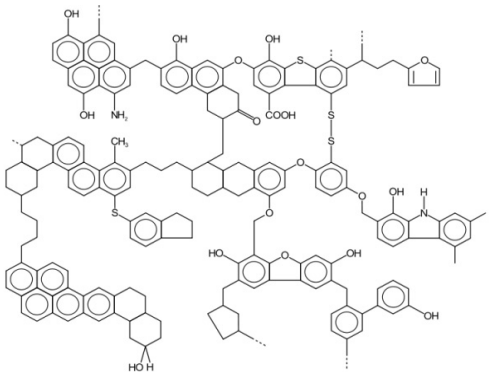

Figure 2.1 Structure of coal

The reactivity and efficiency of combustion purely depends on percentage of carbon burnout obtain in the furnace. Sometimes coal particle takes more time to burn, based on burning rate of char particle after devolatilisation. Research suggests that raw coal quality plays an important role on the level of unburnt carbon in fly ash to produce less NO_x after combustion (Carpenter, 2002). Naturally occurring coal obtained as mixture of combustible solid hydrocarbon, which is identified on the basis of their optical properties referred as maceral and largely incombustible mineral and other inorganic constituents known as mineral matter. An organic component defines the rank and type of coal and it's important for different processes (Ward, 1984; Taylor et al., 1998). It is classified as potential source of hydrocarbon.

The inorganic mineral matter behaves as diluents, displacing more useful organic matter with a non combustible component that leaves an ash residue when the coal is burned. This mineral matter in coal seam is the main component causes problems in utilisation industry (Gupta et al., 1999b).

Further more mineral matter in coal is sum of the minerals and inorganic matter in and associated with coal (Standards Australia 1995, 2000). This definition was considerably true and was defined in the same way by Finkelman (1994), Harvey and Ruch (1986). Thus on the basis of different studies carried out for mineral matters, it can be divided into three basic types of constituents.

- Inorganic elements associated with organic compounds of coal marceals;
- Dissolved salts and other inorganic substance;
- Crystalline or non crystalline particles.

Out of these three, first two types of constituents are non mineral inorganic. In sub-bituminous materials, lignite and in brown coals these non inorganic are in large amount. These mineral matter constituents are also involved in ash formation process for low rank coal deposits (Kiss and King, 1977, 1979; Given and Spackman, 1978; Miller and Given, 1978, 1986; Benson and Holm, 1985; Ward, 1991, 1992). Generally non-inorganic mineral matter is in small amount in bituminous and anthracites. Formulae have been generated to calculate the percentage of mineral matter for any coal sample. In late 30s Parr (1928) and King et al., (1936), both proposed formulae based on percentage of sulphur and percentage of ash yield from coal with few assumptions. But these formulae do not give any accurate amount of mineral matter in coal seam. However, there are many other different methods available to analyse the mineral matter and its behaviour in mined coal sample. Megascopic and microscopic methods, Scanning electron microscopy, Electron microprobe analysis, X-ray diffraction analysis, Rietveld XRD analysis techniques and other analytical methods have been used by different authors to find out proportion of mineral matter in whole coal samples. Out of all these technique Scanning electron microscopy is used with computer-controlled scanning electron microscopy (CCSEM) to visualise distribution of minerals in coal. Thus, it became possible to predict the behaviour of mineral matters in coal during coal combustion. CCSEM is the most adopted technique to determine size, composition, and association of minerals in coal (Wigley et al., 1997; Wigley and Williamson, 1998; Gupta et al., 1998; Virtanen et al., 1999).

2.2 Behaviour of mineral matter during coal combustion

There is an interaction between mineral matters in coal at high temperature at which combustion occurs. For example loss of CO_2 from carbonates, S from sulphides and crystal lattices OH form clay minerals. Theses minerals and other inorganic constituents in coal react, along with the organic particles, when the coal is used in combustion process. However, changes in the mineral matter of coal at high temperature associated with coal combustion have been addressed by several researchers. Literature also shows that alteration of individual minerals and interaction of minerals brought about by exposure to high temperature fuse to form liquid phase, which cools in other parts of the furnace to become crystalline glass in the ash or slag

residue (Ward, 2002).Some mineral interaction is also depending upon the environmental condition inside the furnace, like pyrite and siderite forms iron oxide mineral during combustion process. In detail pyrite goes through exothermic reaction, because of sulphur and oxygen interaction, while siderite undergoes an endothermic reaction to release CO_2. In other cases Ca and Mg from different minerals react to form calcium ferrite, Srebrododlskite, magnesionferrite and many other minerals. Wide range of minerals found at high temperature in coal combustion as shown in Table 2.1. All these minerals have an effect on furnace operation depending upon their hardness and reactivity during combustion procedure. Data suggests that quartz and pyrite may both be abrasive in coal mill but only quartz plays most effective role to cause erosion or abrasion to the different parts of boiler as pyrite rapidly decomposes. Empirical studies show that quartz is two to five times more abrasive than pyrite (Carpenter, 2002). Other then minerals in solid phase, liquid phase of minerals formed at high fusion temperature cool down in different part of furnace, forms ash or slag residue**.** Thus ash formation throws more lights on mineral behaviour during and after coal combustion inside the furnace.

Table 2.1 Principal minerals identified in high temperature with coal utilization during combustion of coal (Ward, 2002)

Mineral	**Composition**	**Mineral**	**Composition**
Quartz	SiO_2	Metakaolin	$Al_2O_3.2SiO_2$
Mullite	$Al_6Si_2O_{13}$	Albite	$NaAlSi_3O_8$
Anorthite	$CaAl_2Si_2O_8$	Sanidine	$KAlSi_3O_8$
Corundum	Al_2O_3	Pyrrhotite	$Fe_{(1-x)}S$
Oldhamite	CaS	Anhydrite	$CaSO_4$
Aragonite	CaCO3	Portlandite	$Ca(OH)_2$
Lime	CaO	Periclase	MgO
Wuestite	FeO	Hematite	Fe_2O_3
Magnenite	Fe_3O_4	Spinel	$MgAl_2O_4$
Magnesioferrite	$MgFe_2O_4$	Calcium ferrite	$Cafe_2O_4$
Srebrodolskite	$Ca_2Fe_2O_5$	Brownmillerite	$Ca_4Al_2Fe_2O_{10}$
Wollastonite	$CaSiO_3$	Gehlenite	$Ca_2Al_2SiO_7$
Merwinite	$Ca_3Mg(SiO_4)_2$	Melilite	$Ca_4Al_{12}MgSi_3O_{14}$

2.3 Ash formation mechanism

In any thermal power station ash related problems are of major concern since it is difficult in predicting the formation and behaviour of ash during combustion. Two important coal characteristics influencing the ash formation process which are

- The mode of occurrence of the inorganic matter;
- During combustion behaviour of coal particles containing both organic and inorganic matters.

Many of inorganic matter present in coals occur in the form of minerals of various types and sizes. These minerals can be closely associated with the organic matter (included minerals), or they occur excluded from the organic matter (excluded minerals). The majority of ash particles are formed from four formation mechanisms as shown in Figure 2.2 below.

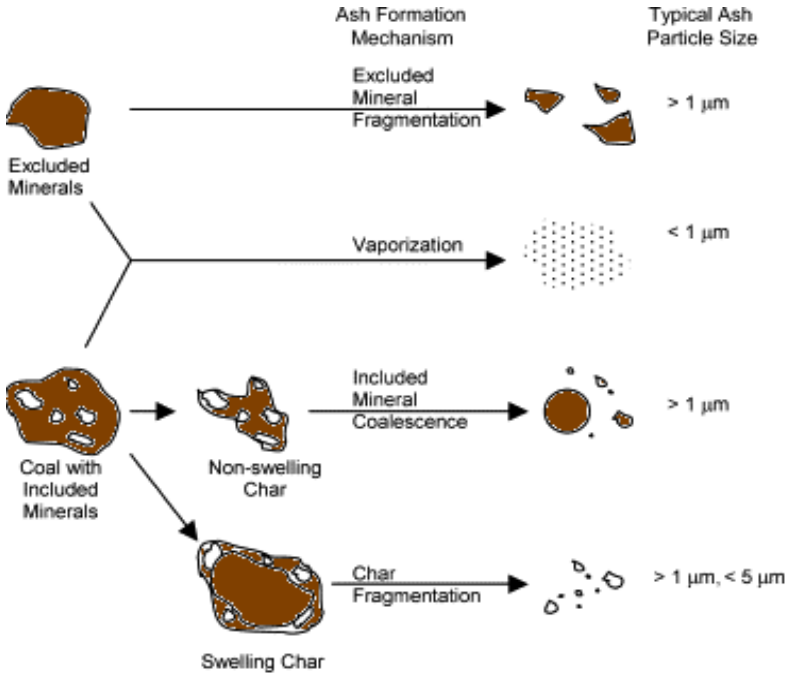

Figure 2.2 Ash formation mechanisms (adepted from Carpenter et al., 2005)

- Included mineral coalescence;
- Char fragmentation;
- Excluded mineral fragmentation;
- Vaporization and subsequent condensation of inorganic matter.

Ash particle formed by first mechanism forms bulk of super micron particles, while ash particle formed by third mechanism is not bulky but super micron sized. Large number of ash particle of micrometer size is produced because of char fragmentation, while last mechanism contributes mainly to submicron size ash particles. However, vaporisation believed to be less important in formation of sub micron size ash particle during low rank coal combustion in utility boiler.

During coal particle combustion, ash particle formed by coalescence of included minerals can be affected by the size, type and distribution of minerals. This happens when char particle remain unchanged means they does not fragment. Sintering is another characteristic of ash particle which will affect the tube spacing. Ash particle below 900 ^{o}C will adhere to the tube surface. It has shown that sintering strength is directly related to the fouling tendency. Thus at such high combustion temperature mineral matter undergo physical and chemical changes. Oxidation, decomposition or calcinations of carbonates to oxides may occur. Some mineral may melt; other may become soft with change in its shape or size. This change depends upon the residence time of mineral particle in hot zone. This is called as ash. Thus ash may be considered as inherent and as adventitious ash depending on the mineral matter involved in it. Iron, calcium, Magnesium, phosphorus, potassium and sulphur are commonly present in inherent ash but iron, calcium, magnesium and sulphur are present in larger quantities in adventitious ash with varied particle size (William, 1984). Moreover, this elemental distribution depends upon the complex interplay of a range of factors such as mineralogy, particle size, mode of occurrence and organic association. However in combustion process non carbonaceous mineral matter end up as solid particles of size which restrict them to enter in to combustion gas as it flows through the system. This is considered as fly ash. Fly ash generated causes mechanical damage to tube wall and furnace wall and other part of utility boiler. This mechanical damage is called as erosion or abrasion described in detailed in the following section.

2.4 Erosion and influencing parameters

Abrasion or Erosion can be define more precisely as when solid particle moves on the surface called as abrasion, while when kinetic energy of particle is high, then it considered as erosion. Thus wear is total effect produced by abrasion and erosion.

In coal power plant wear of metal surface is caused by (1) flow of coal as ash inherent in it; (2) Due to fly ash or bottom ash of poor quality generated after incomplete combustion of coal. However, these two causes are in the content of moisture limit in raw coal. The upper limit of moisture in raw coal is generally 10 %. During the rainy season some coals having hardness varying from 90 to 130 represented by hard grove index (HGI). This is attributed to high clay content containing high moisture. Despite their soft nature, they cause flow problems and consume excessive power for pulverisation. Literature also shows that, when ash in coal increases, in order to maintain the given system output level, the coal flow through the system also increases, because of reduced useful heating value of coal, lower efficiency of equipment, and so on. Hence, it affects the systems in qualitative as well as quantitave manner (Bhatt, 2006).

Erosion is mainly observed for the systems which involve high speed particle movements, causes mechanical wear to the different part of utility equipments such as in regenerators, riser and cyclones of catalytic cracking installations, air mills, tube wall and re heaters in side furnace, fluid bed systems. Since five to six decades, this problem has been investigated by various researchers all over the world to optimise the erosive behaviour of particles and its effects in combustion system. Many experimental studies have been carried out to find out various parameters responsible for particle's erosive nature and to develop the material which does not affect by wear under different operational condition. Major parameters are described in the following sections give more information on solid particle erosion.

2.4.1 Effect of impact angle on metal surface

Impact angle is one of the major factors which decide the type of erosion on the metal surface. (DE Haller, 1939) he found that large impingement angle and small angle of impact causes metal erosion. Study at the microscopic level showed highly deformed surface for large impingement angle and less deformed, scratched surface for small impact angle. (Wellinger, 1949) studied the erosion phenomena using impact angle as a platform. His study was concentrated on mechanical properties of erodent material, which also influence the type of erosion persist. (Davis, 1949) had a different view other then impact angle. According to him repeated deformation could be one of the

main reasons for erosion to occur. He studied that elastic deformation occurs when maximum value of stress does not reach the strength of the material. However during collision the elastic limit is exceeded, plastic deformation reaches the maximum value of stress. On repeating collision this maximum value of plastic deformation become equal to the strength of material. Later on increasing the load, strength of the material is exceeded, the surface layer is destroyed. (Van Riemsdijk and Bitter, 1959) visualised the effect of deformation wear by exposing silver plates to a jet of cast iron pellets impacted at 60°. They also mentioned another type of wear, cutting wear. In cutting wear mechanism, a particle strikes at an acute angle which is less than 90°. For hard and ductile material effect of cutting wear is negligible as compared to deformation wear. On the basis of these two mechanisms Bitter derived the overall erosion rate of particular material. A detailed mathematical model is described later in section 2.6 in this chapter. He showed that total erosion rate is sum of deformation mechanism and erosion due to cutting mechanism. It is well developed that solid particle impingement angle is key factor to find out the erosion rate. For all metal, maximum erosion occurs at angle approximately $20^{\circ} - 30^{\circ}$ from the plane of the surface. Erosion at normal incidence is of less interest because erosion at this angle is only one third of the maximum. But research also shows that erosion occur at normal incidences does have mechanism differ from shallow angles. (Hutchings, 1980) carried out analytical model for erosion considering spherical particle at normal incidence angle. He studied that at normal incidence angle platelet is formed on specimen surface as shown in Figure 2.3 below. These appear to be the main mechanism of metal removal by spherical particle. The platelet mechanism is different from the cutting and deforming processes which are seen in single impacts of angular and spherical both particles at oblique angle. He proposed that critical strain may be one of the main criteria such as removal of a fragment of a material occurs when plastic strain in the fragment reaches the critical value. He further showed that average strain value can be affiliate with each impact with same velocity to find out the erosion rate (Rickerby and Macmillan, 1980). Thus, velocity with impact angle is our second major constrain.

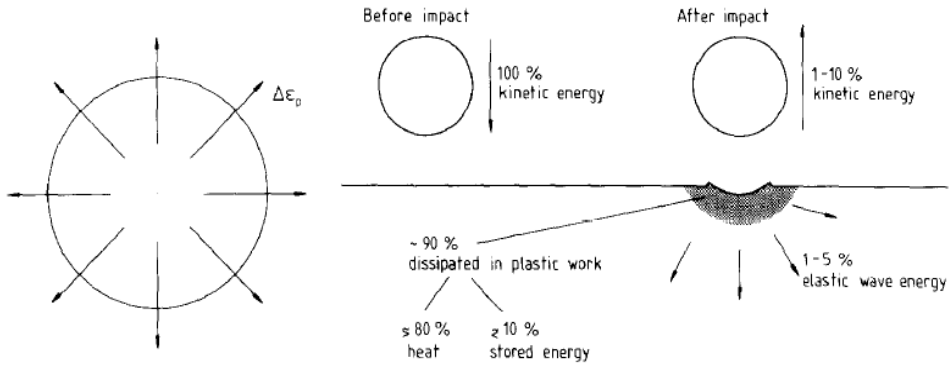

Figure 2.3 The plastic strain associated with impact and the energy balance before and after the normal impact of a spherical erosive particle (adapted from Hutchings, 1980)

2.4.2 Effect of impact velocity and its exponential value

As mention above that velocity is second key factor for the removal of material from its surface. In 1972 Finnie showed relation between volume removed from the surface, particle velocity, mass of the particle, and horizontal component of flow pressure of particle, angle of impact, which was experimentally proven but it has different value for values of α equal to 90°. Study showed that erosion rate differed with large angle of impingement. It was observed that cutting mechanism occurs with an angle range from 0 to 45° due to repeated collision between particle and surface (Finnie and Kabil, 1965). Further this study was carried out with role of particle velocity. The assumed relation $V=U^n$ with value of n=2 was first approximation with actual value of n being noticeable large. Different values of n for different grade of material were shown at different angle. Sheldon reported value of n is equal to 2.36 for electrolytic copper and 6061-0 Al eroded by SiC particle at $\alpha = 20^{\circ}$. Values of n close to 2.3 for a variety of materials were found out by Tilly. This value was confirmed experimentally for 11% Chromium steel. They also suggest that smashing of the particle and growth in secondary erosion occurs at higher velocities (Tilly et al., 1970). In 1965, Sheldon developed a sand blast apparatus to analyse the velocity effect on erosion rate with different thermal diffusivity. For Al and Ti, showed similar velocity exponent value at velocity 39 and 97 m/s, $\alpha = 10^{\circ}$, despite of difference in thermal diffusivity. Prediction from experimental work shows that velocity exponent should increase with angle for given velocities. Bitter studied that particle rigidity is

also one of the major factor effecting type of erosion with certain velocity. If a rigid particle strikes the steel surface with 100m/s velocity, it penetrates to the depth of fraction of particle diameter and forms curvature of same radius to that of particle shape. But with higher velocity forms depth and diameter many time the diameter of particle.

At certain velocities particle will produce stress concentration for brittle material, which results in cracks at depth proportional to particle size. At higher velocity cracks may be formed in directions which are determined by particle velocity (Bitter, 1963). The force and direction of an ash particle's impact on the target surface provides necessary data to determine the erosion rate of that material. For rebounding particle velocity, impact condition and combination of particle and surface are also of importance. Here restitution behaviour which can be defined as momentum lost by particle corresponds to the work done on the material surface and extent of erosive wear suffered by the material. (Grant and Tabakoff, 1975) they developed the empirical correlation of velocity restitution coefficients for silica. The velocity coefficient of restitution mainly depends on the density of the particle, velocity of the particle, and hardness of the target material.

2.4.3 Effect of solid particle rotation

Finnie, 1972 he reported the implication of particle rotation which can influence the erosion rate of metal surface by solid particles. His theory was based on rotational velocity distribution which indicated the effect on erosion rate. (Hutching, 1977, 1979) delivered an impressive theory suggesting that for ductile material, three possible mechanisms occur during erosion. He considered the effect of a particle rotating forwards or backwards after impact. It was suggested that for angular shape particle erosion occur by cutting or micro-machining completely depend upon the direction of rotation before and after impaction, while plastic deformation occurs for spherical shape particle.

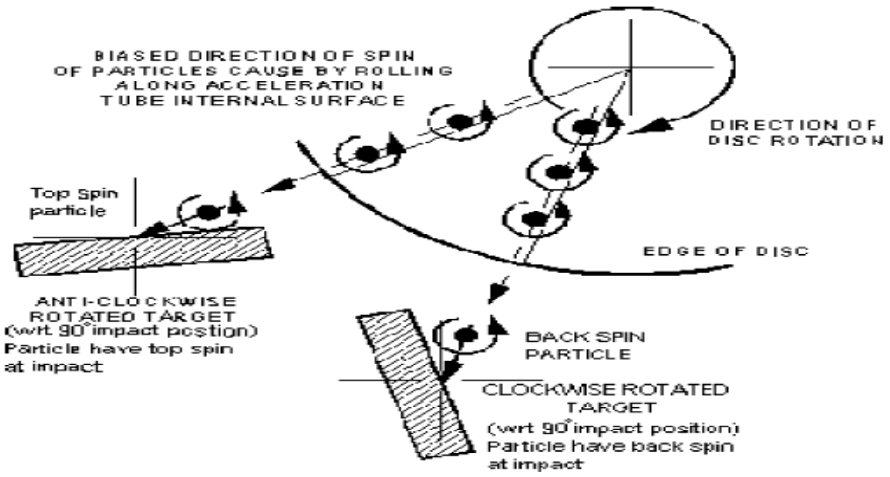

Figure 2.4 Schematic illustration of the effect of target orientation on the spin direction of rotating particles at impact (adapted from Bingley et al., 2003)

Experiment on particle spin in centrifugal accelerator erosion tester was carried out and it was observed that particle strikes the target depending on the speed and direction of rotation of particle will change the effective impact velocity of the particles during their point of contact as mentioned in Figure 2.4. Different angles of impingements were arranged to be close to the 10°, 20°, 30°, 45°, and 60° as possible with same velocity for all tests. The results indicated a higher erosion rate for back spin of particle rather than top spin. Due to back spin particle has a higher velocity at the point of contact leads to high material removal during erosion (Bingley et al., 2003).

2.4.4 Effect of temperature on solid particle erosion

Many of the experimental data obtained on erosion rate are based on temperature at normal room temperature. Sundararajan structured all results and incorporated them in erosion model developed on the basis of room temperature. With the help of different erosion model, important material characteristics were possible to determine for high temperature erosion. Data available from different source show that the erosion behaviour of metals and alloys as a function of temperature can be classified into three groups. First group in which erosion rate initially decreases with increase in temperature, SS 310, SS 304, Al 1100 and Ti-6Al-4V falls in this group. For the second group erosion rate is independent on temperature until it reaches the critical temperature. Once critical temperature is achieved erosion rate of material increase

with increase temperature. SS 310, Al 1100 and lead fall in this group. In third group of metal erosion rate goes higher with high value of temperature (Sundararajan, 1984). Thus tensile properties, interference of oxidation and mechanical properties has an association with erosive behaviour at high temperature. Research shows the presence of a limiting particle above which erosion prevails and below which corrosion occurs. However, erosion behaviour at high temperature is still not studied well. For tube erosion study basic erosion parameter such as impact velocity, impingement angle was analysed at high temperature. Keeping this condition constant, erosive resistance of boiler tube steel was examined and tried to correlate that with steel property to have an idea about the controlling factor for that particular steel. Using different material experiment was carried out with blasting type test equipment at high temperature. Tabakoff showed that velocity exponent for inconel 718 and for Ti-6Al-4V for 25° impingement angle and 60°-1300°F, it decreases with temperature. Also, yield strength decrease with increase in temperature. For low angle, erosion rate is high and temperature would be higher. Thermal parameter such as melting temperature, heat capacity could be the one of key factor for the metal removal. (Smeltzer, 1970)

2.4.5 Erosion rate and material selection

Indenture and erosion of target surface by impact of solid particle, frequently depends on the size and velocity of the particle. For ductile material maximum erosion occur at impact angle of 70° to 80° to the normal (Zukas, 1990). At shallow incidence angles, the indenture and erosion occurs due to cutting and deformation action (Bitter, 1963). During this process plastic flow and friction are prime mechanism of deformation and energy dissipation. Wellinger and co-worker showed that for different material, erosion resistance changes as the angle of impact changed. For harder steel which has Vickers's hardness 840 kg/mm^2, maximum removal of material occurs at jet angles close to 90°. Holtey showed rub and shock, two new phenomena related to erosion action on the metal surface.

On striking particle soft steel are under shock conditions, while harder steel are under rub condition. Mainly the erosion of target surface by solid particle in inert fluid should depend on the number of particle collide with the surface, normal and

tangential component of velocity and direction magnitude of the particle (Finnie, 1960). For brittle material deformation wear is more likely to happen and for ductile material cutting mechanism would be more prominent. As an angle of impact changes from 90° to zero, importance of deformation to cutting wear increases. Different factors which can be considered while selecting material of furnace for its construction.

From surfaces point of view

- Physical properties;
- Change in shape caused by erosion;
- Stress level;
- Presence of oxide (or other) coatings;
- Simultaneous occurrence of corrosion;
- Temperature.

From particles point of view

- Impact angles;
- Impact and rebound velocities;
- Rotation before and after impact;
- Shape and size;
- Volume concentration and surface flux;
- Physical properties (hardness, strength, and density);
- Fragmentation;
- Interactions with surfaces.

2.5 Tube erosion

In most of the power plant apart from furnace wall, re-heater in inlet, primary superheater, secondary superheater and economiser are also prone to erosive wear under combustion condition. This erosive effect can be describe as the mechanical thinning of tube walls by the continuous impact of the ash particle on the mild steel tubes in super heater sections. Figure 2.5 shows photographic view of tube surface eroded due to solid particle impact at different location. Mechanical damage is limited

to localised zones in the vicinity of the gaps between tube bundle and wall. Outlet of gas by pass channel is also affected by high flue gas velocity. Cutting action is dominant in removal of metal at oblique angle of impaction less than $\pi/4$ rad.

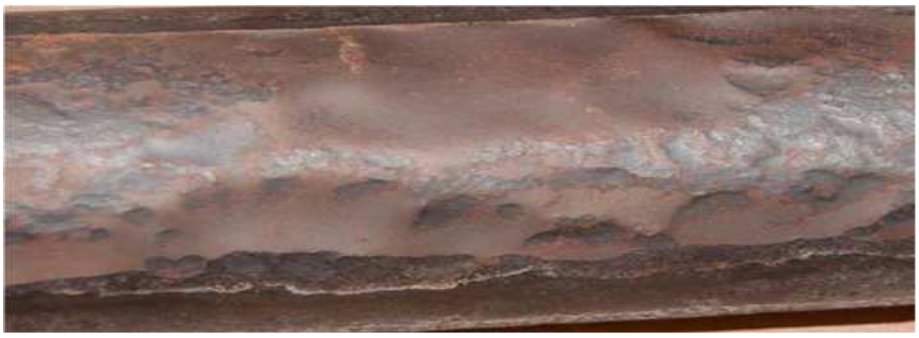

Figure 2.5 Eroded tube surface

Study also shows that during soot blowing due to compressed air jets and impaction of ash particles. Depending upon the concentration of flue gas and particle impact velocity less than 100 to 150 m/s causes less tube erosion. This case is different for oil fired boiler where ash particle velocity of the flue gas rises up to 60 or 80 m/s causes negligible erosion to the tube surface (Raask, 1969). The damaging effect of erosion substantially reduces the operational life of tube at an average rate of $2x10^{-5}$ to$15x10^{-5}$ μm/s. for maximum erosion rate tube failure happened after 16000 hrs in service (Jianren et al., 1999). Thus finally, it could be concluded that key factors for erosion rate analysis for target steel surface are

- Ash particle velocity,
- Ash particle impingement angle,
- Mass fraction of silica contained in the ash sample,
- Average density of ash particles,
- Density of the steel component,
- Yield stress of the steel component, and
- Temperature of the steel component.

On the basis of above mentioned key factors, many researchers have made analytical as well as mathematical equations and models to enhance the scope of erosion phenomena in pulverised coal fired power industry. It is quite interesting to know that when the variables are assembled into mathematical form, they are referred to as wear

equations while a wear model is a listing, description or discussion of the variables that influence wear. Many of the mathematical equations developed by various authors are mentioned in next section for our study.

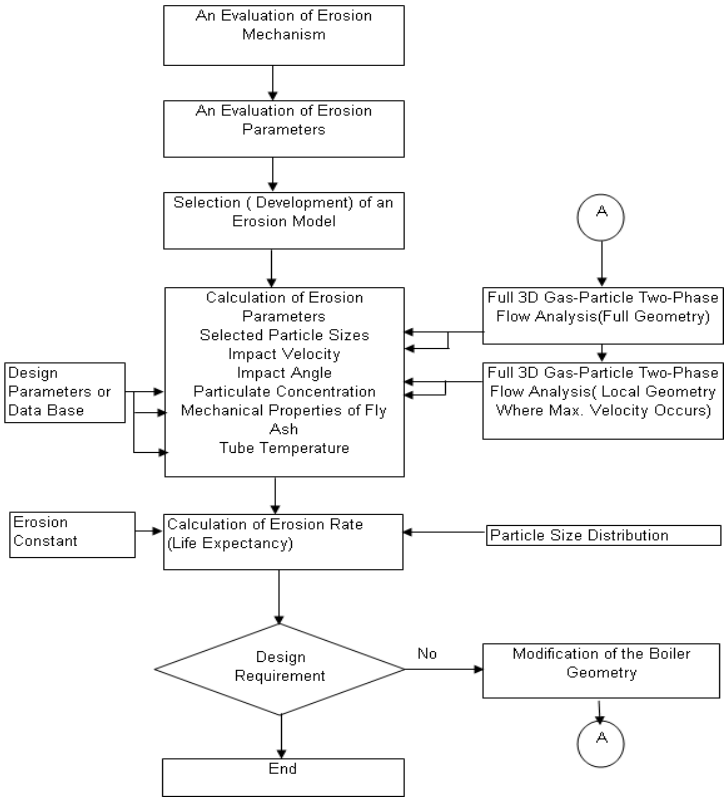

Figure 2.6 Calculation procedure of solid particle erosion rate (adapted from Lee et al., 1999)

2.6 Erosive wear equations

There are number of erosion models and mathematical equations are described in the literature to calculate erosion rate. This section will shows different erosion wear equations developed in past.

(1) J. G. A. Bitter, A study of erosion phenomena, part 1 and 2, wear, 6-1963 pg.5, 169

$$\varepsilon_{VT} = \varepsilon_{VD} + \varepsilon_{VC}$$

$$\varepsilon_{VD} = \frac{1}{2}\frac{M(V\sin\alpha - K)^2}{\delta}$$

$$\varepsilon_{VC1} = \frac{2MV(V\sin\alpha - K)^2}{(V\sin\alpha)^{\frac{1}{2}}}(V\cos\alpha\frac{C(V\sin\alpha - K)^2}{(V\sin\alpha)^{\frac{1}{2}}}\chi) \; for \alpha > \alpha_{p0}$$

$$\varepsilon_{VC2} = \frac{\frac{1}{2}M(V^2\cos^2\alpha - K_1(V\sin\alpha - K)^{\frac{3}{2}})}{\chi} \; for \alpha < \alpha_{po}$$

(2) I. Finnie, Erosion of surface by solid particle, wear, 3 (1960) 87-103

$$\varepsilon_{VP} = \frac{mV^2}{P\psi K}[\sin(2\alpha) - \frac{6}{k}\sin^2\alpha]., \; for \tan\alpha < \frac{K}{6}$$

$$\varepsilon_{VP} = \frac{mV^2}{P\psi K}\frac{K\cos^2\alpha}{6}., \; for \tan\alpha > \frac{K}{6}$$

(3) J.H. Neilson and A .Gilchrist, Erosion by a stream of solid particles,(1968)111

$$\varepsilon_V = \frac{\frac{1}{2}M(V^2\cos^2\alpha - V^2{}_{r)}}{\chi} + \frac{\frac{1}{2}M(V\sin\alpha - K)^2}{\delta} \; for \; \alpha < \alpha_{po}$$

$$\varepsilon_V = \frac{\frac{1}{2}M(V^2\cos^2\alpha)}{\chi} + \frac{\frac{1}{2}M(V\sin\alpha - K)^2}{\delta} \; for \; \alpha > \alpha_{po}$$

(4) J.E. Goodwin, W. Sage and G .P. Tilly, study of erosion by solid particles, Proc. Inst. Mech. Eng. 184 (15), part 1(1969-1970) 279

$\varepsilon_m = K_1 V^a$, Where a = 2 for 25 μm and a = 2.3 for 125 μm

(5) G.L. Sheldon and A. Kanhere, An investigation of impingement using single particles, wear, 21(1972) 195

$$w \approx q^3 = \frac{D^3 V^3 \rho_p^{\frac{3}{2}}}{H^{\frac{3}{2}} V}$$

(6) G.P. Tilly, A two stage mechanism of ductile erosion, wear, 23 (1973) 87

$$\varepsilon = \varepsilon_1 \left(\frac{V}{V_{ref}} \right) \left[1 - \left(\frac{d_o}{d} \right)^{\frac{3}{2}} \frac{V_o}{V} \right]^2 + \varepsilon_2 \left(\frac{V}{V_{ref}} \right)^2 F_{d,v}$$

$$\varepsilon_2 = \varepsilon - \varepsilon_1$$

$$\mathrm{F_{d,v}} = \frac{W_0 - W}{W_0}$$

(7) G. Grant and W. Tabakoff, An experimental investigation of the erosion characteristics of 2024 Al alloy, Department of Aerospace Engineering Tech. Rep. 73-37,1973(University of Cincinnati)

$$\varepsilon = K_1 \{1 + C[K_2 \sin\left(\frac{90}{\alpha_0} \alpha \right)]\}^2 V^2 \cos^2 \alpha \left(1 - R_T^{\,2}\right) + K_3 (V \sin \alpha)^4$$

$C = 1,\ for \alpha \le 3\alpha_0$

$C = 0,\ for \alpha > 3\alpha_0$

(8) I .M .Hutchings, R. E. Winter and J . E .Field, solid particle erosion of metals: the removal of surface material by spherical projectiles, Proc. R. Soc. London A, 348(1976) 379- 392

$W = 5.82 \times 10^{-10} V^{2.9}$

(9) I .M .Hutchings, A model for the erosion of metals by spherical particles at normal incidence, wear, 70 (1981) 269- 281.

$$\varepsilon = 0.033 \frac{\alpha \rho_t P^{\frac{1}{2}} V^3}{\Omega_c{}^2 H_t{}^{\frac{3}{2}}}$$

(10) G. Sundararajan and P. G. Shewmon, A model for the erosion of metals at normal incidence, wear, 84 (1983) 237-258

$$\varepsilon \approx \frac{6.5 \times 10^{-3} V^{2.5} \rho_p{}^{2.5}}{C_p T^{0.75}{}_m H^{0.25}{}_t}$$

2.7 Summary of literature review

Literature shows that major experimental based research is carried out with limited parametric values for solid particle erosion. Finding optimal solutions for each individual practical problem with experiments becomes very tedious and time consuming task. Critical parameters such as flame position, particulate flow pattern, incompleteness of combustion and probable zones under the particulate concentration are difficult to assess during experiments. Apart from being expensive and not easy to perform, experimental measurements may not project reliable results of individual tests to the situations with changed operating conditions. On the other hand, CFD modelling approach can effectively provide detailed and complete information on the process in the furnace.

CFD modelling has proven as an effective tool to communicate the results obtained from simulation studies to potential industrial users and to obtain recommendation from potential users regarding research direction. The results obtained from simulations provide a detailed graphical presentation of local values such as velocity, temperature distribution and species concentrations inside the furnace. Furthermore, it is known from the available literature review, that in order to use analytical or mathematical model that can predict the erosion rate in coal fired large scale furnace, several issues need to be looked into. Firstly, it is vital to have detailed knowledge of the chemical speciation of the organic and inorganic in a coal to be able to predict its behaviour when it is combusted. Research in coal over the year has provided deep insights into coal mineral matter using different available techniques. Secondly, this research will look into ash formation mechanism that will provide essential information on the behaviour of ash particle during coal combustion inside the furnace. The work reported in this thesis will address the different parameters responsible for erosion by solid particles during combustion in boiler. Additionally, this research will also look into various analytical methods as well as numerical approach to predict the erosion rate of different part of furnace. An analysis of coal as received will be used to calculate operating conditions for the given furnace domain. Finally, Knowledge of available computational numerical technique combined with analytical model will be used to predict the probable areas prone to erosive wear and to predict erosion rate.

Chapter 3

Computational Fluid Dynamics Modelling

3.1 Introduction

Inventions in computational technologies have opened the door for improvements in the area of power generation by way of computational fluid dynamics (CFD) modelling. Traditional research on turbo machinery, reactors, and heat exchangers has involved fabrication and testing of actual systems, which is often expensive and time consuming. CFD allows engineers to improve the efficiency and reduce difficulty levels of these systems without fabrication expenses even at laboratory scale level. Predominantly CFD technique was used to perform aerodynamic research, which used to enhance engine efficiency by improving the airflow through the engine. Advance in computing since that time have stimulated the further development and application of these models to more complex structure. But recently, the use of Computational Fluid Dynamics has received increased attention within the boiler manufacturing industry, considerably due to the relatively low cost of computational capacity, but also due to the continuous development of more user friendly CFD code including pre-processing, solver and post-processing. With the help of Computational fluid dynamics it is possible to analyse the complex flow, temperature distribution and combustion pattern in boilers which are very difficult or even not possible to identify experimentally. Today this allows a detailed study to be carried out, for instance fluid flow mixing processes, pollutant formation, particle burnout and many other processes important during the design of new boilers and in the course of trouble shooting. Moreover it also helps designer to optimize the operating conditions, investigate malfunctions in the equipment and evaluate different corrective measure for the same (Carvalho et. al., 2001).

To understand the particle size distribution, char oxidation, local heat release, kinetic parameters for coal devolatilisation, local oxygen concentration during pulverised coal combustion using CFD codes as a tool, it becomes necessary to understand the basic concept of codes which are further divided in three elements available in CFD. CFD consider fluid flow equations which were derived by Navier, Poisson and

Stokes, known as Navier-Stokes equation, as the basis for calculations. But knowledge of function of these elements in context of CFD code is necessary.

3.2 CFD Code

3.2.1 Pre- processor

Before we proceed with CFD work we need to narrow down various criteria for our problem to reduce the difficulty level to an achievable level to get accuracy and desirable results. Keeping end results in mind problem can be divided in to physical and chemical phenomena.

First, decide geometry configuration. Geometry can be made in two dimensions or three dimensions but, three dimensional geometries consume higher computational power. So it could be our one of the main concern to resolve our problem. Detailed geometry with dimension is given in Appendix A. 3D geometry produces more accurate results then 2D geometry, but complex 3D geometry is quite difficult to construct as well. Here, three dimensional geometry was created using GAMBIT- a FLUENT pre-processor. Second step would be boundary conditions applied to geometry by dividing it into different zones. For our study different boundary conditions such as primary and secondary inlet and furnace out let, radiation zone, conduction zones etc.

Next important part as pre-processing is discretisation of flow field in to computational domain which leads to grid generation or creating mesh. Grid generation or creating mesh is defined as set of points distributed over a calculation field for a numerical solution of a set of partial differential equations (Thompson et al., 1999). Hence, grid generation divides the domain into a smaller number between the regions of our interest. This is possible with CFD based software GAMBIT. User must generate mesh of proper size with minimum skewness error to obtain accurate result. User should be aware of consequences of size selection, affecting the accuracy of numerical solution. Major amount of time spent on project is devoted to geometry creation, defining the domain geometry and grid generation. The choice influences the accuracy of the approximation.

Considering these factors grid type can be decided. There are two type of grid, which are structured and unstructured. Structured grid can be defined as, “when domain geometry is equally divided into intersection of curvilinear co-ordinate surfaces or mapping the flow field domain equally into hexahedral or quadrilateral element.” Figure 3.1 shows structured meshing scheme for two dimensional pipe structures. This type of grid gives more precise results then unstructured grid but has disadvantages over unstructured grid as well. It consumes high computational power and higher computational time required which is not beneficial for instantaneous result oriented projects.

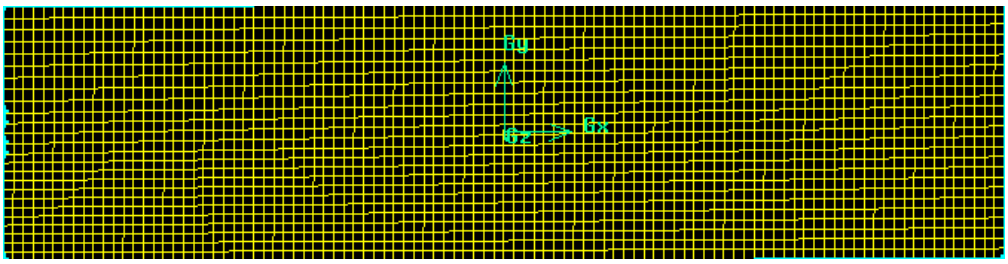

Figure 3.1 Schematic of structured meshing scheme

Unstructured grid can be defined as, “when domain geometry is divided into triangular or tetrahedral element is known as unstructured grid.” Figure 3.2 shows unstructured meshing scheme for two dimensional pipe structures. An unstructured grid can be describe as a limiting case of a multi block grid where each individual cell is treated as a block. The advantage of such an arrangement is that no implicit structure of co-ordinate lines is imposed by the grid. It requires less storage space, less computational power and less computational time to concentrate where ever it needed.

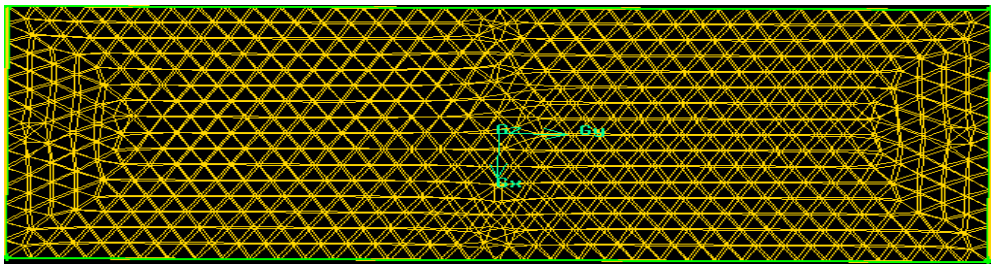

Figure 3.2 Representation of unstructured meshing scheme

Due to complexity of geometry and computational power availability. In next chapter detailed furnace geometry is described with graphical presentation.

Grid dependency is another one of the major concern in order to achieve desirable results. Different size of grid shows distinguished results for the same type of geometry. Small exercise is carried out to show difference in results for the same size of object but with different size of grid size. Fluent equipped with visualisation capability make much easier for the user to analyse useful information in terms of temperature - velocity profile, particle trajectory etc. CFD code fluent also calculates mass balance, heat transfer rate at any time of simulation.

3.2.2 Solver

The choice of solver depends on the grid type and the number of nodes involved in each algebraic equation. Partial differential equations are solved mainly be three numerical techniques in CFD.

- Finite difference method;
- Finite elemental method;
- Finite volume method.

Fluid flow problems are generally solved by numerical algorithms consists of summation of fluid flow equations over control volumes of the domain, Discretisation of integral equation in to algebraic equations system and solution of the algebraic equations by an iterative method (Versteeg and Malalasekera, 2007).

3.2.3 Post – processing

Rapid growth in computing world has provided a useful platform to designer with its graphical effects in post processing field. Graphical representation gives clear idea to the user about operation to be performed. This element of CFD is used to visualise versatile data such as,

- Grid display;
- Sweep surface in any three dimensional direction at any point;
- Temperature and velocity contours or vectors plots;
- PDF display;
- Particle flow pattern;

- Colour postscript output.

As in computer aided engineering, the graphical image of output in CFD code have shown new way to the science industry. Still research is continued for many other post-processing techniques to make it more and more better. FLUENT is mainly associated with post processing element which is used here as well.

3.3 Basic fluid flow modelling

Basic fluid flow modelling is based on fundamental principals from the laws of physics in form of governing equation which are as followed,

- Conservation of mass-- Continuity equation;
- The rate of change of momentum equals the sum of the forces on a fluid particle-- Newton's second law;
- The rate of change of energy is equal to the sum of the rate of heat addition;
- The rate of work done on a fluid particle-- First law of thermodynamics.

In modelling of pf coal combustion, fluid is assumed as a continuum and interaction of gas and coal particle is considered. In other word for fluid flow analysis, distance between the molecules is negligible which may be ignored, so it appears as a continuous gas phase region. Basic governing equation along with chemical species transport and chemical reaction during combustion provides platform for combustion modelling. Because of turbulent flow occurs in compressible fluid flow, these three conservation equations mentioned above should to be treated in time and space average forms (Eaton et al., 1999).

3.3.1 Basic governing equations

Conservation equation of Mass

This is usually defined as,

Rate of increase mass in fluid elements = Net rate of flow of mass into fluid element

$$\frac{\partial \rho}{\partial t} + \frac{\partial}{\partial x_i}(\rho v_i) = S_i \tag{3.1}$$

Where, S_i is the mass source in the system, ρ is a density of the fluid and v_i is the velocity component in x direction.

This mass balance for more than one component system,

$$\frac{\partial}{\partial t}(\rho m_i) + \frac{\partial}{\partial x_i}(\rho v_i m_i) = -\frac{\partial}{\partial x_i} H_{i',i} + M_{i'} + S_i \tag{3.2}$$

Where, m_i = local mass fraction of each species;

$H_{i,j}$ = Diffusion flux of species i;

$M_{i'}$ = mass rate of removal or formation by chemical reaction;

S_i = mass source in other system.

Conservation equation of momentum or Navier-stokes equations

$$\frac{\partial}{\partial t}(\rho v_i) + \frac{\partial}{\partial x_i}(\rho v_i v_j) = -\frac{\partial p}{\partial x_i} + \frac{\partial \tau_{ij}}{\partial x_j} + S_{mi} \tag{3.3}$$

Where p = static pressure,

τ_{ij} = stress tensor,

S_{mi} = Momentum in particular direction.

Conservation equation of energy or First law of thermodynamics

$$\frac{\partial}{\partial t}(\rho h) + \frac{\partial}{\partial x_i}(\rho h v_i) = \frac{\partial p}{\partial t} + v_i \frac{\partial p}{\partial x_i} - \frac{\partial}{\partial x_i}\left(k \frac{\partial T}{\partial x_i}\right) - \frac{\partial}{\partial x_i}\sum_j h_j J_i + \tau_{ik} \frac{\partial v_i}{\partial x_k} + S_h$$

where,

$$h = \sum_j m_{j'} h_{j'} \tag{3.4}$$

$$h_{j'} = \int_{Tref}^{T} c_{p,j'} dT$$

3.3.2 Generalised equation for fluid transport

All these above conservation equation can be outlined in one generalised transport equation.

$$\frac{\partial}{\partial t}(\rho\phi)+\frac{\partial}{\partial x_j}(\rho\phi v_j)=\frac{\partial}{\partial x_i}\left(\Omega_\phi\frac{\partial\phi}{\partial x_i}\right)+S_\phi \tag{3.5}$$

Where, Ω_ϕ is diffusivity for scalar variable ϕ. It is very tedious task to solve these equations. There are many other techniques are available which can be used to solve conservation equations. A brief review of these techniques is discussed in the following section.

3.4 Fluid dynamics with numerical techniques

Diverse numerical techniques are available to obtain algebraic equations but solutions to these equations are very complex. Thus, different types of approximations such as Moment averaging, vortex methods, spectral and direct numerical simulation have been suggested for solving these equations. Out of these four approximation methods moment averaging is widely used in simulating large scale industrial combustion problem. Major advantage of this method is that different commercial software programs such as PHOENICS, FLUENT, FLOW 3D, TEACH, PCGC-3 and GENMIX are easily available to solve combustion problems. In this method turbulent velocity components are reduced to average and fluctuating terms and solved with $k-\varepsilon$ closure equations. Mainly three numerical techniques are used to simulate turbulent flows. Finite difference, finite element and finite volume either of these is used to discretise the computational domain. Methodology by which the flow variables are approximated is the main difference between these three methods (Baukal et al., 2000).

In finite difference method nodes of grid co ordinate lines are used to describe the unknown variables. Based on Taylor series these co ordinates determine the number of algebraic equations (Smith, 1985). In finite elements methods the computational domain is divided into number of finite elements. Piecewise functions are applied to

show change in flow variables. In finite volume method computational domain is divided into small number of finite volumes. Then integration of mass, momentum and energy equations is performed over the all finite volumes. Then finite difference type approximations are substituted for the terms in the integrated equation. This results in to a series of algebraic equations which are finally solved iteratively. This technique is widely used in industry to solve combustion problems with semi implicit method for pressure linked equations approach under steady state assumption (Zienkiewicz and Tylor, 1991).

3.5 Turbulent flow modelling

Different turbulence models have been used to optimise flow field (mainly flow fluctuation) situation in any process including combustion modelling. But due to their limitations of each and every model is not useful for all processes. Here user will have to narrow down parameters requires for modelling. The literature available for all these turbulence models, user will have a clear idea about the model to be used for particular reactions.

Different Turbulence models:

- Spalart – Allmaras model or one equation model;
- $k-\varepsilon$ model;
- Wilcox $k-\omega$ model;
- Addon model;
- Reynolds stress model;
- Detached eddy simulation model;
- Large eddy simulation model.

Most flows encountered in engineering practice are turbulent. Characteristic properties of turbulent flow are, fluctuation of flow on a large range of length and time scale, diffusive behaviour due to increase in rate at which conserved quantities are stirred, time dependent, three dimensional and dissipative flow (Ferziger and Milovan, 1999). Generally all basic governing equations for homogeneous Newtonian fluid flow are based on set of partial differential equations which can not be solved numerically because of it laminar flow pattern. Consequently, turbulence

through mixing is key factor for efficient combustion (Kjäldman,1993).By using dimensional analysis, it is known that in order to capture all length scale, it requires computational mesh in high grid order Re 9/4 with time step in order of Re3/4 .Subsidiary relationships are required to provide the effects of turbulence on the transport processes. To overcome this problem idea of averaging Navier-Stocks equations were developed, which has known as Reynolds-averaged conservation equations (RANS). Since this method was mainly dependent on mean value of the turbulent flow thus additional turbulence model required (Warnatz et al., 1993).

Research showed that effect of turbulence can be modelled by dividing the direct properties ϕ (scalar variable) in conservation equations into mean $\bar{\phi}$ and fluctuating ϕ' components (Bird et al, 1960, Kjäldman, 1993, Warnatz, 1993, 2001).

Based on Reynolds decomposition theory,

$$\phi = \bar{\phi} + \phi' \tag{3.6}$$

Therefore $\phi' = 0$, when conserved scalar variable is averaged. Combustion processes are associated with density variation in huge amount. Thus, another averaging flow field method was introduced as Faver-averaging method which based on density weighted average concept. So time- average continuity equation can be written as,

$$\frac{\partial \rho}{\partial t} + \frac{\partial (\rho \mathbf{V}_i)}{\partial t} = S_i \tag{3.7}$$

Where, $\rho, \mathbf{V}_i$, and S_i are mean variable.

RANS can be written as,

$$\frac{\partial(\rho v_i)}{\partial t} + \frac{\partial}{\partial x_j}(\rho v_i v_j) = \frac{\partial}{\partial x_j}\left\{\mu\left(\frac{\partial v_i}{\partial x_j} + \frac{\partial v_j}{\partial x_i}\right) - \frac{2}{3}\mu\frac{\partial v_r}{\partial x_r}\right\} - \frac{\partial p}{\partial x_i} + \frac{\partial}{\partial x_j}\left(-\rho\overline{v_i' v_j'}\right) + S \tag{3.8}$$

Here, $-\rho\overline{v_i' v_j'}$ is Reynolds stress modelled from Boussinesq hypothesis shown in the following equation.

$$-\rho\overline{v_i' v_j'} = \mu_t\left(\frac{\partial v_i}{\partial x_j}+\frac{\partial v_j}{\partial x_i}\right)-\frac{2}{3}\left(\rho k+\mu_t\frac{\partial v_i}{\partial x_i}\right)\delta_{ij} \quad (3.9)$$

Where, μ_t is the turbulent viscosity, needs to be modelled.

Time- averaged transport equations incorporating mean variable ϕ eq. (3.9) can be written as

$$\frac{\partial(\rho\phi)}{\partial t}+\frac{\partial}{\partial x_i}(\rho\phi v_i)=\frac{\partial}{\partial x_i}\left(\Omega_\phi\frac{\partial\phi}{\partial x_i}\right)+\frac{\partial}{\partial x_i}\left(-\rho\overline{v_i'\phi'}\right)+S_\phi \quad (3.10)$$

$$-\rho\overline{v_i'\phi'}=\Omega_t\frac{\partial\phi}{\partial x_i}.$$

Here Ω_t is transport coefficient of turbulent for mean conserved scalar variable ϕ.

3.5.1 The standard $k-\varepsilon$ model

A form of $k-\varepsilon$ model was first proposed by Harlow and Nakayama; this was revised by launder and Spalding in 1972, 1974 as standard $k-\varepsilon$ model. According to them the standard $k-\varepsilon$ model is a semi-empirical model based on model transport equations for the turbulent kinetic energy (k) and its dissipation rate (ε). The model transport equation for k is derived from the exact equation, while the model transports equation for ε was obtained using physical reasoning. This model is applied to fully turbulent flow on assumption of negligible effects of molecular viscosity in flow and turbulence is assumed to be isotropic.

RANS were used as a platform to develop $k-\varepsilon$ model in further extension of time-averaged method.

As shown in eq. (3.9) for Boussinesq hypothesis

μ_t Is turbulent viscosity, which can be assumed as shown in following relation,

$\mu_t = A\rho VL$

Here various model constants depend upon process considerations and application of empirical methods. A is a dimensionless constant, L is turbulent length scale and V is the turbulent velocity scale.

Thus turbulent viscosity in the form of kinetic energy and dissipation rate shown as

$$\mu_t = A\rho\frac{k^2}{\varepsilon}$$

$$\frac{\partial}{\partial t}(\rho k)+\frac{\partial}{\partial x_i}(\rho v_i k)=\frac{\partial}{\partial x_j}\left[\left(\mu+\frac{\mu_t}{\sigma_k}\right)\frac{\partial k}{\partial x_j}\right]+G_k+G_b-\rho\varepsilon \tag{3.11}$$

And

$$\frac{\partial}{\partial t}(\rho\varepsilon)+\frac{\partial}{\partial x_i}(\rho v_i\varepsilon)=\frac{\partial}{\partial x_j}\left[\left(\mu+\frac{\mu_t}{\sigma_\varepsilon}\right)\frac{\partial\varepsilon}{\partial x_j}\right]+A_{1\varepsilon}\frac{\varepsilon}{k}(G_k+(1-A_{3\varepsilon})G_b)-A_{2\varepsilon}\rho\frac{\varepsilon^2}{k} \tag{3.12}$$

In these equation G_k represents the generation of turbulence kinetic energy due to mean velocity gradients. G_b Is the generation of turbulence kinetic energy due to buoyancy, can be described by the Prandtl number (Pr) for temperature and β , a thermal expansion coefficient.

3.5.2 RNG $k-\varepsilon$ Model

This model for turbulence is derived from the instantaneous Navier-Stokes equations, using a mathematical technique called “renormalization group methods”. It is similar to standard $k-\varepsilon$ model but differ in few ways such as it has an additional term of heat dissipation rate which is responsible for accurate strain flows and streamline curvature, swirling effect on turbulence for swirling flow, uses analytical equations for turbulent Prandtl numbers. This model is useful for analysing the effect of low Reynolds number with the help of viscosity calculated analytically (Fluent, 2003).

$$\frac{\partial}{\partial t}(\rho k)+\frac{\partial}{\partial x_i}(\rho k v_i)=\frac{\partial}{\partial x_i}\left(P_k\mu_{eff}\frac{\partial k}{\partial x_i}\right)+G_k+G_b-\rho\varepsilon \tag{3.13}$$

$$\frac{\partial}{\partial t}(\rho\varepsilon)+\frac{\partial}{\partial x_i}(\rho\varepsilon v_i)=\frac{\partial}{\partial x_i}\left(P_\varepsilon\mu_{eff}\frac{\partial\varepsilon}{\partial x_i}\right)+C_{1\varepsilon}\frac{\varepsilon}{k}(G_k+C_{3\varepsilon}G_b)-C_{2\varepsilon}\rho\varepsilon^2/k-R \tag{3.14}$$

Values for P_E and P_K = 1.393 for high Re number. G_k and G_b is same as $k-\varepsilon$ model.

$$R=\frac{C_\mu\rho\eta^3(1-\eta/\eta_0)}{1+\beta\eta^3}\frac{\varepsilon^2}{k} \tag{3.15}$$

Here, $\eta_0 = 4.38, \beta = 0.012$, also values for $C_{1\varepsilon}, C_{2\varepsilon}$ is 1.42 and 1.68 respectively and model constant for buoyancy term $C_{3\varepsilon} = \tanh\left[\frac{u}{v}\right]$. u and v both are velocity components.

The effective viscosity can be modelled by

$$d\left(\frac{\rho^2}{\sqrt{\varepsilon\mu}}\right) = 1.72\frac{\hat{u}}{\sqrt{\hat{u}^3} - 1 + C_u}d\hat{u}$$
$$\hat{u} = \frac{\mu_{eff}}{\mu}, C_u \approx 100 \tag{3.16}$$

As we can see that the only difference between standard and RNG $k-\varepsilon$ models equation is addition of few term like reciprocal effective Pr number P_E and P_K, and R term in the equation. This R term has significant effect in such a way that as a result in largely strained flow this model gives less turbulent viscosity then standard $k-\varepsilon$ model.

3.5.3 The $k-\varepsilon$ model via convective heat and mass transfer

Turbulent energy transport equation for convective heat and mass transfer is given by

$$\frac{\partial}{\partial t}(\rho\varepsilon) + \frac{\partial}{\partial x_i}(v_i(\rho E + p)) = \frac{\partial}{\partial x_i}\left(K_{eff}\frac{\partial T}{\partial x_i} + v_j(\tau_{ij})_{eff}\right) + S_h \tag{3.17}$$

Where, K_{eff} is the effective conductivity and E is the total energy.

The correlation between Effective Viscosity and Effective stress tensor is shown by following equation.

$$(\tau_{ij})_{eff} = \mu_{eff}\left(\frac{\partial v_j}{\partial x_i} + \frac{\partial v_i}{\partial x_i}\right) - \frac{2}{3}\mu_{eff}\frac{\partial v_i}{\partial x_i}\delta_{ij} \tag{3.18}$$

Relation between mass transfer and diffusivity, it can be shown by following equation.

Here D_{eff} is the effective diffusivity, m_i is the local mass fraction and R_i is the chemical rate of reaction by mass creation.

$$\frac{\partial}{\partial t}(\rho m_i) + \frac{\partial}{\partial x_i}(v_i \rho m_i) = -\frac{\partial}{\partial x_i}\left(D_{eff}\frac{\partial m_i}{\partial x_i}\right) + R_i + S_{h'} \tag{3.19}$$

3.6 Radiation models

Different five radiation models are available with FLUENT- such as

- Discrete Transfer Radiation Model;
- P-1 Radiation Model;
- Rosseland Radiation Model;
- Surface-to-Surface Radiation Model;
- Discrete Ordinates Radiation Model.

Radiation plays an important role in combustion processes to transport energy to surrounding surfaces in entrained flow particle. Two approaches were developed by researchers. First approach was based on predictions of radiative properties at microscopic level, while in second approach radiative interactions by means of adsorption, emission and scattering of radiant energy was focused. For steady state radiative heat transfer equation is given by following equation.

$$\frac{dI(s,\Omega)}{ds} + (a+\sigma_s)I(s,\Omega) = a\frac{\sigma T^4}{\pi} + \frac{\sigma_s}{4\pi}\int_0^{4\pi} I(s,\Omega)\Phi d\Omega \tag{3.20}$$

Where, s is a path length σ_s is the scattering coefficient, σ is the Stefan Boltzmann constant (5.672 X 10^{-8} W/m^{2}k^4), Φ is the phase function, and $(a+\sigma_s)$ is the optical thickness and T is a local temperature.

3.6.1 P-1 Radiation model

For combustion applications where the optical thickness is large, the P-1 model works reasonably well. The P-1 radiation model is actually the lowest order approximation of the more general P-N model. In the P-1 model, N is set equal to 1 as suggested by

the name of the model. For the P-1 model, the RTE is a diffusion equation, which requires less computational power (Fluent, 2007). In addition, available P-1 model can easily be applied to complicated furnace geometries with many coordinates. The P-1 radiation model considers the effects of scattering (Stockwell et al., 2001).

In radiative heat transfer approximation equation radiative intensity is formulated as a multiplication of angular and special functions which results in series different orders moments' equations and also deducts the integral part of RTE. This model does not consider small concentration of species produced in pf coal combustion which neglects the effects due to scattering. For this project uneven particle shape is assumed to determine the absorption coefficient and scattering for sub bituminous coal combustion. The main limitation of this model is that it does not go through sever calculation and does not give accurate results. A result in loss of accuracy also depends on the complexity of geometry. Basis equation for this model can be expressed as follows.

$$I(s,\theta,\phi)=\frac{1}{4\pi}\left(I'^{(0)}+3I'^{(1)}\cos\theta+3I'^{(2)}\sin\theta\cos\phi+3I'^{(3)}\sin\theta\sin\phi\right) \tag{3.21}$$

So, path length with intensity

$$I'^{(0)}(s)=\int_0^{4\pi} I'(s,\omega)d\omega \qquad \text{And} \qquad I'^{(i)}(s)=\int_{\omega=0}^{4\pi} l_i I'(s,\omega)d\omega$$

So relation between radiation flux q_r and I' can be reduce to

$$q_r=-\frac{1}{3(a+\sigma_s)-C\sigma_s}\nabla G \tag{3.22}$$

The transport equation for incident radiation G in form of σ Stefan-Boltzmann constant is shown as

$$\nabla\times(\Omega\nabla G)-aG+4a\sigma T^4=S$$

$$\Omega=\frac{1}{3(a+\sigma_s)-C\sigma_s} \quad ,$$

Here in both above equation C is phase function.

Therefore radiation flux q_r can be represented as

$$-\nabla \times q_r = aG - 4\sigma T^4 a$$

For scattering is assume due to particles, energy equations can be expressed as

$$-\nabla \times q_r = 4\pi\left(a\frac{\sigma T^4}{\pi} + E_p \right) + \left(a + a_p\right)G \qquad (3.23)$$

3.7 Combustion model

In any combustion when a high number of species are involved it becomes impossible to determine the reaction rate, to overcome this problem it is advisable to use combustion model which will solve the conservation scalar equation from which individual species concentrations are derived. This combustion model is called as PDF formula or mixture fraction formula (Stockwell et al., 2001).

Arrhenius rate equation and eddy dissipation approach are also available to solve the same combustion problem. Reaction rate can be calculated using these two approaches if we know the factor control the combustion process or species concentration fluctuates due to mixing of turbulent eddies which gives rise to a time averaged form. Therefore certain assumptions are made to simplify the model. These assumptions are correlates to both reaction time scale and turbulent mixing time scale. Simulation which offers both reactions and turbulent mixing time-scale at same level (Magnuseen and Hjertager, 1976) also incorporate eddy break up model have been developed for premixed combustion systems or laminar reaction systems or diffusion flames systems (Spalding, 1970).For this project third approach which is mixture fraction or PDF approach is considered.

In this both coal and oxidiser flows in two different stream and contacted intimately on molecular level before they enter into combustion zone. Thus, fast chemistry was assumed. In other word mixture fraction model is divided in two options and neither of those options emphasis on reaction mechanism. A first option is flame sheet where mass; momentum and energy balance is required, not useful for single step reaction. Hence, reactants never coexist. Reaction in this approximation is so fast that as reactant mix, they become burned. Another option is equilibrium assumption which predicts in between species concentration.

For a mixture fraction of variable f defined as follows

$$f = \frac{Z_k - Z_{ko}}{Z_{kF} - Z_{ko}}, \tag{3.24}$$

Where, Z_k is the mass fraction and subscript o and F denotes oxidiser and fuel inlet stream respectively.

Mixture fraction from time-averaged transport equation can be formulated as

$$\frac{\partial}{\partial t}\left(\rho \overline{f}\right) + \frac{\partial}{\partial x_i}\left(\rho v_i \overline{f}\right) = \frac{\partial}{\partial x_i}\left(\frac{\mu_t}{\sigma_t}\frac{\partial \overline{f}}{\partial x_i}\right) + S_m \tag{3.25}$$

If value of variable f is known, mixture fraction at any point in flow field can be found out using above equation. Thermodynamic properties of fluid are linked with mixture fraction. If value of variable is known other important properties can be known without going through individual transport equation. Jones and Whitelaw developed transport equation to show above theory correctly to end turbulence chemistry model.

$$\frac{\partial}{\partial t}\left(\rho \overline{f^2}\right) + \frac{\partial}{\partial x_i}\left(\rho v_i \overline{f^2}\right) = \frac{\partial}{\partial x_i}\left(\frac{\mu_t}{\sigma_t}\frac{\partial \overline{f^2}}{\partial x_i}\right) + C_g \mu_t \left(\frac{\partial \overline{f}}{\partial x_i}\right)^2 - C_d \rho \frac{\varepsilon}{k}\overline{f^2} \tag{3.26}$$

Where, $\overline{f^2}$ is mixture fraction variance, and C_g and C_d having values 2.86 and 2 respectively.

For Non adiabatic system thermodynamic property of fluid is function of mixture fraction and enthalpy. This leads to PDF approach to our discussion.

3.7.1 PDF approach

This mainly consists of two mathematical models.

The double delta function and the beta function. Out of these two beta functions is

$$\frac{dI(s,\omega)}{ds} = -(k+\sigma_s)I(s,\omega) + kI_b + \frac{\sigma_s}{4\pi}\int_{4\pi} I(s,\omega)\Phi d\omega \tag{3.25}$$

Where I is the radiative intensity, k and σ_s are local absorption and scattering coefficients respectively, Φ is phase function, ω represents gradient of intensity in the specified direction. Right hand side of equation shows change in intensity due to absorption and out scattering, emission and in scattering respectively (Eaton et al., 1999).

3.8 Discrete phase modelling

The deposition and erosion of furnace wall or tube material due to solid or air born particle impact are observed in two phase flow region in most of the power plant. In multiphase flow system, hydrodynamic behaviour can be analyse, once there is an exchange of mass, momentum and energy between particulate in confine gas- particle flow occurs. Here one phase is in conjunction with another phase, could be solid, liquid or gas. DPM is able to evaluate this inter exchange between solid-liquid, gas-solid or gas- liquid using two basic approach. Eulerian- Eulerian approach and Eulerian- Lagrangian approach.

In Eulerian- Eulerian approach both phases are treated as separate interpenetrating continua and are solved separately using separate boundary conditions. According to phasic volume fractions, volume fractions are assumed to be continuous functions of space and time. There are three different multiphase models available for this approach in fluent. Although it requires low computational time, this approach is not useful for any dilute phase. Difficulty with this frame is to predict the erosion, because it gives mean value of particulate over small control volume.

In Eulerian- Lagrangian approach gas phase is treated as continuum and discrete method for particulate phase as single particle. Velocity of particle, impact angle, density of particle, important particle properties can be obtained in Eulerian method. This approach is useful to model particle wall impaction. Basic assumption made that dispersed phase attains small volume fraction and particle trajectory for individual particle is possible at any time of simulation in flow domain. Lagrangian formulation yields a detailed physical behaviour of each particle, also it is based on FLUENT uses stochastic way, where mean velocity and particle concentration can be identify near wall surfaces from particle trajectory (Fluent, 2003).

3.9 Submodels used for combustion reaction

I would like to end this chapter by discussing different sub model available and used here for furnace simulation. Coal particle in pulverised coal or char in form of particle or droplet after combustion are linked with vaporisation, devolatilisation and char oxidation operations. For our coal combustion computation, devolatilisation and char oxidation operations are considered. Coal Devolatilisation is modelled with Arrhenius equations to determine the rate of reaction. Single rate reaction is considered due to first ordered combustion reaction. After this process remaining combustible fractions reacts with oxidiser on particle surface. Different heterogeneous surface reaction models are available with FLUENT. Kinetic/diffusion limited rate model is considered on assumption of equal value of oxidiser diffusion rate and char oxidation rate (Jones and Wille, 1996, Speziale, 1987).

Chapter 4

Modelling Approach

4.1 Introduction

In this day and age, the electricity generation from coal around the world accounts for the approximately 1/3rd of the total generation. At the same time, the environmental requirements for gas and particulate emissions are more and more restricted. In order to sustain the harmony between efficient and clean combustion, the development of clean combustion technologies to improve combustion efficiency is required. Coal fired power plants are usually of old technology or facilities and they are always in search of a technology which could enhance their efficiency without an additional cost. Generally, a research trend is to analyse the operation strategies that involve an efficiency improvement in pulverised coal power plant. But, this analysis requires detailed study and characterisation of some processes take place inside boiler, such as coal combustion, fluid flow, fly ash formation, wear etc.

Since 1970s, tremendous growth in computer world, it has become much easier to characterise various phenomena and has fasten the development of numerical flow, combustion and heat transfer modelling. With this advancement, simulation of the furnace of 330MWe is possible using computational fluid dynamics (CFD) codes. CFD modelling is capable of predicting qualitative and quantitative information, with sufficient accuracy to justify the change in design parameter of commercial boiler plant. Codes are used to solve physical model for gas flow, particle dynamics, particle combustion, gas phase mixing and combustion, and energy transport. It is known that CFD codes has certain limitations as well, despite of these it has undergone a series of progressive enhancement as the focus of application has shifted (Vuthaluru and Vuthaluru, 2006). Despite of the limitations, CFD has lightened up new areas which are difficult and sometimes not possible to visualise in experiments. In this chapter, furnace is simulated under different operating conditions and an attempt is made to identify the fluid flow pattern and its possible effect on different part of the furnace. Before that it is necessary to have brief information regarding furnace geometry which is used for our study.

4.2 Geometry description

This section will describe detail dimensions of the geometry and meshing technique adopted. The three dimensional opposite wall pulverised coal fired is considered in this study is 330 MWe unit, and is shown schematically in Fig. 4.1. This furnace geometry is created using GAMBIT – a FLUENT pre-processor. The height up to top wall of furnace is 42.53m; the horizontal cross section in the furnace has width of 14.4 m and depth of 10.9 m. The specification of furnace geometry is given in Table 4.1. In super heater section plates are incorporated instead of tubes in tube bundles. Tube bundles of reheater and economiser are not considered in this geometry.

Table 4.1 Furnace geometry specification

Parameter	Values (m) and m^2
Total travel path from burner to outlet	51.025
Distance between last burner row and hopper	2.215
Horizontal distance between burners	2.286 and 2.350
Vertical distance between burners	3.00
Surface area of inner burner	0.2826
Surface area of outer burner	0.5024

In order to make effective firing system within the furnace, 20 burners are arranged in series of 5 burners in one raw mounted at different level on front and rear wall of the furnace. Provision of extra 5 burners is made on front wall of furnace as standby. Single raw of burners on each side of the furnace wall are oil burners used as start up burner for initial furnace firing. To achieve qualitative results, all these burners are meshed with Quad Pav meshing scheme dividing each burner surface in to 20 nodes interval count. The swirl angle is not considered for the present study.

Moreover, geometry of furnace hinders its solution mainly because of variation in scale between burners and large volume of the domain (Vuthaluru and Vuthaluru, 2006). To overcome this problem tetrahedral unstructured mesh is used wherever needed. Coarse grid is used to mesh the complete geometry, which contained 384,522 elements with tetrahedral cell for all zones.

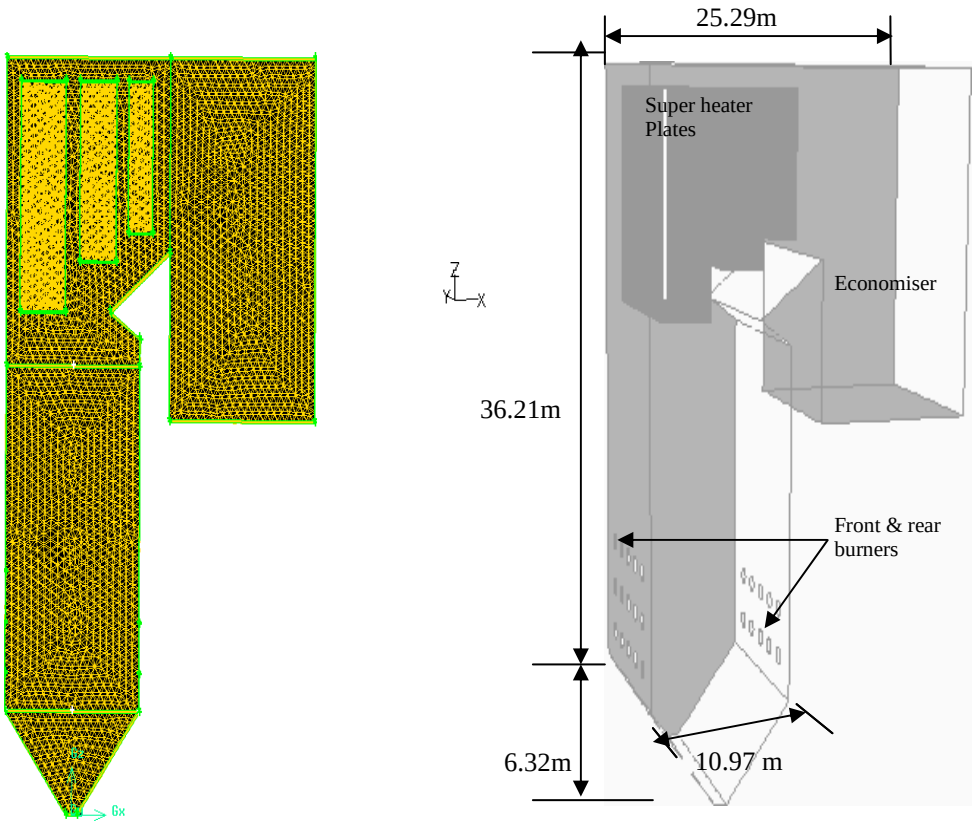

Fig 4.1 Schematics of (a) meshing scheme used and (b) dimensions of furnace

Once, the geometry is constructed, input data as boundary conditions for simulation is calculated using engineering equations. The main furnace operating condition considered in this project include five cases explain in detailed in section 4.4 in this chapter. Prior to basic input data calculations, it is necessary to determine the numerical simulation method and models selection out of different models explained in previous chapter 3. The following section will elaborate on simulation procedure and models adopted for furnace simulation.

4.3 Numerical Simulation Technique

- Gas Phase Model

The gas flow is described by the time mean conservation equations of global mass, momentum, enthalpy and species mass fractions. The gas phase conservation equation in three dimensions can be framed in the following form:

$$\frac{\partial(\rho u_j \phi)}{\partial x_j} = \frac{\partial}{\partial x_j}\left(\Gamma_\phi \frac{\partial \phi}{\partial x_j}\right) + S_\phi \tag{4.1}$$

Where ϕ, represents three momentum components, the turbulent kinetic energy k and its dissipation ε, the enthalpy and mass fraction of gas species (mixture fraction). Γ_ϕ, is the diffusion coefficient of the transported variable ϕ. For the particular case of the mass conservation equation, variable ϕ is set to unity and the right hand side of the equation is zero. S_ϕ, the generalized source term of which depends on the geometry, transport coefficients, and other dependent variables (M. Xu et al, 2001). Since the flow is turbulent, turbulent model must be coupled to the Navier stoke equation in order to overcome the turbulence problem. The standard $k-\varepsilon$ model proposed by (Launder and Spalding, 1972; Launder and Sharma, 1974) has been chosen with an assumption of negligible effects of molecular viscosity in flow and turbulence is assumed to be isotropic. It has been also validated for a large amount of industrial turbulent flow. Thus turbulent viscosity in the form of kinetic energy and dissipation rate shown as

$$\mu_t = A\rho \frac{k^2}{\varepsilon}$$

$$\frac{\partial}{\partial t}(\rho k) + \frac{\partial}{\partial x_i}(\rho v_i k) = \frac{\partial}{\partial x_j}\left[\left(\mu + \frac{\mu_t}{\sigma_k}\right)\frac{\partial k}{\partial x_j}\right] + G_k + G_b - \rho\varepsilon \tag{4.2}$$

$$\frac{\partial}{\partial t}(\rho\varepsilon) + \frac{\partial}{\partial x_i}(\rho v_i \varepsilon) = \frac{\partial}{\partial x_j}\left[\left(\mu + \frac{\mu_t}{\sigma_\varepsilon}\right)\frac{\partial \varepsilon}{\partial x_j}\right] + A_{1\varepsilon}\frac{\varepsilon}{k}(G_k + (1 - A_{3\varepsilon})G_b) - A_{2\varepsilon}\rho\frac{\varepsilon^2}{k} \tag{4.3}$$

In words the equations are

Rate of change of k or ε + Transport of k or ε by convection = Transport of k or ε by diffusion + Rate of production of k or ε - Rate of destruction of k or ε

In these equation G_k represents the generation of turbulence kinetic energy due to mean velocity gradients. G_b Is the generation of turbulence kinetic energy due to buoyancy, can be described by the Prandtl number (Pr) for temperature and β , a thermal expansion coefficient. The standard $k-\varepsilon$ model employs values for the constant that arrived at by comprehensive data fitting for a wide range of turbulent flows: A= 0.09, σ_k= 1.00, σ_ε= 1.30, $A_{1\varepsilon}$ = 1.44, $A_{2\varepsilon}$= 1.92 (Versteeg, 1995).

- Particle Phase Model

The heterogeneous nature of pulverised coal combustion and the relatively slow particle combustion rates require the particle trajectories are accurately modelled. In Lagrangian framework the particle field is represented as a series of trajectories through the gas continuum. The Lagrangian equations of continuity, momentum, and energy are used to calculate the particle properties and trajectories. Particle trajectories are tracked throughout the computational domain, and interactions between the particles and gas are incorporated by an exchange of source terms (particle source in cell method) for mass, momentum and energy. Particles are assumed to be composed of raw coal, char, ash, and moisture. In the Lagrangian treatment, formulated by Megdal and Agosta, the flights of statistically representative particles are tracked through the combustion chamber from entry to exit. There are three principal advantages weighing in favour of the Lagrangian and against the Eulerian treatment: particle slip in the fluid is very much more easily accounted for; the computer storage requirement does not increase with the number of particle-size groups, the drag, heat transfer, devolatilisation, and other laws which govern the particle behaviour are more readily and obviously applied (Lockwood et al. 1980).

The particle momentum equation can be written as;

$$m_p \frac{du_{pi}}{dt} = \frac{1}{2} C_D \rho \left(u_i - u_{pi}\right)^2 + m_p g_i \tag{4.4}$$

The drag coefficient C_D is a function of Reynolds number. m_p, is mass of particle, ρ is a particle density, u_i and u_{pi} are velocity component in i direction (Boyd, 1986).

However, here we are considering interaction between gas and solid phase, both Eulerian and Lagrangian approach has been adopted for this project.

Combustion of pulverised coal is modelled as a non premixed kinetics/diffusion-limited process with the mixture-fraction/probability density function (PDF) approach for the reaction chemistry. It is assumed that the PDF mixture consists of 13 volumetric species (Filkoski et.al, 2006). In the present study, a commercial finite-volume-based CFD solver Fluent is used to solve discretized equations. There are two advantageous features in finite-volume methods: physically, the conservation of mass, momentum, and energy is assured in the formulation itself and, numerically, unstructured grids and arbitrary geometries are accommodated without coordinate transformation (Chung, 2002,). Fluent applies an unstructured grid solver, which cannot exploit all the benefits related to grids of hexahedral cells (Saario and Oksamen, 2007). Furthermore, study shows that the mean mass fractions of fuel, oxidant and products are obtained from mean and variance of the mixture fraction, using an assumed form for the Pdf of the mixture fraction. Here, a beta function was assumed.

- Particle Combustion

The coal combustion model considers coal combustion as a two global step process. During the first step, considered as homogeneous, volatile gases escape from the coal particle, which is nothing but devolatilization and the combustion in the gaseous phase takes place, leading to the generation of the volatile combustion products. The second stage is considered heterogeneous because the combustion of the solid phase (char) occurs, giving off gaseous products of the heterogeneous combustion (Iranzo, 1985). The particle devolatilization is modelled by considering a pair of parallel, first

order reactions and rate constant is expressed in an Arrhenius form. Badzioch and Hawksley proposed expression for single kinetic rate model that assumes the rate of devolatilization is first order dependent on the amount of volatile remaining in the particle.

$$-\frac{dm_p}{dt} = k\left(m_p - (1 - f_{vo})m_{po}\right) \tag{4.5}$$

Here, m_p is the particle mass (kg), f_{vo} is fraction of volatile present in the particle, m_{po} is the initial particle mass (kg), k is the kinetic rate (s-1) defined by input of an Arrhenius type pre- exponential, A and activation energy

$$k = A_1 \exp(-E/RT) \tag{4.6}$$

In above equation A is a constant, E is activation energy, R is ideal gas constant and T is temperature (^oC) (Sahajwalla et al., 1997).

Char oxidation is a much slower process than devolatilisation, and determines the burnout time of pulverised coal in the furnace. The char oxidation is modelled as a global reaction of order unity. The reaction rate is calculated on the assumption that the process is limited by the diffusion of oxygen to the external surface of the char particle and char reactivity. When coal combustion is modelled, it is necessary to combine the combustion models with particle transport calculation. Thus, Lagrangian approach discussed earlier in this section has been adopted (Field MA et al., 1998).

Radiation heat transfer is computed by the simplified P-N model, based on the expansion of the radiation intensity into an orthogonal series of spherical harmonics, widely known as P-1 model. One of the important issues in the case of coal combustion modelling is the inclusion of the effect of discrete phase presence (coal and ash particle) on the radiation absorption coefficient. Moreover, the P-1 model has several advantages over other radiation models, treating the radiative transfer equation as a diffusion equation that is relatively easy to solve. It can be easily applied to complicated geometries. To model emissivity coefficient of combustion products, WSGGM (weighted-sum-grey gas) model is used. Detailed formulation is shown in previous chapter in section 3.6 (Filkoski et.al, 2006).

4.4 Overall Simulation Method

This section will explain simulation methodology and model chosen for coal combustion inside the furnace. The solving phase of the CFD simulation consists of the numerical solution of the governing equations. The work presented here implies the simulation of turbulent flow field, coal combustion, particle transport, and radiative heat transfer in the furnace. Numerical calculations are carried out using commercial CFD code FLUENT based non premixed combustion model available in it. The combustion simulation begins by solving the gas flow field equations assuming that the particle, energy and radiation equations are disable.

- The gas flow is modelled by solving the Navier- Stokes equations along the solution domain. The time averaged Navier-Stokes equations are solved using the SIMPLE – pressure velocity coupling algorithm to predict the flow, temperature, and concentration of gas species within the boiler.
- Since the flow is turbulent, a turbulence model, standard $k-\varepsilon$ model based on density and turbulent viscosity is coupled. Here, standard wall function option is considered.
- The simulation procedure is based on finite volume formulation. It is also assumed that the flow field is at unsteady state and the solution procedure is simplified by solving an unsteady state form of the equation of motion.
- Once converge solution is obtained for fully developed flow, Energy equations are active. Next step would be modelling of pulverised coal combustion with non-premixed kinetic-diffusion limited process with mixture fraction or PDF approach for reaction chemistry. Species and chemical reactions are modelled using PDF approach. The species composition in terms of atom fraction of C, H, N, O with specific heat capacity of the fuel are used as data available from local power plant. The fuel composition inputs are defined using proximate and ultimate analysis data shown in Table 4.2 and Table 4.3 respectively. PDF table for a pulverised coal fuel is prepared using pre-PDF pre-processor for medium volatile coal. The reacting system is treated using infinitely fast chemistry, chemical equilibrium calculations, or non equilibrium calculations. The chemical equilibrium is assumed in this study. Single kinetic rate model is used to derive elemental composition of the volatile stream. This model also suggests

that a volatile gas produced during reaction is given by a first order reaction and the rate constant is expressed in terms of Arrhenius equation form.

- Furthermore, the char combustion has to be modelled due to the fact that the two stage of combustion are considered. The char oxidation is much slower process than devolatilization and it therefore determine the burnout time of pulverised coal in the boiler (Iranzo, 1985). For this study kinetic / diffusion surface reaction rate model was applied for the modelling of the char combustion. However, it is assumed that surface rate reaction is determined either by kinetic or by a diffusion rate (Fluent, 1999). All physical properties of chemical species and equilibrium data are obtained from the chemical database. The particle emissivity, reflectivity, and anisotropic scattering are effectively included in the calculation (Bolsevic et al.2006,).
- One of the important issues in the case of coal combustion modelling is the inclusion of the effect of discrete phase coal and ash particles on the radiation absorption coefficient (bolsevic et al.2006). For our study WSGGM (weighted-sum-of-gray-gases-model) is used, which specifies a composition dependent absorption coefficient (Vuthaluru and Vuthaluru, 2006).
- When all criteria for coal combustion model are set, it is necessary to activate the radiation model using P-1 radiation model. The P-1 radiation model is simplest approximation of the P-N model, which is based on the expansion of the radiation intensity in to an orthogonal series of spherical harmonics.

Table 4.2 The Proximate analyses of coal (as received)

Proximate Analysis (% dry base)	Average value
Moisture	25
Ash	8
Volatiles	29.8
Fixed Carbon	37.7
Total Sulphur	0.7
Specific Energy (MJ/Kg) 19.6	

- Lastly, when we have prepared non- adiabatic PDF table, above mentioned radiation model and discrete phase model (DPM) are activated. Discrete phase

model is used to calculate particle transport equations. In this case, a Lagrangian approach has been adopted in combination with Eulerian approach. Using DPM injections of fixed number of particle stream is introduced to each burner as per their location point.

- Particle size distribution is assumed to fit Rosin-Rammler diameter distribution with spread parameter equal to 3.30. Trajectories formed by those injected particles are tracked throughout the computational domain.
- Spherical drag low is considered in discrete phase modelling with two – way coupling between particle and gas phase in turbulent flow field. Inter action between the particles and gas is incorporated by an exchange of source terms of mass, momentum and energy. The dispersion of particles due to gas turbulence is predicted using stochastic tracking model which includes the effect of instantaneous turbulent velocity fluctuations of the gas on the particle trajectories. Discrete random walk model is used as stochastic tracking model. Particles are assumed to be composed of raw coal, char, ash and moisture (Fan et al., 2001).
- Before we decide boundary condition and operating conditions, material type for PDF mixture is specified.
- Simulation of coal combustion can be controlled with adjusting under relaxation factors, plays an important role for convergence criteria.
- Gravitational force and default value for operating pressure is considered under operating condition section. After incorporating operating condition, boundary condition selection would be the last step before initialising simulation.

4.5 Boundary conditions

This section will describe the boundary conditions chosen for different cases considered in this study. The principal theory behind choosing the different cases is that the several experimental and computational studies have contributed to understand the role of mechanism of solid particles eroding the material surface of an individual tube. Although these studies are useful but research conducted so far suggests that it is too difficult to relate to full scale boiler. There is very little reported work in literature in which full scale boilers were simulated and the erosion distribution evaluated from the mean particulate velocity or from the impact angle.

The complexity of flow generated within a power utility boiler has compelled designers to make use of empirical information, often complemented by pilot plant experiments, in order to tackle problems associated with the erosion reduction. Such design practices are rather expensive, inefficient and often valid for restricted range of parameters. Thus, using trend analysis approach one can predict the detailed flow and particulate distributions under different operating conditions and could possibly enable to identify the location of maximum erosion wear and the consequences in or around those locations. Using different feed flow rate and different firing scenarios, optimization of boiler configurations to minimise erosion rate could then also proceed in a more cost effective way.

Therefore, once the problem was defined in terms of necessary equations, the establishment of the boundary conditions is required. Boundary conditions for present situations are inlets, wall and outlet. Boundary conditions will vary for four different cases explained in section 4.5. For inlet, primary and secondary air inlets are considered as velocity inlet. These velocities are calculated as a function of mass flow rate, density and inlet section area. Necessary calculations are shown below in this section below. Table 4.4 shows calculated air and coal flow rate for base case (full load) of 330MW furnace considered for study. Turbulent intensity of 3 % to 7 % is considered.

Hydraulic diameter is set equal to inlet diameter of the boiler. It is assumed, for the calculations, that the gas pulverised coal mixture temperature is 400 K and the secondary air temperature is 543 K.

Boundary condition calculations:

- Case 1: Full load (100%)

Fuel: Sub-bituminous coal

Calorific Value (CV): 5135 Kcal/kg

Type of Furnace: Pulverized coal fired furnace

Power generation (PG): 330 MW

Boiler efficiency (BE): 77 % = 0.77

Turbine efficiency (TE): 38% = 0.38

Excess air (EA): 20%

Primary air distribution: 30%, Secondary air distribution: 70%

Cross sectional area of inner burner (From General Arrangement (GA) drawing) =0.2826 m^2

Cross sectional of outer burner (From General Arrangement (GA) drawing) = 0.5024 m^2

Total Number of inner and outer burners in operation = 50

Calculations:

1. Coal flow rate calculations

$$\text{Coal Flow rate} = \frac{\text{PG (KW) / (hour) * 860 (Kcal / KW)}}{\text{CV (Kcal/kg) * BE (\%) * TE (\%) *3600 Sec/hr}} \quad (4.7)$$

$$= \frac{330 * 1000 * 860}{5135 * 0.77 * 0.38 * 3600}$$

$$= 52.47 \text{ kg/S}$$

2. Air flow rate calculations

For typical sub- bituminous coal, the air requirement as per stoichiometry comes out as 8 Kg per Kg of Coal. The calculations are as below:

Calculation for Requirement of Theoretical Amount of Air

Basis: 100 kg of sub-bituminous coal.

Table 4.3 The Ultimate analysis of sub bituminous coal

Ultimate analysis of sub-bituminous coal	Average (wt %)
Carbon	73.5
Hydrogen	4.8
Nitrogen	1.2
Sulphur	1.0
Oxygen	19.5

The exothermic chemical reactions are:

$C + O_2 \rightarrow CO_2$

$H_2 + ½ O_2 \rightarrow H_2O$

$S + O_2 \rightarrow SO_2$

Constituents of fuel

$C\ (12) + O_2\ (32) \rightarrow CO_2\ (44)$

12 kg of carbon requires 32 kg of oxygen to form 44 kg of carbon dioxide therefore 1 kg of carbon requires 32/12 kg i.e 2.67 kg of oxygen

$(73.5)\ C + (73.5 \times 2.67)\ O_2 \rightarrow (269.5)\ CO_2$

$H_2\ (2) + ½ O_2\ (16) \rightarrow H_2O\ (18)$

2 kg of hydrogen requires 16 kg of oxygen to form 18 kg of water, therefore 1 kg of hydrogen requires 16/2 kg i.e. 8 kg of oxygen

$(4.8)\ H_2 + (4.8 \times 8)\ O_2 \rightarrow (4.8 \times 9)\ H_2O$

$S\ (32) + O_2\ (32) \rightarrow SO_2\ (64)$

32 kg of sulphur requires 32 kg of oxygen to form 64 kg of sulphur dioxide, therefore 1 kg of sulphur requires 32/32 kg i.e 1 kg of oxygen

(1) $S + (1 \times 1) O_2 \rightarrow (2 \times 1) SO_2$

Total Oxygen required = 235.65 kg

(196.25+38.4+1)

Oxygen already present in 100 kg fuel (given) = 19.5 kg

Additional Oxygen Required = 235.65 – 19.5 = 216.15 kg

Therefore quantity of dry air required = (216.15) / 0.23

(air contains 23% oxygen by wt.)

= 939.76 kg of air

Theoretical Air required = (939.76) / 100

= 9.40 kg of air / kg of fuel

=@ 8 kg of air / kg of fuel

(As the ultimate analysis of the fuel was varying at the plant site, it was recommended by plant operator to take 8 kg of air / kg of fuel for further calculations.)

Excess air was considered 20% for the pulverised coal firing furnace.

Therefore, Total air required = 8 kg of air / kg of coal * 52.47 kg of coal / Sec * 1.2

= 503.70 kg of air / kg of coal

As per plant practice, 30% of the total air was supplied as primary air and rest 70% as secondary air.

Therefore, Primary air flow rate (from inner burner) = 503.62 * 0.3 = 151.11 kg/s

Secondary air flow rate (from outer burner) = 503.62 * 0.7 = 352.59 kg/s

3. Air velocity calculations (Boundary condition for Fluent)

Flow rate (m^3/s) = cross sectional area (m^2) * velocity (m/s)

Therefore, Primary air velocity (m/s) (through each burner)

= Flow rate (m^3/s)/(cross sectional area of burner(m^2) *Total number of running burners)

(Density of air = 1.2 kg / m^3)

Primary air velocity (m/s) = (151.11 / 1.2) / (0.2826 * 25) = 17.82 = @18 m/s

Secondary air velocity (m/s) = (352.59 / 1.2) / (0.5024 * 25) = 23.29 = @ 23 m/s

4. Coal injection value (Boundary condition for Fluent)

Total number of inner burners in operation from which coal will be injected = 25

Coal injection from each burner = 52.47/25 = 2.10 kg/s

From the above calculations, the boundary conditions applied for base case is as follows:

Table 4.4 Boundary conditions of Base Case for 330MWe furnace

Parameter	Values
Total primary air flow rate (kg /s)	151
Total secondary air flow rate (kg/s)	352
Coal feed rate from each burner (Kg/s)	2
Primary air velocity (m/s)	18
Secondary air velocity (m/S)	23
Total number of burners (inner + outer)	50

A pressure out flow is considered as outlet condition with 1300 K back flow temperature. Wall temperature and emissivity value of 0.5 to 1 for different walls are considered as wall boundary conditions. Boundary conditions for three other cases are shown in Table 4.5, Table 4.6, and Table 4.7. Detail calculations are shown in Appendix G.

Table 4.5 Boundary conditions for case 2 (excess air -20%)

Parameter	Values
Number of active burners (inner + outer)	40
Total primary air flow rate	121 (kg/sec)
Total secondary air flow rate	282 (kg/sec)
Total coal flow rate	42 (kg/sec)

Table 4.6 Boundary conditions for case 3 (excess air -20%)

Parameter	Values
Number of active burners (inner + outer)	30
Total primary air flow rate	91 (kg/sec)
Total secondary air flow rate	212 (kg/sec)
Total coal flow rate	31 (kg/sec)

Table 4.7 Boundary conditions for case 4 (excess air -30%)

Parameter	Values
Number of active burners (inner + outer)	50
Total primary air flow rate	174 (kg/sec)
Total secondary air flow rate	411 (kg/sec)
Total coal flow rate	50 (kg/sec)

4.6 Calculated cases

This section will describe operating conditions of burners considered for this project. Purpose of this study is to investigate characteristics of fluid flow pattern and behaviour of different parameter such as fluid velocity, particle trajectories temperature etc. inside solution domain under different firing pattern. Table 4.8 shows operating condition of burners for four diverse cases. These cases cover different set up of the burners and fuel load in accordance with different operating range. In this table “NA” indicates that burners which are not in service during operation while, “A” indicates that burners which are in service during combustion process. For case 1 all five rows of burners are in service and furnace is operated in full load conditions. Input data of total air and fuel consumption for this case is calculated using empirical equations as shown in detail in section 4.5.

In case 2, burner number 11 to 15 are not in service and can be considered that furnace is operated on 80 % fuel load. For case 3 burner number 11 to 15 and 21 to 25 are not in service. That means only three rows of burners are in service out of five and can be said that furnace is operated on 60% fuel load. All these cases are considered with 20 % excess air to achieve complete combustion inside the furnace using different firing pattern.

Table 4.8 Operating conditions of burners for different cases

Burner Number	Case 1 Full load (base case) (3-2 firing)	Case 2 2-2 firing	Case 3 2-1 firing	Case 4 Full load with (excess air 30%)
1 to 5	A	A	A	A
6 to 10	A	A	A	A
11-15	A	N/A	N.A	A
16 to 20	A	A	A	A
21 to 25	A	A	N/A	A

A= Burners are in service, N/A= Burners are not in service.

Moreover, in this project author has tried to investigate diverse case scenario by considering 30% excess air as case 4 for the pulverised coal firing furnace. It is true that 15-20% excess air is realistic operating condition in the case of pulverized coal (Turner WC et al., 2006, Devendra C, 2005). Higher the excess air lower will be the overall efficiency of the furnace due to higher stack gas flow rate. However, the advantage of higher excess air is that it can reduce CO_2 and CO percentages well below the standard limits. Thus, it can lead to complete combustion (Devendra, C, 2005). Even in the case of the higher moisture, higher excess air is recommended (N Magasiner et al.,). Moreover, as per new practice, partly (15-20%) flue gas

recirculation in the pulverizer has been put in the practice to get higher efficiency of the pulverizer (Bhattacharya C. et al., 2007).

Despite of the standard 15-20% excess air limit, looking to the increased price of the raw coal and pulverizing, some industries have been experimenting 30% excess air in the case of pulverized coal (Arand JK. et al., 1985, Rodrigues et al., 2005). Also, it was suggested by industrial personal to carry out simulation considering higher excess air than ideal to analyse boilers efficiency and its operation. That was the reason that this case was studied at 30% excess air. However, it is just a scenario modelling.

Results regarding simulation of all these cases mentioned below are shown and discussed in the following chapter five results and discussion.

However, calculated values of input data shown in boundary condition are used to run simulation for the given furnace. Results obtained from simulations are used to do parametric study and are combine with erosion model developed be Mbabazi and colleague to calculate erosion rate for the given furnace condition. Selection of this model is based on coal chemistry criteria and its operating conditions used for experimental study. They have considered different impact angle and various impact velocities to calculate erosion rate for the given specimen. These two parameters are of our main concern out of all other parameter responsible to cause wear effect. Next section describes analytical model developed by Mbabazi et al for their study.

4.7 Erosion Model: - (adopted from Mbabazi et al,. 2001)

In a high speed system when solid particle strike the metal surface, it removes or damage the surface material layer by layer. This process can be termed as erosion or abrasive wear of that target material. The extent of abrasive wear is generally calibrated as mass or volume removed by striking solid particle. Cutting wear and plastic deformation are two type of action by which material is removed. Finnie and McFadden (1978) carried out experiments to analyse the behaviour of particles which are at low velocities and at undesirable angle. Results showed that the material removed by these particles is negligible, while particles at an acute angle and velocity higher than critical do remove material in similar fashion as a cutting action. Bitter mentioned that when particle impacts on a flat surface at an acute angle, the material

is accounted for shear over an area same as vertical cross section of part of particle which has impacted onto the surface. When shear strain exceeds, destruction starts. This is known as cutting action.During the cutting action, stresses acting at the contact surface are constant. Thus, impacting particle should exert sufficient amount of energy to overcome the deformation resistance of material. Kragelsky et al. developed the equation of motion for impacting particle with mass m_p and diameter of d_P is showed below.

$m_P \frac{d^2h}{dt^2} = -\pi \frac{dp}{2} hc\sigma_y$ Where t is the time, σ_y the yield stress of the target material, and c is equal to 3, a shape factor for sphere.

When particle strikes a target surface at an angle of impact β, and impacting velocity V, normal component of velocity is equal to initial rate at which particle strike the surface.

For t = 0, depth of penetration is equal to the $V \sin\beta$ (normal component of velocity). Integrating equation, the following equation is obtained.

$$\frac{dh}{dt} = \pm\sqrt{V^2 \sin^2\beta - \frac{9\sigma_y h^2}{\rho_p {d_p}^2}} \tag{4.8}$$

For maximum depth of penetration,

$$h^3{}_{\max} = \frac{{d_p}^3}{9} V^3 \sin^3\beta \left(\frac{\rho_p}{\sigma_y}\right)^{\frac{3}{2}} \tag{4.9}$$

Volume of the material removed away from the material is proportional to $h^3{}_{\max}$, thus mass of the material removed by single particle will be proportional to the value of maximum height. Therefore mass using eq. (4.9) is given by

$$m = K_c \rho_m h_{\max}{}^3 = \frac{K_c \rho_m \rho^{\frac{3}{2}}{}_p d^3{}_p V^3 \sin^3\beta}{9\sigma^{\frac{3}{2}}{}_y} \tag{4.10}$$

Where, K_c is a constant and ρ_m is the density of the erodent material. Cutting action is defined as ratio of mass of the material and mass of impacting particle. Thus erosion due to cutting mechanism is given by the following relation.

$$\varepsilon_c = \frac{m}{m_p} = \frac{K_1 \rho_m \rho_p^{\frac{1}{2}} V^3 \sin^3 \beta}{\sigma_y^{\frac{3}{2}}} \tag{4.11}$$

Where K_1 is a constant

When particle strikes the target surface, removal of material takes place by the joint extrusion- forging process. Platelets are extruded from shallow craters made by the impacting particle. These platelets are then hammered into strained condition, in which they can be easily removed from the surface. This is known as plastic deformation. During plastic deformation, normal component of particles' kinetic energy is used. This is given by the following equation,

$$E_1 = \frac{1}{2} \frac{\pi d_p^{\ 3}}{6} \rho_p V^2 \sin^2 \beta \tag{4.12}$$

Where $d_p and \rho_p$ are the particle diameter and particle density respectively. Sheldon and Kanhere showed relation between force and diameter of the crater formed in the target surface.

Thus work done by the normal force is given by,

$$E_2 = \frac{\pi H_v}{4} \int_0^{h_{\max}} \delta^2 dh \tag{4.13}$$

Where, H_v is the Vickers hardness number for steel

Comparing E_1 and E_2 maximum depth of penetration from eq. (4.12) and eq. (4.13) is given by

$$h^3_{\max} = \frac{d^3_p V^3 \sin^3 \beta \rho_p^{\frac{3}{2}}}{H_v^{\frac{3}{2}}} \tag{4.14}$$

Since crater formed is of same dimension to that of the maximum height, and mass of the material removed is proportional to maximum height given by the following expression. Using eq. (4.14)

$$m = K_p \rho_m \rho_p^{\frac{1}{2}} \frac{d^3{}_p V^3 \sin^3 \beta}{H_v^{\frac{3}{2}}} \tag{4.15}$$

Where, K_p is a constant

The erosion rate due to plastic deformation using eq. (4.15) is given by,

$$\varepsilon_p = \frac{m}{m_p} = \frac{K_2 \rho_m \rho^{\frac{1}{2}}{}_p V^3 \sin^3 \beta}{H_v^{\frac{3}{2}}} \tag{4.16}$$

Relation between Vickers hardness and yield stress of material is given by Tabor.

$$H_v = 2.7\sigma_y \tag{4.17}$$

Using relation shown in eq. (4.17) the overall erosion rate considering both mechanisms using eq. (4.11) and eq. (4.16) is given by the following equation,

$$\varepsilon = \frac{K_e I_e(x) \rho_m \rho_p^{\frac{1}{2}} V^3 \sin^3 \beta}{\sigma_y^{\frac{3}{2}}} \tag{4.18}$$

Where, is $K_e and I_e$ a constant and erosion index (as shown in Table A.2 in Appendix A) of the ash respectively and x is mass fraction of silica contained in an ash sample.

I_e = 3.5 x $^{4.95}$

Thus equation (4.18) for overall erosion rate is given by

$$\varepsilon = \frac{K(x)^{4.95} \rho_m \rho_p^{\frac{1}{2}} V^3 \sin^3 \beta}{\sigma_y^{\frac{3}{2}}} \tag{4.19}$$

K is the overall erosion constant

An empirical eq. (4.19) for overall erosion rate considering both erosion mechanism used by Mbabazi and colleagues, has been adopted for this work. This equation includes all major parameters which are responsible for metal erosion process including yield stress for steel.

Chapter 5

Results and Discussion

This section will explain parametric study carried out from simulation using simulation technique mentioned in previous chapter. This study includes the effect of temperature distributions, flue gas flow, an impact angle effect and particle trajectories for described combustion process. Thus, as discussed in previous chapter, four cases including full load case have been calculated for the analysis of physical processes inside the coal fired boiler to classify the most susceptible area or faces of the furnace, which may be under the influence of mechanical wear. Therefore, to evaluate, number of horizontal as well as diagonal cross sections of furnace at different height is considered. Figure 5.1 shows the different cross sections considered for post processing analysis. Plane Y_1 is a Vertical cross (width wise) section used to show temperature distribution, velocity distribution for all cases. Plane x_1 is Located at furnace exit or at cross over path, shows temperature distribution at furnace exit for all cases. Plane Z_1 is a horizontal cross section at Z_1= 8.301mt in burner zone (last burner row) to show velocity as well as temperature distributions for different case scenario. Similarly, Plane Z_2 and Plane Z_3 are horizontal cross section at Z_2=11.4314 mt and at Z_3= 14.315mt in burner zone, second burner row and top burner row respectively, used for the same. Likewise, Plane Z_4 at Z_4= 29.033mt, lower part of nose section, Plane Z_5 at tip of nose section (beginning of super heater zone) and Plane Z_6 at Z_6= 37.246mt in between super heater section and at the end of nose section are all horizontal cross sections considered for flow pattern analysis and temperature distributions in upper furnace region. Plane XZ is an inclined plane considered along the inclined nose surface to observe the activity around the nose section. Lastly, Plane X_1, X_2, X_3, X_4 all are vertical planes considered along the height of the furnace to have an idea regarding the vector directions towards the plates as well as wall surface. Moreover, author has mentioned various reference planes throughout results and discussion section to explain observation made during post processing. The required calculations have been performed on a Microsoft Windows2003 platform. The post processing tools of the FLUENT 6.3.26 with Intel Core 2 Duo 2.3 GHz processor, 2GB RAM with 300GB storage capacity.

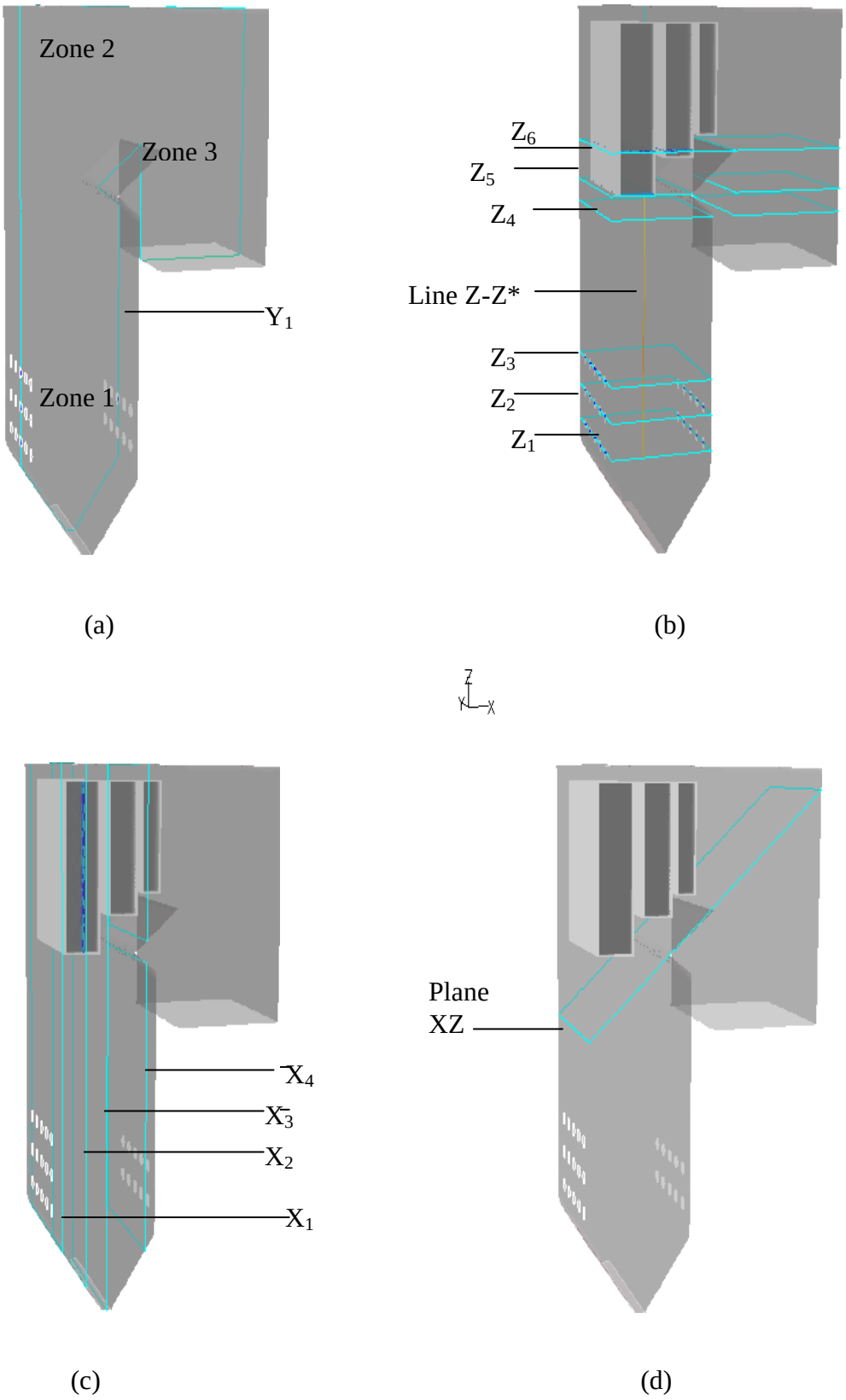

Figure 5.1 Reference cross sections used for post processing study and result analysis

5.1 Temperature distributions

This section will discuss effect of temperature and analysis made mainly on the basis of full load case. All twenty five burners were in service during full load operation. The temperature distributions for case 1(full load) along the cross sections Z_1, Z_2, Z_3, x_1 and Y_1 in accordance with Figure 5.2 is shown below. Initially general observations are made from the analysis of the temperature distribution, and then each case is compared. The temperature distribution for each case is shown at a chosen vertical plane (along the furnace height) Y_1= 7.239 m from the furnace wall. A temperature distribution for all other cases along the cross section Y_1 is shown in FigureB.1 in Appendix B. Similarly, horizontal cross sections in burner zones are considered for all cases at different height to show temperature distributions inside the furnace. For base case, maximum temperature is observed in the centre of the furnace in burner zone (zone1), where combustion takes place. Then temperature decreases gradually as it move toward upper furnace region. This decrease in flue gas temperature is mainly due to heat exchange between wall and flue gas. The maximum temperature is about 1890 K near the burner region, which ensures the non slagging furnace operation (Vuthaluru and Vuthaluru, 2006). A good mixing of the combustion air and pulverised coal seems to be appropriate in the burner region. It can be seen that flame has a proper length but due to flow from the top burner row it inclines slightly towards opposite burner wall.

Moreover, the amount of the combustion air and fuel supplied ratio has a huge influence on the temperature distribution inside the combustion chamber. This is clearly observed in the Figure 5.2 (a) that the peak temperature is around 1890 K near the burner region. This hot region in burner zone occurs may be due to rapid devolatilisation or inadequate particle radiation losses (Boyd and Kent, 2006). Therefore, maximum temperature range in burner and radiation zone determines the criteria for material of construction of different parts of furnace. Finally, temperature then gradually decreases as it approaches the super heater platen region. Mean temperature of 1420 K is observed inside the solution domain. Moreover, at the furnace exit or at the cross over path (plane x_1) nearly flat profile for temperature is observed. Temperature distribution along cross over path is shown in Figure 5.3. The

average temperature at the furnace exit is about 1039 K. This predicted value shows a decent agreement with the available literature as shown in Table 5.1.

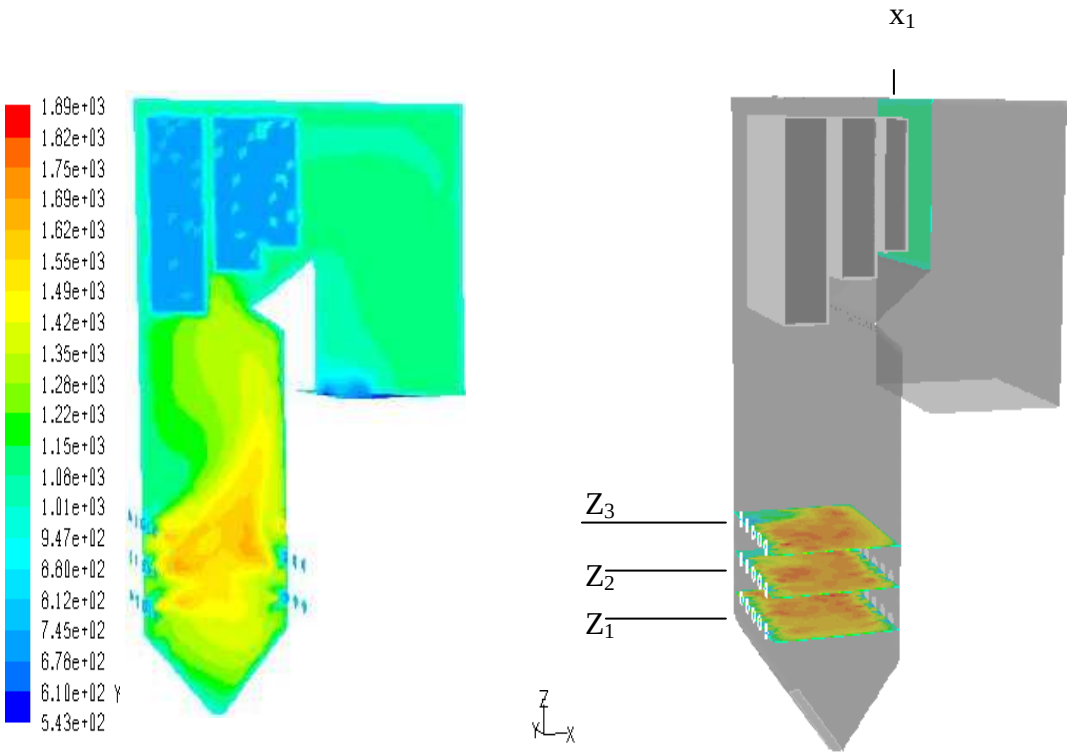

(a) (b)

Figure 5.2 (a) Temperature distributions along cross section Y_1, (b) Temperature distributions in burner zone along cross section Z_1, Z_2, Z_3 and along cross section x_1.

However, in the thesis, average temperature value along the furnace exit (plane x_1) is provided for comparison and not the specific value. Prediction of specific temperature value is very hard through simulation. Besides, due to lack of plant data availability it is not possible to compare the temperature range obtained from simulation with real plant data. Thus, simulation results are compared with literature data obtained from the furnace which were designed to produce electricity of 350 MWe. Rear part or furnace without economiser is considered for their study with same height and nearly same depth of the furnace similar to the current model reported by the author. Similar numerical techniques are adopted for both these models. Similar coal particle density is considered for both models. Although there are certain discrepancies the

comparison shown in the thesis is satisfactory. Besides, a different firing technique is considered in literature apart from what author has considered for current model (Belosevic et al., 2008). Temperature distribution for case 2, case 3 and case 4 is shown in Figure B.1 (b), Figure B.1(c) and Figure B.1 (d) in Appendix B respectively.

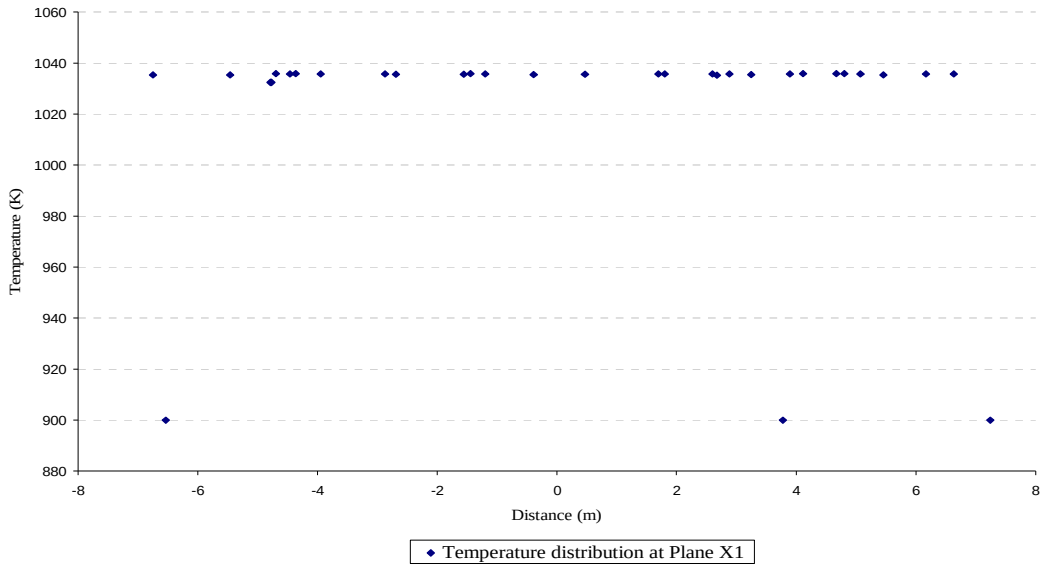

Figure 5.3 Temperature distributions along cross over path / furnace exit for case 1(full load) (fig.5.2 (b))

In case 2 twenty burners (except burner no 11-15) mounted at the same level on opposite walls are in service. It is observed that temperature is equally distributed along the vertical plane and influence of top row burners is absent. The peak temperature near burner region for this case is about 1830 K , which is 60 K less then temperature observed in case 1. Temperature at the cross over path has a similar pattern as analysed in case 1. The average value of temperature 1033 K is observed at the cross over path. The amount of air supplied is lower for this case as compared to case 1. This leads to low temperature profile inside the furnace. Temperature distribution on furnace exit is plotted along x_1 plane as shown in the Figure B.2 in Appendix B.

For case 3, only fifteen burners were in service. A short flame is observed which can cause instability of combustion. It is observed that flame is inclined towards the furnace wall and gradually approach the superheater plates. The highest temperature for this case observed is about 1810 K, less then case 1 and case 2. Figure B.1(c) is

shown in Appendix B for reference. The average value of temperature at the cross over path is about 1021 K, as shown in Figure B.3 in Appendix B.

Table 5.1 Literature value and obtained average value of temperature distribution at the furnace exit for different cases

Temperature (K)	Case 1	Case 2	Case 3	Case4(excess air)
Obtained value*	1039	1033	1021	1009
Literature value	1294	-	-	1263

* Average value considered along the furnace exit (plane x_1) (fig.5.2 (b))

For case 4 where excess air is supplied with increased flow rate of air as compared to case 2 and case 3. Here, all burners were active for combustion process. It is important to notice that temperature has peak value in burner region but reduces as it moves in super heater region. This downturn in temperature is due to additional cooling of flue gas provided by higher flow rate of excess air. It is also observed that temperature at cross over path reduces and has a low value of approximately 1009 K as compared to other cases. Apart from temperature there are other equal responsible factors as well, causing erosion in coal fired boiler are described in the following section.

5.2 Particle trajectories

Particle tracks provide another view on the situation inside the boiler. This exercise will help to quantify the residence time of different streams, which could be one of the important factor for our study. Therefore, during post processing, trajectories of fixed number of particles from selected burners of each row are closely analysed. It was observed that these particle streams strike the furnace wall more repetitively in particular area. In quite a few locations trajectories shows increased activity in different zones such as along nose section surface, top wall surface of the furnace, and in platen region. Moreover, literature also shows that tube failures occurring in coal-fired boilers are the results of erosion wear caused by frequent impaction of ash particles. In addition, particle impacting on metal surface gives rise

to surface layer deformation of furnace wall or tube wall due to repeated collisions (Raask, 1969). However, computational study does not provide the information regarding particle shape but velocity vector direction, impact angle and velocity magnitude which provides the necessary platform to predict the erosive wear for any particular zone. Therefore, on the basis of all these explanations the probable areas are assumed to be under the influence of erosion wear. Thus, detailed analysis of randomly selected burners from each row for each case is carried out to know the behaviour of each stream inside the furnace during combustion process. To do so, stream of fixed number of particles are released from selected burners, are shown in Figure 5.4 for case 1.

For case 1, it is evident that the particles from lower burners initially move in hopper section and eventually travel up in high temperature zone. However, particle stream spend less time in burner zone whereas, spend more time in super heater and economiser section before it leaves the furnace. This indicates that complete combustion of carbon is ensured prior to its exit the furnace (Vuthaluru and Vuthaluru, 2006). During the post processing it was visualised that stream from lower burner row impact on front or opposite furnace wall. This could result in damaging the wall surface and lead to wear effect in this particular area. Furthermore, an upward motion of stream was observed in radiation zone but more vigorous flow was noticed in platen heater regime which could lead to repetitive collision of particles or particle-wall collision. A probability of denting or scratching in this area could be very high too.

Trajectories from second burner row would be affected due to the flow from the above and opposite burners. Thus, this would disturb flow field and vary residence time of the particles, lead to uneven proportion of unburnt carbon inside the furnace. Moreover, time for any char particle for the nearly complete combustion usually lasts from several milliseconds to five seconds in the furnace. Particle residence time inside the furnace may vary due to several obstructions on its way to chimney (i.e. particle-particle, particle-furnace wall, particle-tube wall collisions etc.). In the present study with Fluent, particle residence time obtained by resolving particle trajectories using the continuity equation of mass, momentum and energy are estimated to be in the range of 14-21 seconds.

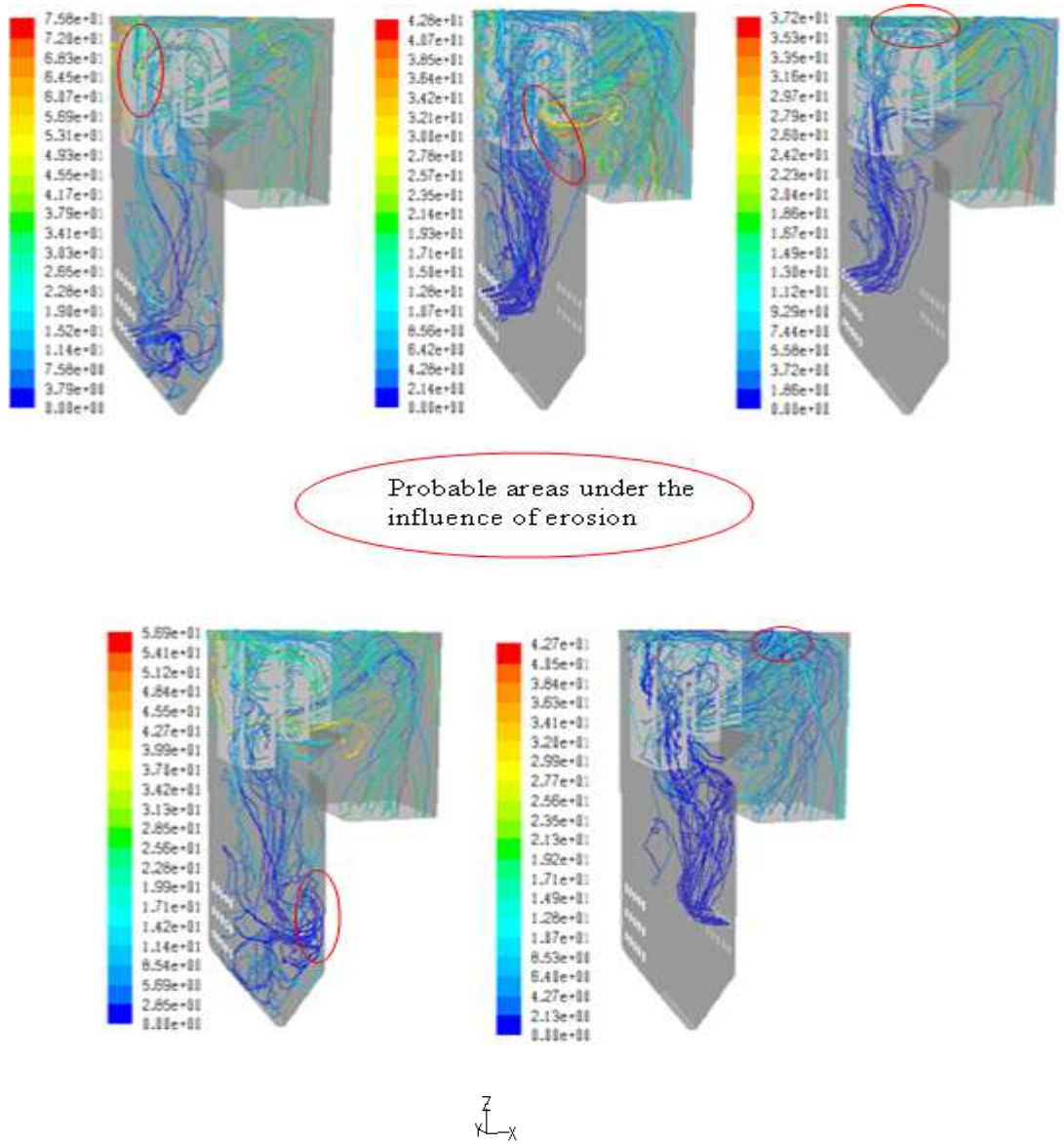

Figure 5.4 Particle trajectories selected burner from row of burners for Case 1

Some of the literature with CFD exercise also shows that particle stream has average residence time of 22 sec to exit the furnace (Choi and Kim, 2009). Model considered from the literature has tangential firing pattern without any plates or heat exchanger in super heater section and has nearly same outer geometry as of our study case. Also, widely reported studies on coal fired furnace do not consider nose section in their furnace design even though the residence time comes about 20-22 sec in 300 MW capacity furnaces(Choi and Kim, 2009). In current model, opposite wall firing technique is used for this study. In super heater section plates with narrow gaps and nose section in radiation zone are created to match real plant furnace design. Due to

increased impaction of the char particles inside the furnace, particle will reside in the furnace even after combustion for a quite considerable time.

For case 2, trajectories are shown in Figure C.1 in Appendix C different burners are selected for study purpose. A strong recirculation flow is observed in the bottom ash zone. It is necessary to take into account that the particles in area, where it is possible to reach the melting temperature, they sometimes do not fully burn out and hit the wall, which could cause mechanical damage to that surface. It is observed that particle from the second burner row spend high amount of time inside the domain, especially in super heater region and after cross over path. It is also seen in post processing that particle stream circulates and strike the furnace wall very frequently. Top surface of the furnace and surface of platen heater could be affected and may be under the influence of abrasive wear. Here, for this case the average residence time of the flue gas approximately 18 seconds is noticed.

A complete opposite behaviour is observed in case 3. It shows very strong circulation in burner zone as well as in the region of platen heater. It is also observed that particle has high residence time and more active movement in radiation zone as shown in Figure C.2 in Appendix C. It is interesting to observe that particle strikes the opposite wall as soon as they released from the burners as shown in Figure C.2(c) in Appendix C. less active flow is observed near nose region and it may have less effect in that region. An average residence time for case 3 is approximately 23 seconds which shows sufficient time for char conversion.

In case 4 where excess amount of air is supplied trajectories has different behaviour as compared to case 1. It is observed that flue gas flow from second and third rows of burner moves directly in upward direction and travel around plates in super heater zones. It has moderate residence time as compared to case 2 and case 3 where air and fuel supplied ratio is less. Upward movement of trajectories also shows that it might hit the plate wall in vertical direction, which would not ripple but would have deforming effect in those regions. Trajectories from another two burner row on opposite wall shows same flow pattern and have average residence time of approximately 17 to 19 seconds.

In general, for all cases particle stream spend few seconds in burner zone and radiation zone. But it shows more time in upper furnace region and area after cross over path. Table 5.2 shows common observation made from particle trajectories during post processing.

Table 5.2 Summary of observation made for particle trajectories during post processing

Zone	Common observations	Causes
Radiation Zone	Trajectories from all burners show upward movement except few. It inclines toward opposite wall as soon as it released from the burners. During particle tracking it was observed that some of the trajectories hit the opposite wall and side furnace wall repetitively. Due to repeat collision of particle and wall that particular wall surface area may be eroded by the particle impact at certain angle. There could be a formation of crater effect in that particular area.	Repetitive collision between particle and wall or particle- particle, weaken the material integrity or weaken the structural bond of material. This leads to failure of material in high temperature zone.
Convection Zone	Strongly active uneven flow field is observed in superheater plate section. Flow stream enters the heater area at different angle. Due to high gas stream velocity and due to high particle concentration plate surface is most likely to suffer a mechanical damage. This may leads to rapture of metal from that particular surface area.	It reduces the heat transfer efficiency. Due to solid Ash particle impact at various angles can cause circumferential erosion on the tube surface. This also increase the maintenance and unwanted shut down of the plant.
Economiser Zone	Gas flow with less velocity is noticed after cross over Path. This may be due to flow is been restricted by plates in super heater section. Walls of furnace suffer erosive wear due to stream flow through gap between plates and furnace side walls. Stream flow through narrow gap impact directly on the front wall and little down to the exit.	In this section due to solid gas particle velocity wall surface would be plastically deformed as stream flowing down along the surface reduce operational service life.

5.3 Effect of ash particle velocity

The aim of the present investigation is to study erosion phenomena combining the results obtained from numerical simulation and analytical model developed for erosion rate in the past by many researchers. Therefore, an attempt has been made to achieve complete combustion for current furnace model and to make a use of simulation data obtained during post processing. It would be much more practical if the obtained results compared with the real plant data. However, it is difficult to get the information about maximum erosion rate and its location from power station, this study is narrowed down to predict erosion rate using analytical model developed by Mbabazi et al for lethabo power plant in south Africa. Selection of this power plant was based on few point such as, firstly, study was carried out on erosion on air heater surface by fly ash particle inside the boiler. Secondly, fly ash chemistry mentioned in the literature has a similarity with the fly ash composition (adopted from Wee, 2006) considered for current model as shown in Table 5.3. They have considered air at speeds of 18- 28 m/s for conveying ash particles in the range of 0.2- 410 μm.

Table 5.3 Chemistry of the fly ash (adopted from Wee, 2006)

Mineral matter	Fly ash (%)	Mineral matter	Fly ash (%)
$Si0_2$	52.3	MgO	1.3
Al_2O_3	24.2	Na_2O	0.63
Fe_2O_3	15.4	K_2O	0.88
TiO_2	1.4	SO_3	0.1
Mn_3O_4	0.15	P_2O_5	1.4
CaO	1.9		

Moreover, mean particle diameter mentioned in literature has small difference with the diameter considered for current project. Lastly, silica content of fly ash has similar value as of fly ash considered for current study. On the basis of silica content as shown in Table A.3 few predictions has been made as shown in Table A.4 in Appendix A.

In this section we will discuss about effect of impact velocity studied during simulation process.

The parameter chosen here is the impact velocity, which is dominant factor to cause erosion by the ash particle in combustion process. Flue gas flow distributions along the cross section Y_1 and velocity vector distribution at different level Z_1, Z_2, and Z_3 in burner region as well as in superheater region at different level Z_4, Z_5, and Z_6 are shown in Figure 5.5 below. Velocity vector distribution at different cross sections in the burner zone are analysed to have a better understanding of flow in the boiler, as shown in Figure 5.6. It is observed that flue gas moves in vertical direction along the height of the furnace. Some part of flow goes downward along the furnace wall in hopper section and then moves upward towards furnace centre.

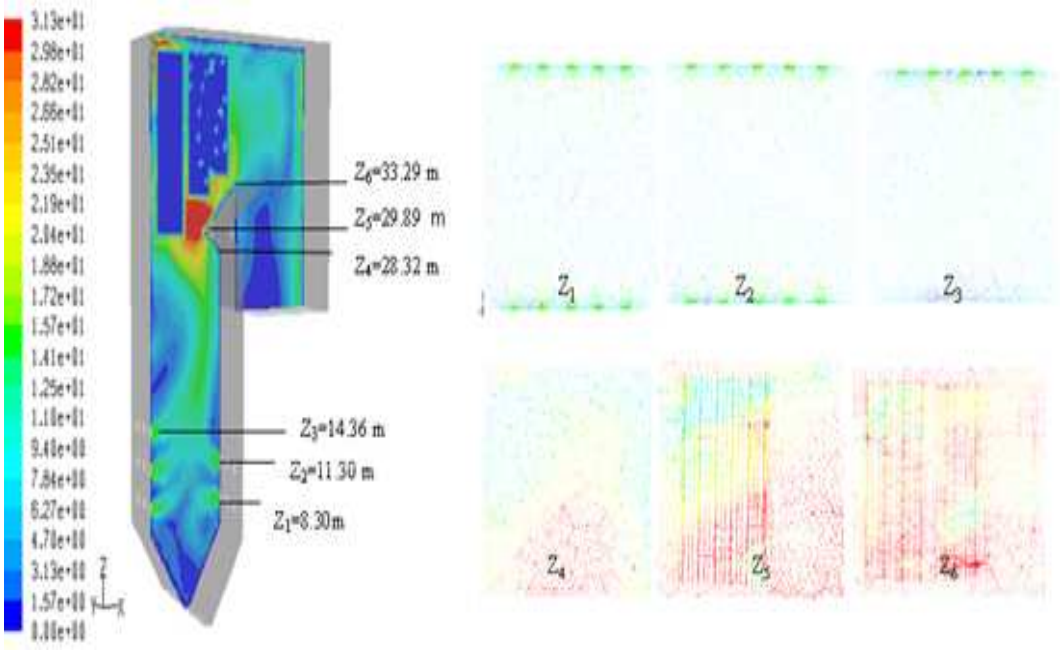

Figure 5.5 Velocity magnitude along vertical cross section Y_1 and Velocity vectors distribution in burner region (Z_1, Z_2, Z_3) and along nose section (Z_4, Z_5, Z_6)

From Figure 5.5 it can be seen that flow is parabolic in nature as it comes out of the burners. This shows even distribution of flow on burner surface. The flow moves upward steadily and inclined towards the furnace wall. Also, it can be seen that after several impactions, flow is not evenly distributed around the nose section and in

platen region. It shows different velocity magnitude in different region such as approximately 25 to 29 m/sec near top furnace wall, 17 to 28 m/sec in superheater section and approximately 19 to 31 m/sec around the nose section." Another reason for change in magnitude can be attributed to the scaling on the furnace walls. This could lead to improper temperature distribution in the radiation zone. It is observed that flow field is disturbed when flow enters in plate region. Uneven flow is obtained in between the plates, also between the plates and furnace side wall as shown in Figure 5.5 for cross section of Z_4, Z_5, and Z_6. After cross over path a reduced flow is observed due to plates in upper part of furnace. It reduces gradually as it enters the rear pass and ceases to exist in some regions of rear pass. It can be seen that velocity magnitude varies from 10 to 22m/s in burner zone. Figure 5.6 shows velocity distribution in burner zone. It remains steady and drastically increases to more than 30m/s as it approaches plate section. It is also observed that velocity before cross over path has maximum magnitude and likely to be responsible for removal of material, depending upon the particle impact angle in that region. Different areas such as plate wall, nose, upper wall corner of furnace, wall opposite to the nose are possible area for mechanical damage.

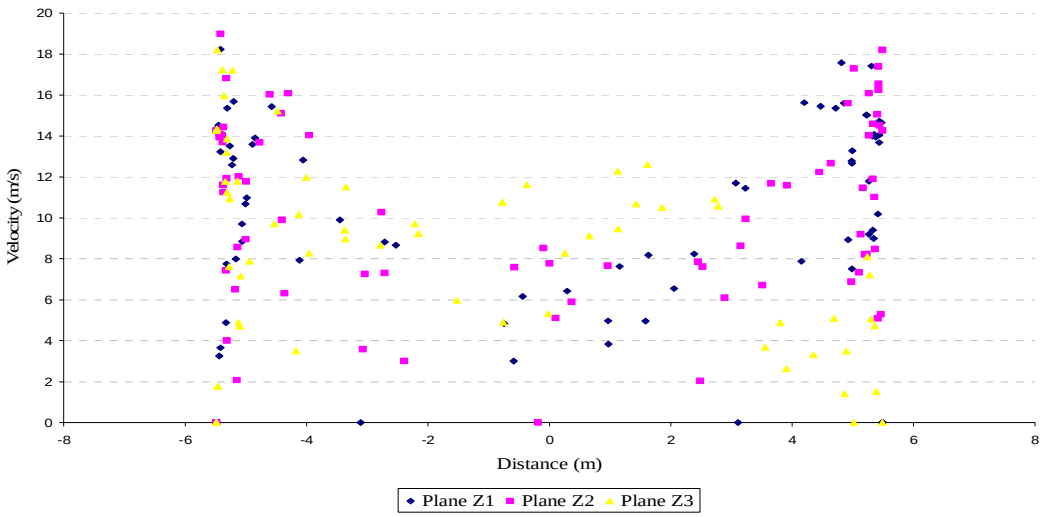

Figure 5.6 Velocity distributions at level Z_1, Z_2 and Z_3 (fig. 5.1) in burner zone for case 1

Similar procedure is followed for case 2 where five burners in top row are not active for burning. In this case less velocity is noticed near furnace wall but flow in the centre of the furnace is more active. Flow near the burners shows more activity then

in other locations. Moreover, Flue gas has peak velocity as it exits burner throat but it reduces as it approaches the radiation zone. The main difference between case 1 (base case) and case 2 is that low velocity region around nose and low velocity after the cross over section was observed for case 2. Hence, less erosive behaviour can be predicted near nose in case 2. Also, wall of furnace at different height and in different zones could be less affected by the particle flow because flow field in those regions is not intensive. Figure D.2 in Appendix D shows that velocity distribution between sections Z_4 and Z_6 for case 2.

Detailed study of velocity vector for different section of the furnace was carried out to approximate the impact angle. To analyse the effect of low velocity impact, another batch of simulation was carried out where only fifteen burners out of twenty five were active for combustion process. In case 3, furnace was supplied with less air and fuel flow rate as compared to case 1. As a result of 2-1 firing uneven firing pattern, an inclined flow field was developed as shown in Figure D.1. Moreover, the average velocity of the char particle calculated by FLUENT comes 32 m/s for Case 1 while it is 12 m/s for Case 3. Case 1 is a full load condition where coal flow rate is high around 52.47 kg/s while Case 3 is 60% loading condition where coal flow rate is 31.47 kg/s. The velocity is proportional to flow rate, increases with increase in flow rate.

It is true that velocity in Case 3 is even less than the proportional value which is 19 m/s. This may be due to firing pattern. In, Case 3, only 30 burners are running with coal and air flow rate decreases by 40%. Hence, the coal particle will have less travelling velocity compared to 50 burners in operation.

One would notice that inclined flow impacting on opposite furnace wall could be major factor for erosive wear of that wall on along which flow occurs. However, it is difficult to identify the particle shape with numerical approach but with magnitude of impact velocity on or around that wall, it is possible to approximate the erosion rate for that burner wall surface. Similar results were analysed for super heater section with low impact velocity. On contrary high velocity was noticed near top furnace wall and wall corner. Generally volume removed is proportional to the mass of eroding particles, except for particles approaching at 90° to the surface (Finnie and McFadden, 1978).Table 5.4 shows different value of erosion rate with different

impact velocity magnitude estimated for constant impingement angle during post processing. Thus, impact angle in conjunction with velocity shows similar pattern for prediction of erosion rate for any particulate flow stream.

Study was further extended by simulating furnace with excess air supply to have an idea of flue gas flow stream with high velocity. For particular scenario flow profile obtained is similar to the case 1 but seems less inclined towards the wall or nose. This would be because of the less temperature in radiation zone due to excess combustion air supplied. Secondly, flow field is evenly distributed in super heater section and near furnace exit (cross over path). Figure D.3 to D.5 and Figure D.6 to D.9 shows the velocity distribution for burner and superheater section respectively in Appendix D.

Table 5.4 Variation of erosion rate with impingement velocity at constant angle of 30°

Velocity (m/s)	Erosion rate (mg/kg)*
18.80	5.04
21.94	6.20
23.51	7.52
25.08	7.52
26.68	9.03

* The unit describes the metal loss in mg per kg of fly ash throughput in the present study.

Finally, Results analysed from numerical simulation are compared with experimental values obtained for Lethabo power plant (South Africa) (Mbabazi et al., 2004). Particulate values such as mass fraction of silica 0.52(%w/w), fly ash density 1700kg/m^3, velocity exponent equal to 3 and mechanical properties for steel, such as density is 7860kg/m^3 ,yield stress is 254kgf/m^2 is considered. Reasons for comparing with the lethabo power plant are that the coal used in both case has nearly similar physical and chemical properties. The velocities of the sections are also nearly same. The mean particle diameter mentioned in the literature has minimal difference with simulation case study. Silica content in both the cases is also nearly same.

The only difference being that Mbabazi's studies reported that erosion rate for lethabo plant for air preheater and for small to medium scale furnace. Mbabazi's efforts have been extended further in the present study for higher scale furnace and for different sections other than air preheater. Due to lack of validation data of actual running installation, in this case only trends have been compared. This model works well and shows that erosion rate increases with increasing velocity and impact angle. The probable zones for higher erosions rates have been obtained through FLUENT simulations by tracking particle trajectories. This model later should be validated with real plant data in future studies.

Furthermore, figure 5.7 shows that erosion rate increases with increase in velocity and shows similar pattern as predicted for Mbabazi's model. The difference in erosion rate value between obtained and literature value is approximately 30% when measured at 30° impact angle. This is quite huge difference which may be because predicted value of erosion rate is obtained considering velocity magnitude by simulating full scale boiler. Mbabazi has obtained the erosion rate value only on the air preheater study. It can be also seen from the graph that for constant impact angle (20°) with different impact velocity, the average deviation is about 4.9% which is quite acceptable.

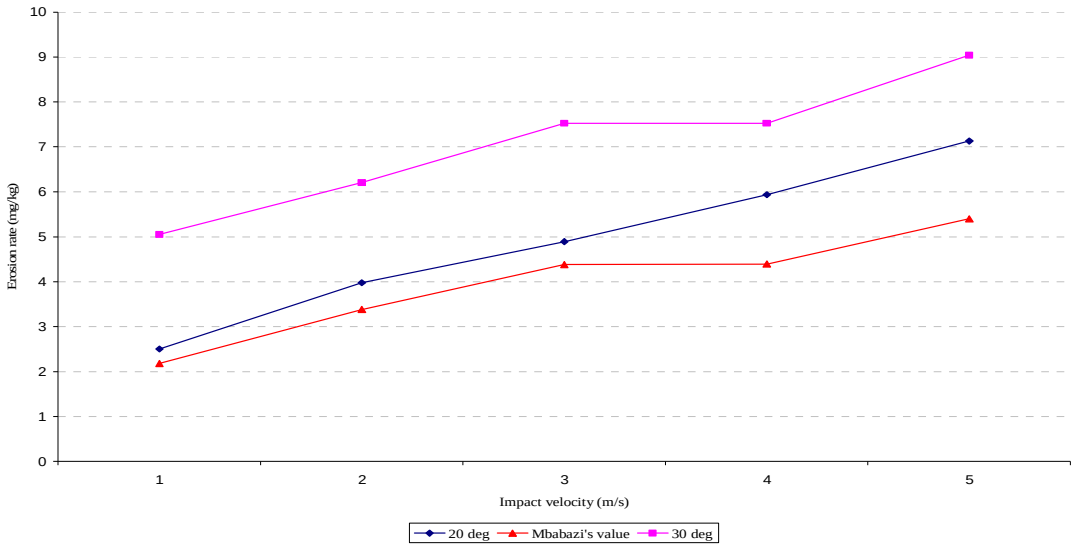

Figure 5.7 Comparison of erosion rate for different velocity between predicted and literature value at constant impact angle of 20° and 30°

It is also observed that there is a steady increase in erosion rate with increasing particle velocity in all other cases as shown in Figure E.4, Figure E.8 and Figure E.12 in Appendix E. Propensity of Erosion rate of surface material depends mainly on the velocity magnitude. Figure 5.8 shows Comparison of percentage of erosion rate for different velocity for all cases. Predicted erosion rate for all cases for different impact velocity at constant impingement angle (20°) is shown in Appendix F.

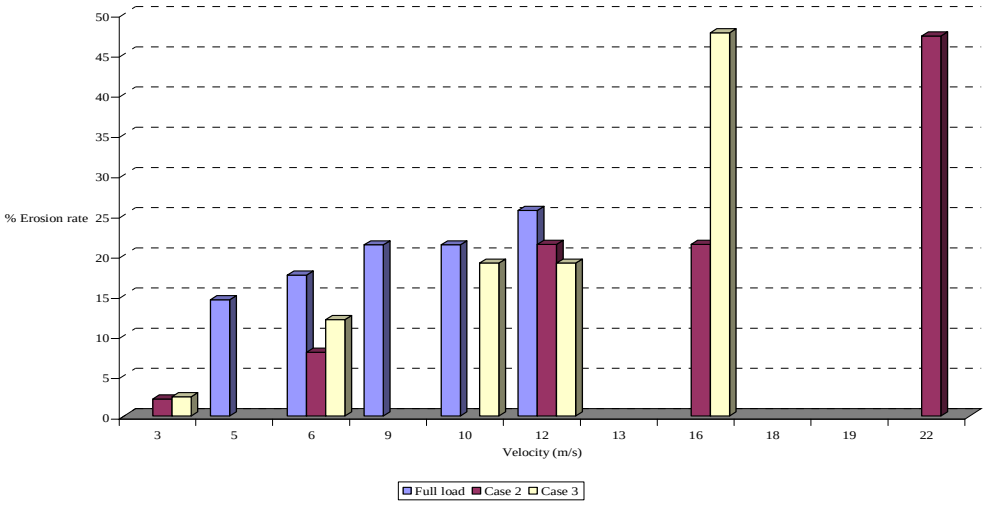

Figure 5.8 Comparison of percentage of erosion rate for different velocity for all cases

As mentioned earlier that impact velocity and impingement angle together gives clear view about wear effect. Thus, from here we move to our next section effect of impact angle once all necessary data related to velocity have been gathered. Next section will give insight analysis of impingement angle at different location, which will help us to predict the erosive behaviour in power utility boiler.

5.4 Effect of impact angle

Analysis is further extended to impact angle of different particles on the basis of particle trajectories which is usually defined by flue gas path line. However, accurate quantification of different angle is difficult with this approach. Literature data available for impact angle is purely based on experimental research. Most of the research relies on experimental set up and consider very limited number of parameters. Generally, in any experimental test particle stream containing one or two

particles with particular shape and size is injected at fixed angle and with fixed velocity which strike the test specimen. Frequent observation of specimen surface is made after each trial. Thus, using different impact angle with fixed velocity or fixed angle with different velocity, it is possible to justify wear effect on the surface of target material. While in real power plant boiler it is not possible to do so as the flow distribution is much more complex. Therefore, CFD post processing technique together with IMAGEJ software is one of the alternatives to overcome this situation and approximate the angles for velocity vectors, obtained from simulation. As shown in Figure 5.9 circled vectors are considered to analyse the impact angle. Different angles are measured along different magnitude of velocity. Close view of circle area showed that there can be different angle for same velocity magnitude.

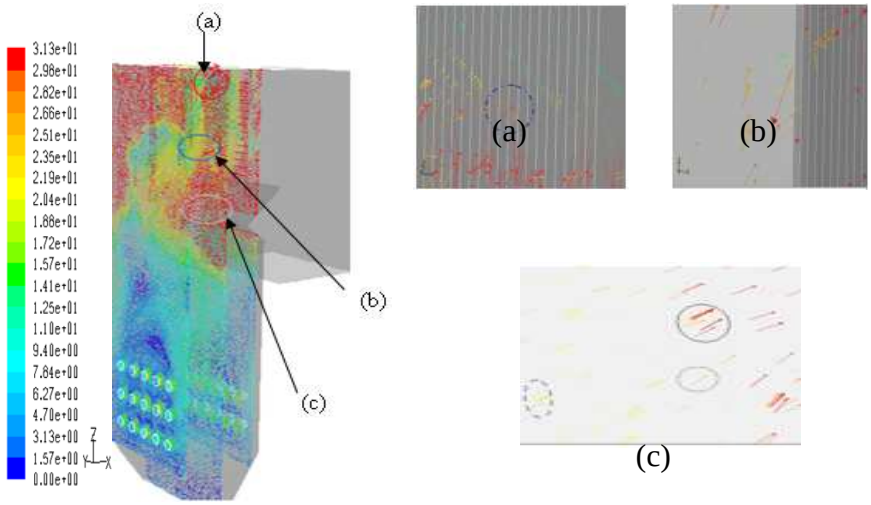

Figure 5.9 Diagrams of velocity distributions on different cross section in X direction for Case 1 (a) Close view of directional vectors between top furnace wall and plates (b) Close view of flow vectors in between secondary platen heater (c) Close view of flow vectors in nose region

Different cross section along furnace height is analysed to obtain the dominant velocity on that particular plane as shown in Figure 5.9. Close view of plate zone and zone near nose clearly shows different velocity magnitude and its direction in that region. All calculations are carried out with defined material and fly ash particle properties using erosion model developed by Mbabazi et al. It is observed from Figure 5.10 that maximum erosion rate occurs at 20° and gradually decreases with

increase in impingement angle. It is also observed that there is not much of difference in erosion rate value between 20° and 30° impact angle. But it decreases suddenly between 30° and 45° impact angle.

Table 5.5 Erosion rate at different angle at constant velocity (26m/s)

Impingement Angle (deg)	Erosion rate (mg/kg)
12.26	0.23
20.32	8.57
30.01	8.39
45.07	5.36
58.72	4.48

Hutchings showed that for all metal maximum erosion occurs in between range of 20°-30° by ash particle in high temperature region. Table 5.5 shows the different erosion rate for different impact angle at constant velocity for base case. Erosion rate at different angle at constant velocity for all other cases are tabulated in Appendix F.

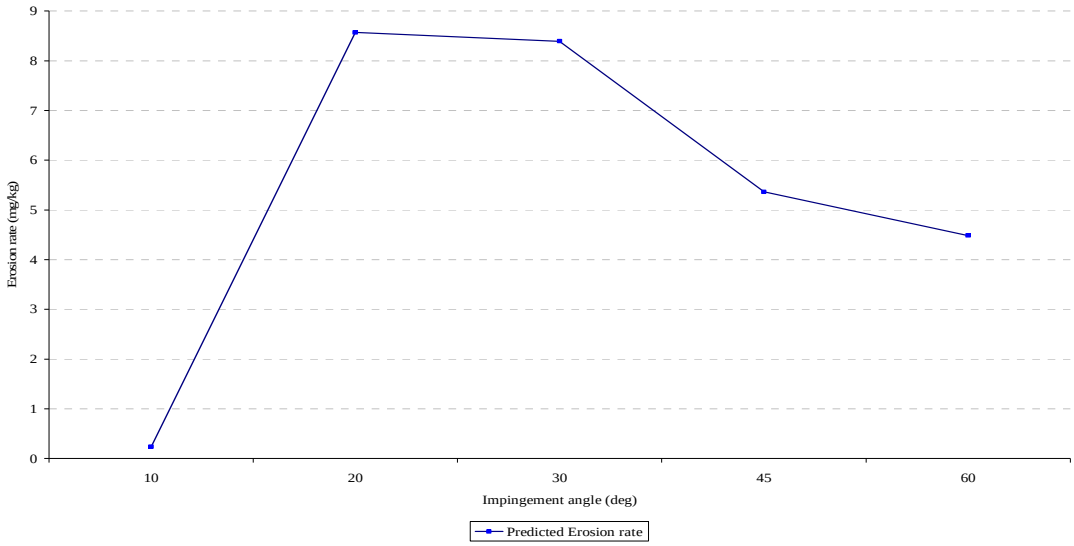

Figure 5.10 Predicted erosion rate for different impingement angle at constant impact velocity

Figure 5.10 shows erosion rate predicted for different impingement angle at constant impact velocity. This analysis was based on randomly selected velocity vectors found near furnace wall approaching towards wall during post processing. Although, it was tedious and time consuming job, in this modelling study, 500-600 particles were analysed for each case.

Chapter 6

Conclusions and Recommendation

6.1 Conclusions

- Model development

The characteristics of the flow, combustion and temperature in the 330 MWe opposite wall fired furnace have been numerically investigated using CFD commercial flow solver FLUENT for combustion process. A complex evaluation of the model has been performed, with grid independent study. Qualitative and quantitative analysis has been performed for various geometrical and operational conditions. The detailed results obtained in this study enhance the understanding of complex flow patterns, combustion processes and erosive behaviour in opposite wall fired pulverised coal furnaces. Moreover, the predictions of different cases based on the full load lay a foundation for the boiler operating expert system.

- Model results

In the absence of experimental support and plat data, the presentation of more results of the parametric studies is difficult to justify. However, Simulations were performed for varying combinations of burners in operations and results were compared. It was observed that for different air to fuel supplied ratios, selection of these burners had a substantial impact on the flow rate and temperature distribution inside the boiler. Simulation carried out with excess air indicated that the temperature at the furnace exit or at cross over path decreases. Thus, it is important from the design point of view that a careful selection of burners in operation must be made. Also it is imperative that the all the selected burners should be maintained for a smooth combustion process to avoid unexpected breakdown of the boiler. Results obtained from simulation shows deviation of approximately 18% with previously published experimental data, may be due to difference in firing technique, different boiler configuration and different grade coal is used as row material.

Predicted particle trajectories show variation in particle residence times inside the boiler. Particle from the bottom of the burner row shows longer average residence time inside the domain for certain cases may lead to poor combustion process which is not desirable for efficient working of power plant boilers.

The numerical investigation combine with analytical model described here shows that erosion rate on a mild steel surface subjected to stream of fly ash particles varies with particle impingement angle. For low value of the impingement angle, the erosion rate increases with an increase in impingement angle, with maximum erosion rate occurring at 20°. Thereafter, the erosion rate decreases with further increase in the impingement angle. Thus, results obtained from this study are in good agreement with literature available.

The calculated erosion rate for predicted velocity shows a steady increase in erosion rate with increase in particle impact velocity. Range of velocity obtained from simulation results are used to calculate erosion rate at constant impinging angle shows average deviation of 4.9 % when measured at 20° angle. The percentage of deviation obtained is very small and can be neglected. This shows good agreement with the previously published experimental value. This numerical modelling study endeavours to exemplify the effect of impact velocity and impingement angle in evaluating erosion potential of fine ash. Furthermore, effect of impact velocity and impingement angle for discrete sizes of silica particles could be responsible for excessive wear on furnace walls. These discrete sizes of silica particles are not considered in the present analysis due to lack of real plant data.

Overall, current model in conjunction with erosion model can provide useful insight into the erosion phenomena for different grades of coals. Model results from the present work can complement full scale experiments and engineering calculations for better judgement for arriving at optimum operating conditions to control erosion phenomena in utilities.

6.2 Recommendation

Future work should focus on the influence of the shape and rotation angle of the ash particles on the erosion rate with appropriate erosion model. Quantitative analysis should be performed on studying various grades of coal with minimum amount of silica content. Investigations must also be performed on the effect of this silica content on the erosion in coal fired furnaces.

One of the commonly used modifications in the industrial scale furnaces involves use of tertiary air inlets to improve the mixing characteristics in these processes. It is presumed that with higher supply of tertiary air and decreased secondary air may lead to better mixing of flue gas inside the furnace and decreasing of temperature in the down-streams of the furnace. It would be worthwhile to carry out modelling study that incorporates these tertiary air inlets in the boiler geometry. Verification of these claims could be topic for future development.

For the purpose of modelling it is generally assumed that the coal particle size and shape remains even and uniform. Whereas, it is unlikely that in practical scenario such phenomenon would be occur. Thus, quantitative work is required to analyse the effect of non uniform particle size and shapes for a wide range of mean particle diameters. From the modelling point of view in future it is recommended to use and compare other gas solid modelling approaches such as discrete element method and Eulerian- Eulerian approach.

It would be interesting to incorporate the wall effect of various materials of construction and coatings that are generally used in industrial operations. Phenomena's such as sticking, reflecting, impacting and repulsing as an effect of wall coating must be investigated to develop a better understanding of the erosion in coal fired furnaces.

6.3 Protective and remedial measures

Operational and equipmental measures are generally considered. It starts with evenly distribution of coal flow rate from pulveriser mill to burner section of the boiler. During coal selection for thermal power plant, extra attention should be given to silica and other hard minerals content to avoid erosion. Ensure complete combustion only in radiation section. Due to incomplete combustion, large lumps of unburnt char particle may impact directly on the wall surface. The most obvious action would be to reduce the air and coal particle velocity as much as possible with in allowable pressure drop limit to reduce the particle concentration on wall surface of furnace.

In equipmental measures, material of construction for furnace wall and plates in superheater section can be decided considering severe conditions such as fuel silica content, extreme temperatures, thermal shock, and intensity of impact of solid ash particle inside the combustion chamber. Non destructive tests should be carried out to analyse the surface condition of tubes as well as walls inside the furnace. Proper preventive measures should be taken to reduce sudden and unwanted shutdown. Although the measured shown above would not cure erosion problem but at least it will extend the operational life of this equipment.

Appendix A

Table A.1 Proximate and ultimate analysis

Proximate Analysis	**Average**	**Range**
Moisture	25	22-28
Ash	8	4-10
Volatiles	29.8	22-34
Fixed Carbon	37.7	36-48
Total Sulphur	0.7	0.3-1.0
Specific Energy (MJ/Kg)	19.6	18.8-21.5
Ultimate Analysis (% daf)	**Average**	**Range**
Carbon	73.5	73-76
Hydrogen	4.8	4.2-4.9
Nitrogen	1.2	1.2-1.5
Sulphur	1.0	0.3-1.3
Oxygen	19.5	18-20
Mineral matter	**Average**	**Range**
$Si0_2$	47.3	30-55
Al_2O_3	24.3	20-30
Fe_2O_3	17.1	5-22
TiO_2	1.54	1.-2.5
Mn_3O_4	0.19	0.05-0.22
CaO	2.14	1-3
MgO	1.67	0.5-2
Na_2O	0.54	0.2-1
K_2O	0.73	0.3-0.9
SO_3	0.90	0.3-1.8
P_2O_5	1.52	0.05-4.0

Table A.2 Erosion indices of fly ash for silica contents (Raask, 1985)

Silica (SiO_2) content of ash (Wt %)	**Erosion indices**
Less then 40	Low, less than 0.02
Range 40-50	Medium, 0.02-0.08
Range 50-60	Medium to high, 0.04-0.28

Table A.3 The chemistry of the mill reject ash, bottom ash, fly ash (Wee, 2006)

Mineral matter	**Fly ash**	**Furnace wall**	**Superheater**	**Reheater**
$Si0_2$	52.3	67.14	65.40	72.24
Al_2O_3	24.2	15.36	12.26	11.34
Fe_2O_3	15.4	11.83	17.05	12.85
TiO_2	1.4	1.07	0.83	0.97
Mn_3O_4	0.15	0.07	0.07	0.04
CaO	1.9	1.01	1.17	0.68
MgO	1.3	0.64	0.60	0.41
Na_2O	0.63	0.11	0.10	0.10
K_2O	0.88	0.91	0.41	0.93
SO_3	0.1	0.02	0.05	0.09
P_2O_5	1.4	1.06	1.43	0.60

Table A.4 Summary of Erosion rate for different zones on the basis of silica content (Wee, 2006)

Zone	**Probable areas under erosion influence**	**Dominant impact Velocity (m/s)**	**Approximate Erosion rate (mg/kg)**	**Erosion effectiveness (%)**	**Intensity of erosion**
Zone 1 Radiation Zone	- Side wall of furnace - Burner walls - Lower part of nose section - Hopper section	14.28	2.86	5.52	Medium
Zone 2 Convection zone	- Super heater section	30.19	24.51	47.38	High
	- Upper furnace walls - Upper part of nose section - Edge of nose section	28.14	22.58	43.64	High
Zone 3 Economiser Zone	- Side walls of furnace	12.33	1.78	3.44	Medium

Appendix B

B.1 Temperature distribution

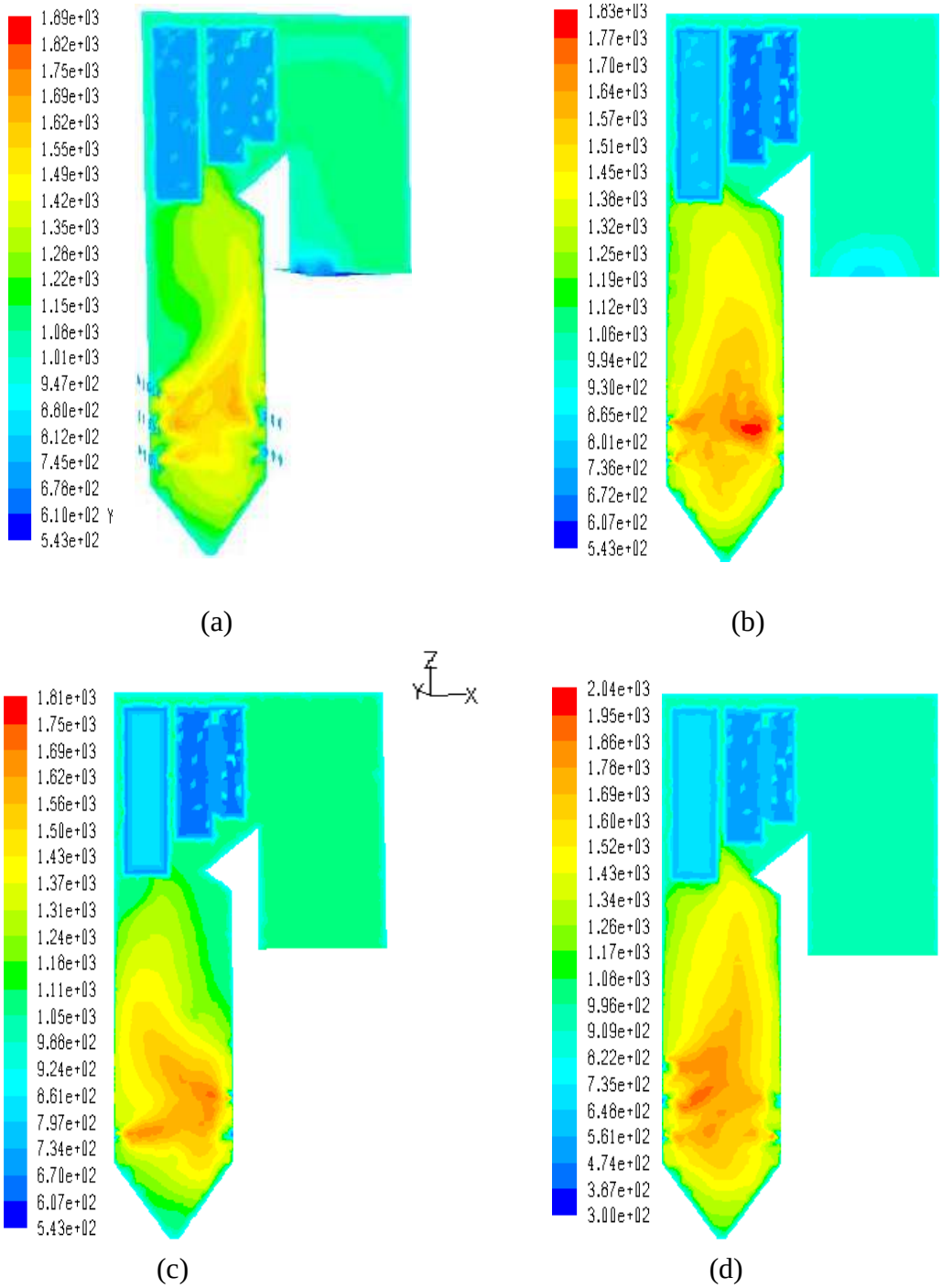

Figure B.1 Temperature distribution along plane Y_1= 7.2395 m in Z direction, (a) Temperature distribution for case 1. (b) Temperature distribution for case 2, (c) Temperature distribution for case 3, (d) Temperature distribution for case 4

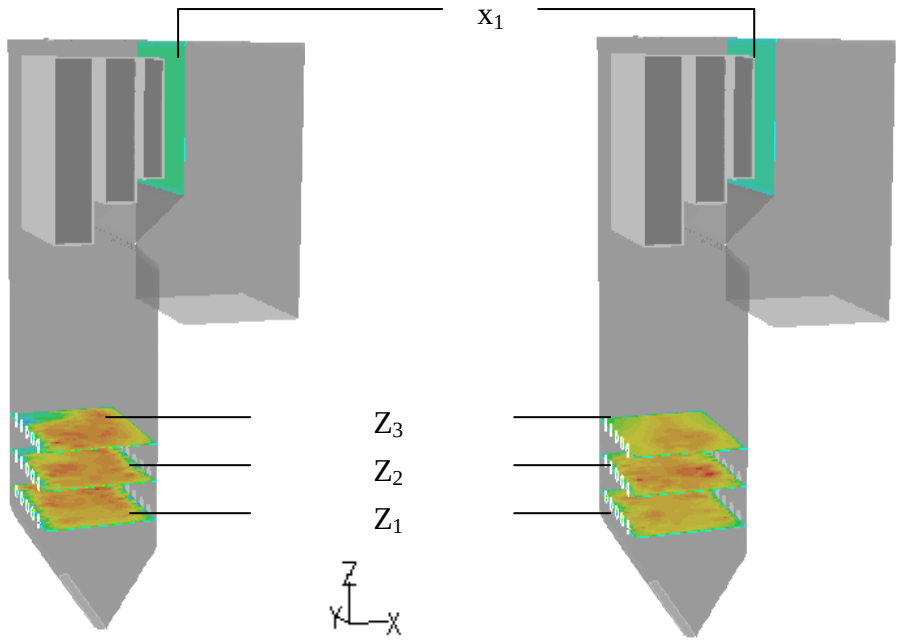

(a) (b)

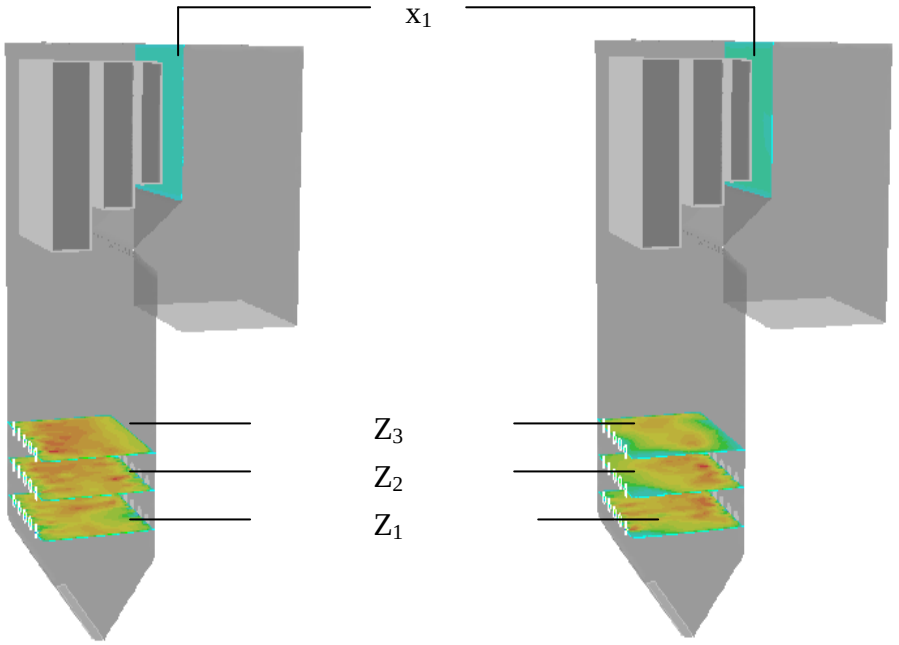

(c) (d)

Figure B.2 Temperature distribution on planes Z_1, Z_2, Z_3 and x_1(Z_1=8.30m, Z_2=11.30m, Z_3=14.36m, and x_1= 7.89m) for (a) Case 1 (b) Case 2 (c) Case 3 (d) Case 4

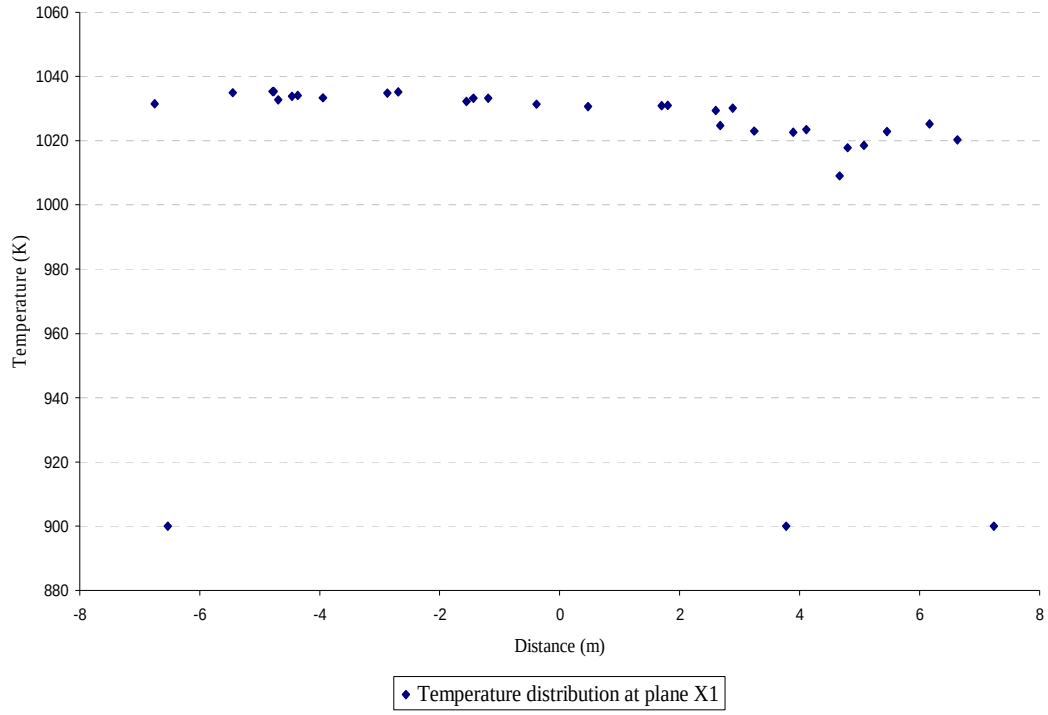

Figure B.3 Temperature distributions at cross over path for case 2

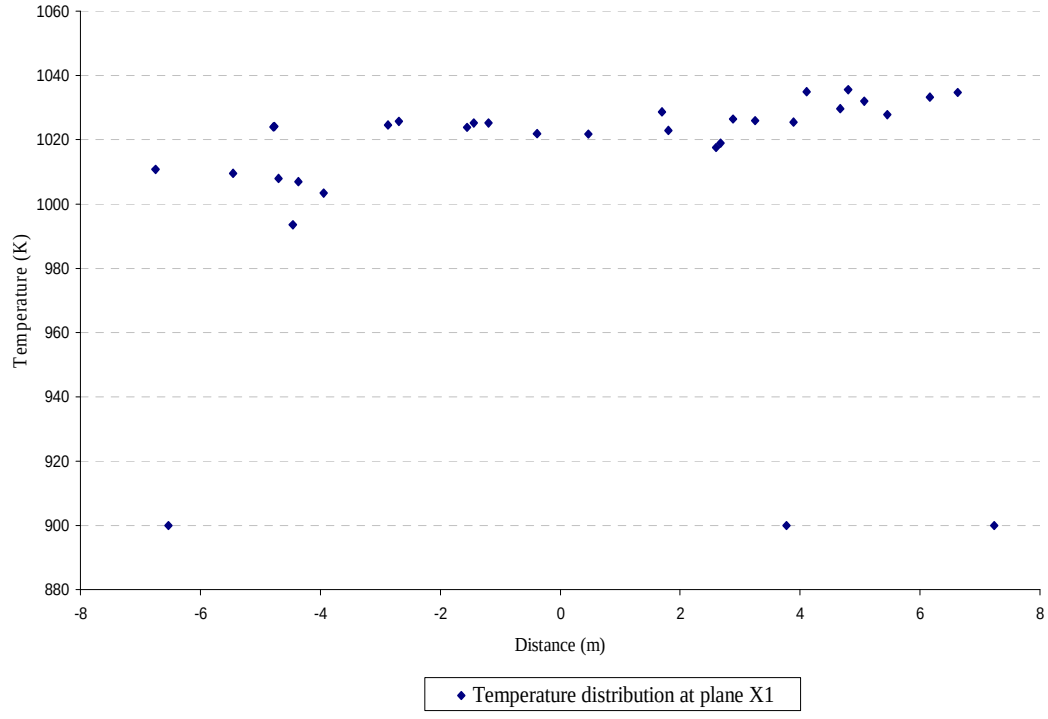

Figure B.4 Temperature distributions at cross over path for case 3

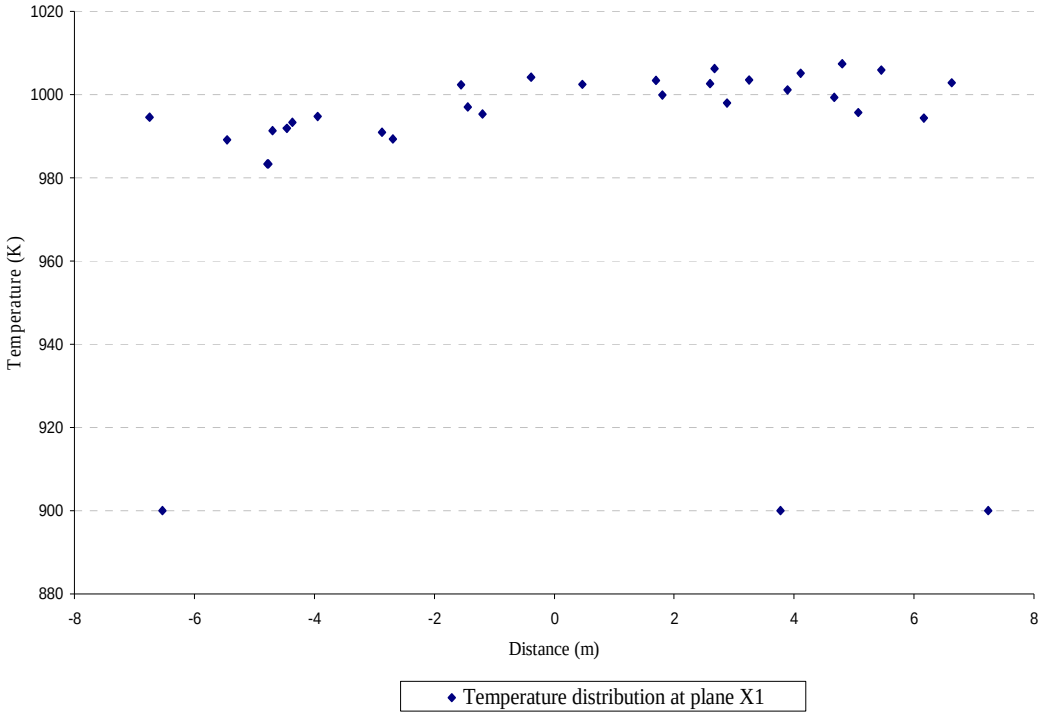

Figure B.5 Temperature distributions at cross over path for case 4

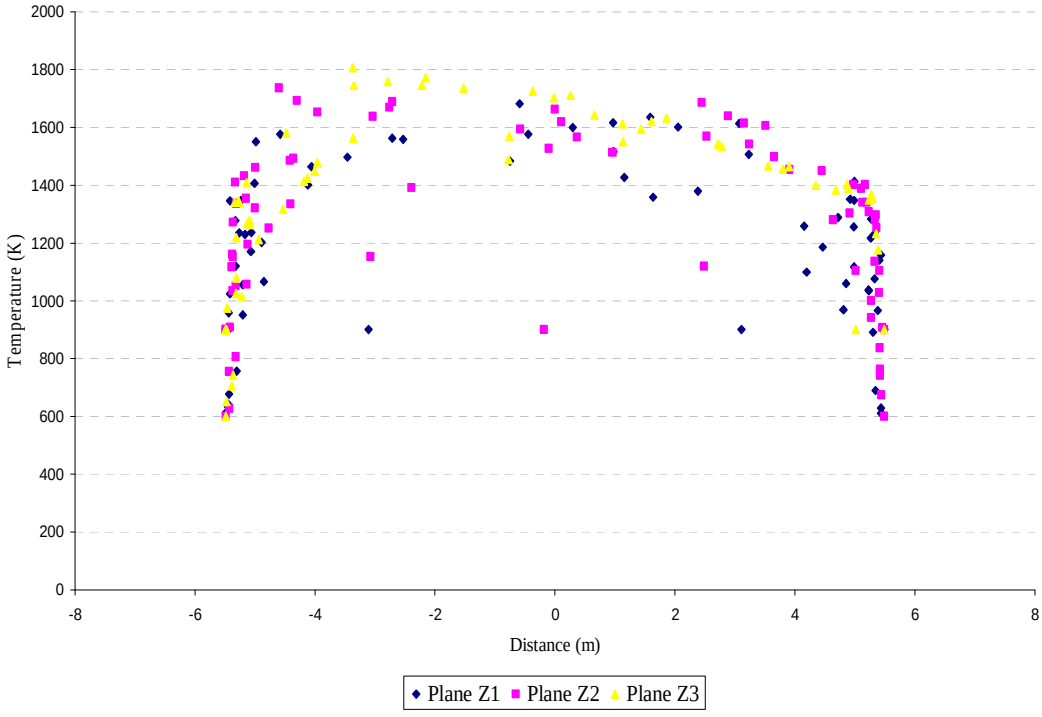

Figure B.6 Temperature distributions in burner region for case 1

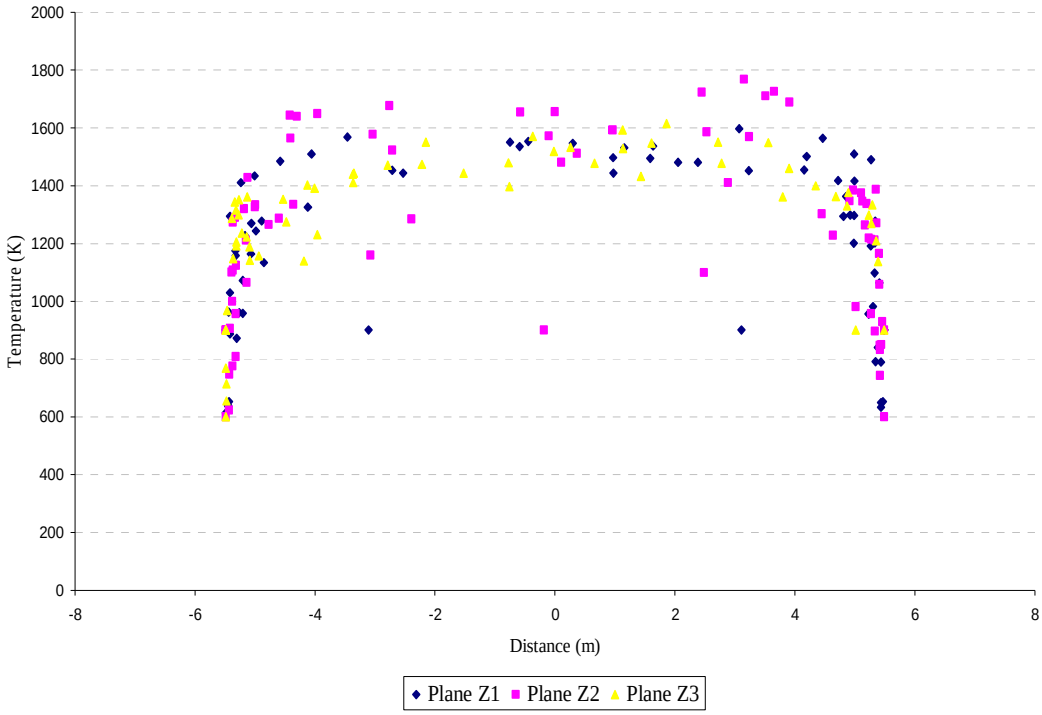

Figure B.7 Temperature distributions in burner region for case 2

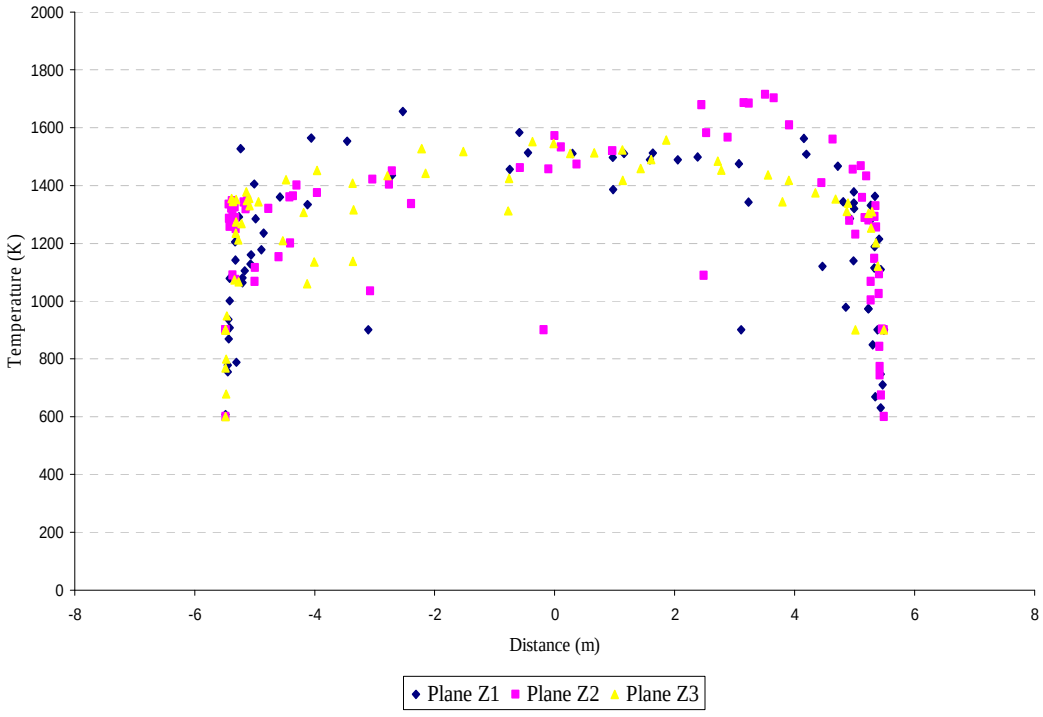

Figure B.8 Temperature distributions in burner region for case 3

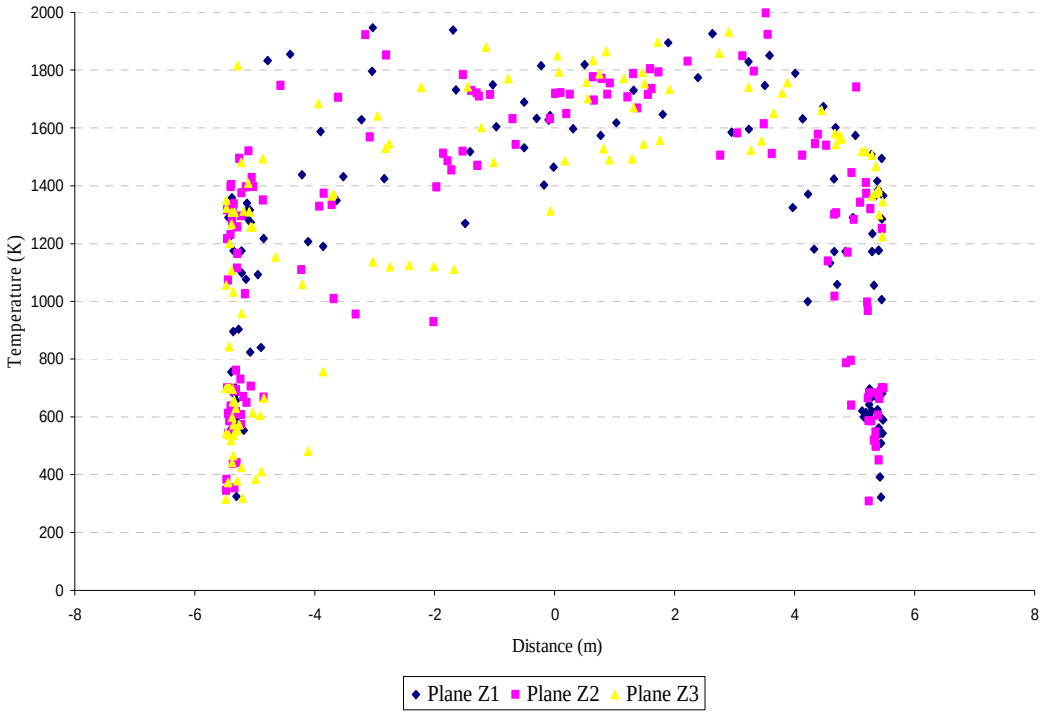

Figure B.9 Temperature distributions in burner region for case 4

Appendix C

C.1 Particle trajectories – case 2

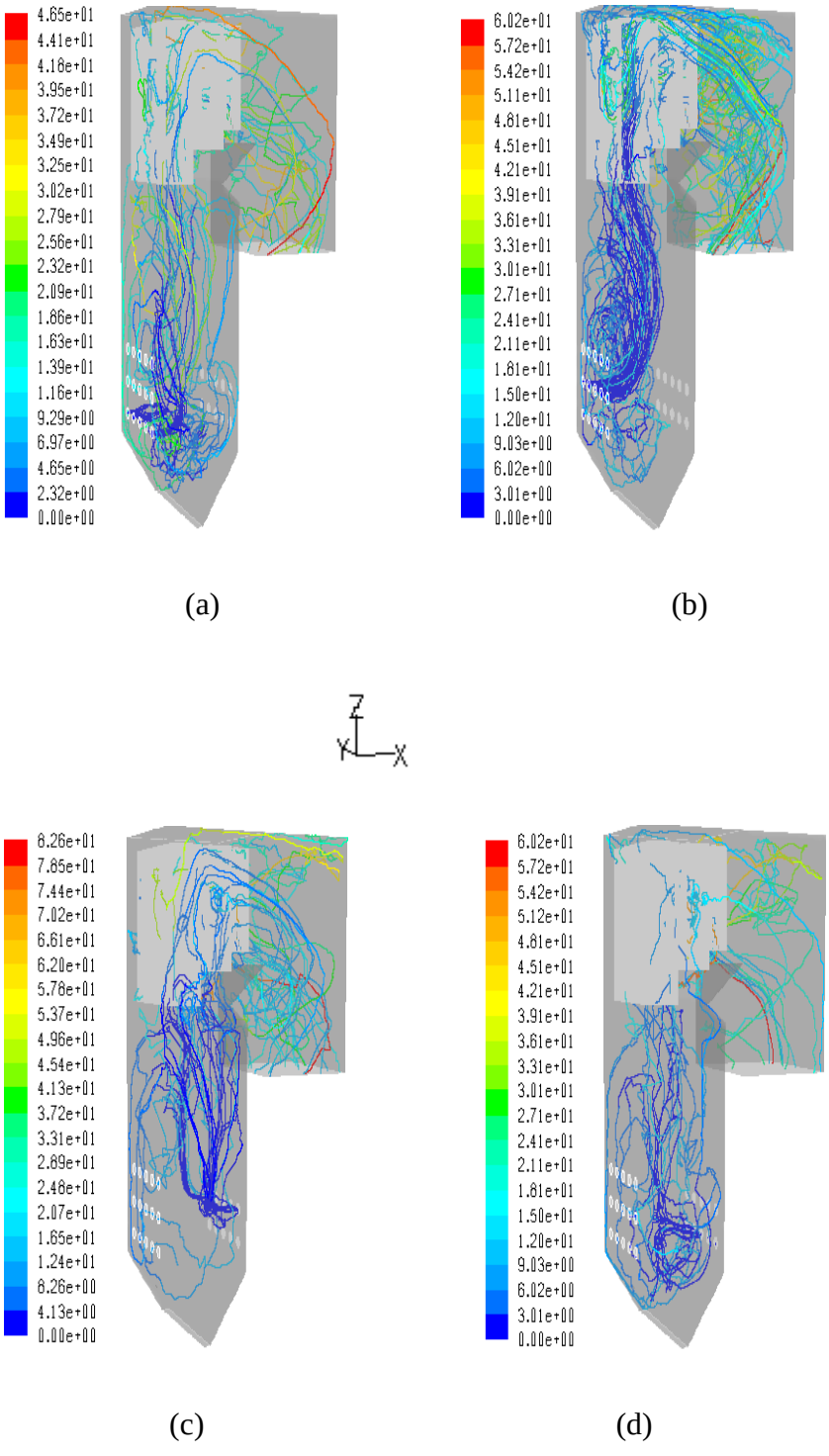

Figure C.1 Particle trajectories for case 2, (a) Burners 1 to 5 (b) Burners 6 to 10 (c) Burners 16 to 20 (d) Burners 21 to 25

C.2 Particle trajectories - case 3

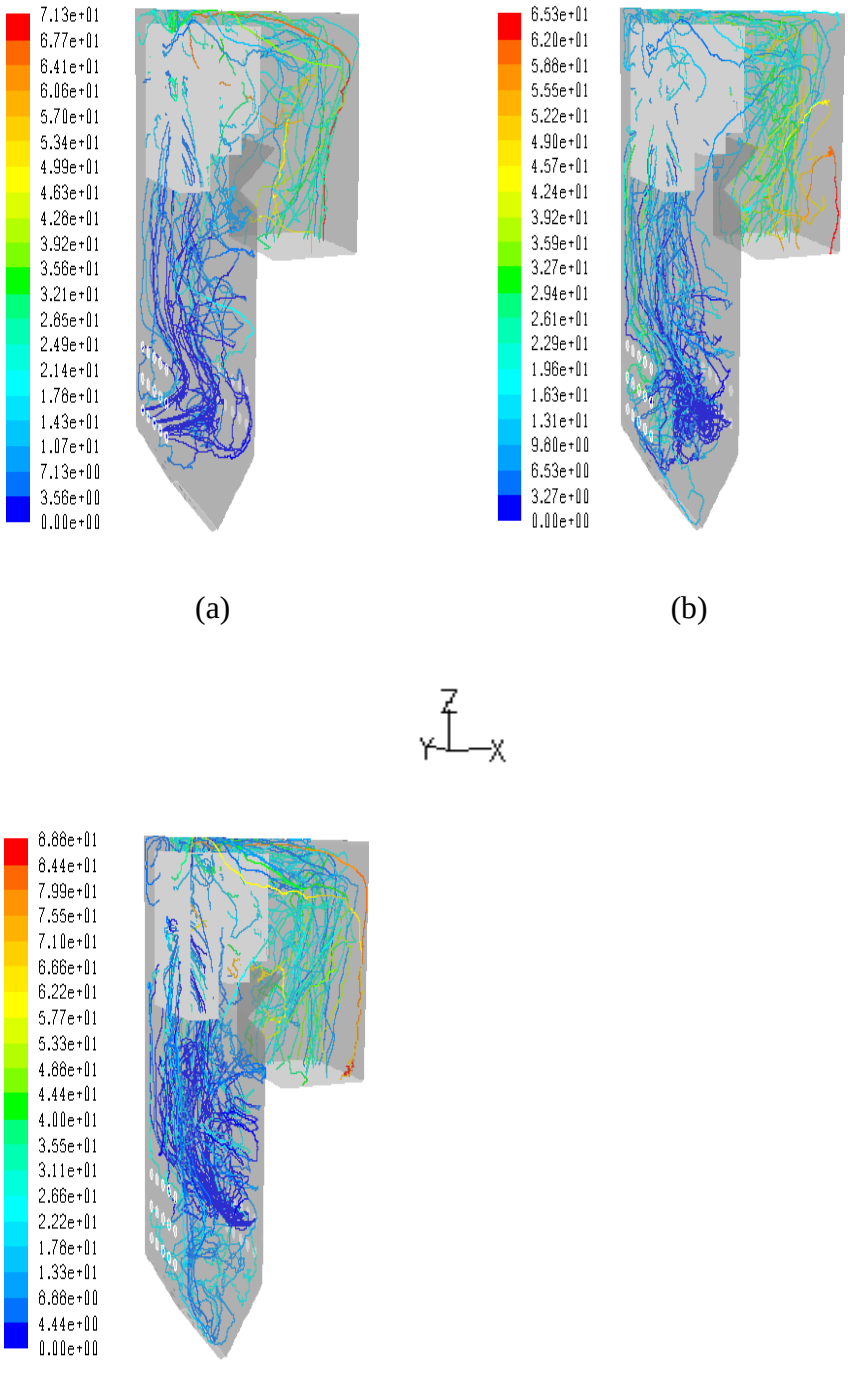

Figure C.2 Particle trajectories for case 3 (a) Burners 1 to 5 (b) Burners 16 to 20 (c) Burners 21 to 25

C.3 Particle trajectories – case 4

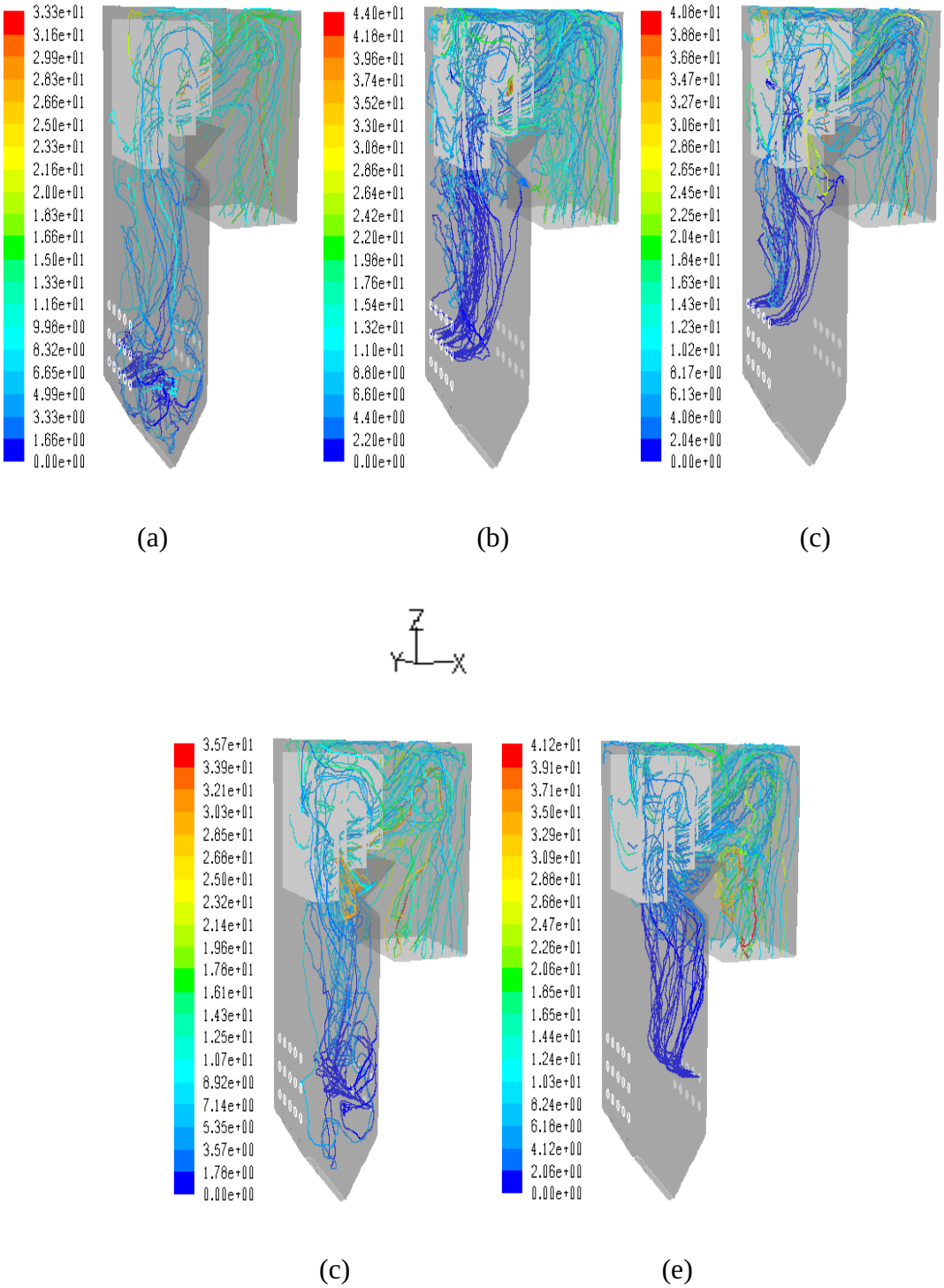

Figure C.3 Particle trajectories for case 4 (a) Burners 1 to 5 (b) Burners 6 to 10 (c) Burners 11 to 15 (d) Burners 16 to 20 (e) Burners 21 to 25

Appendix D

D.1 Velocity distribution

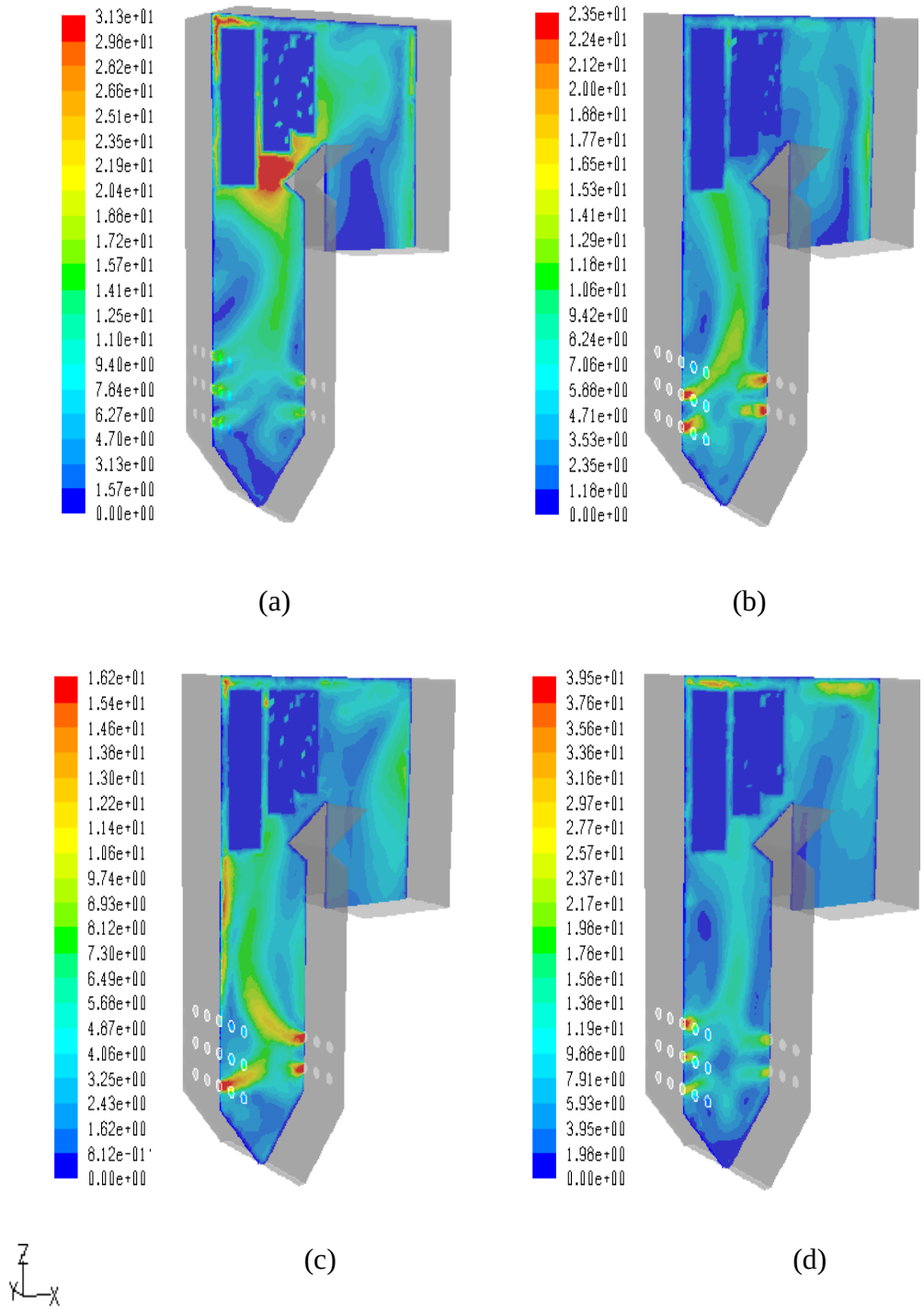

Figure D.1 Velocity magnitude along plane Y_1= 7.2395 m in Z direction (a) Case 1 (b) Case 2 (c) Case 3 (d) Case 4

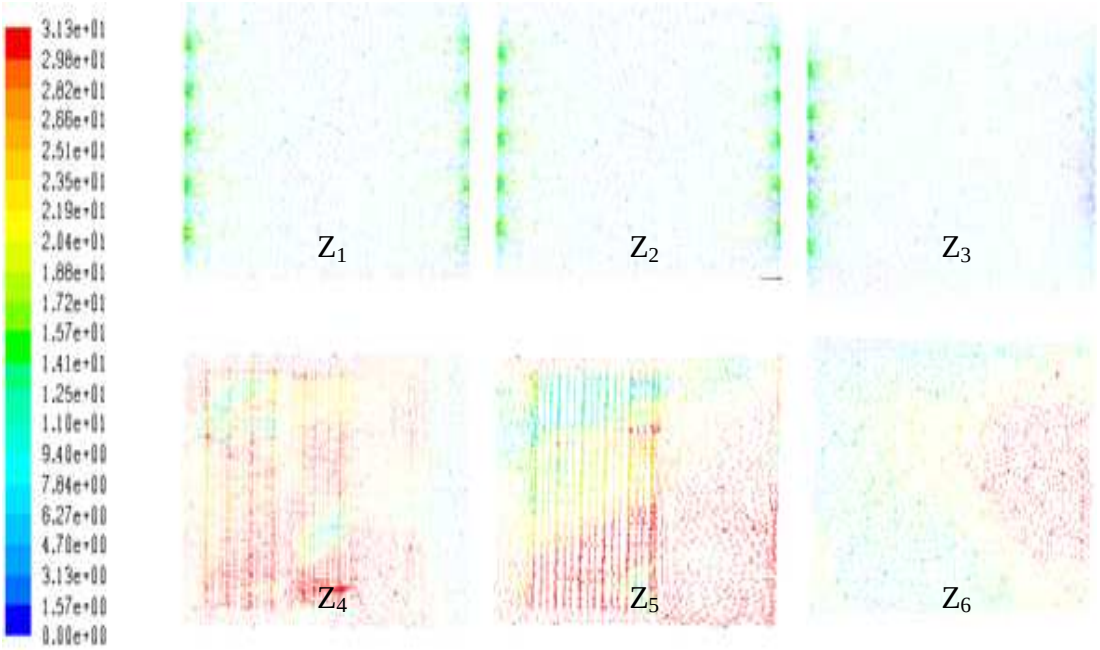

(a)

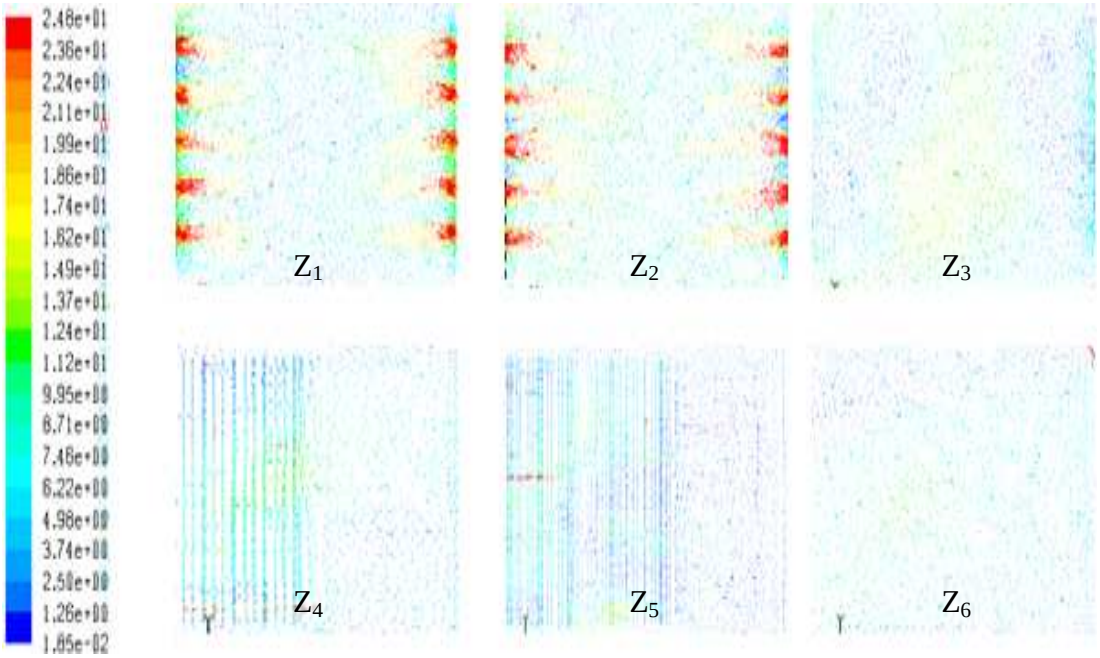

(b)

Figure D.2 Velocity distribution on plane Z_1, Z_2, Z_3, Z_4, Z_5, Z_6 for (a) Case 1 (b) Case 2

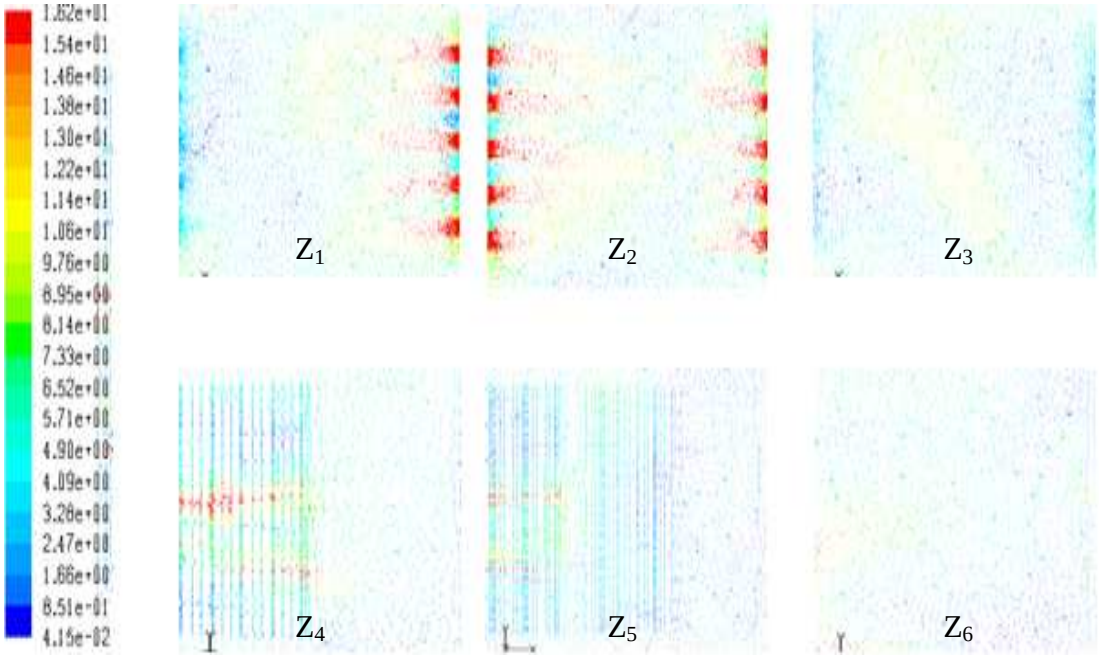

(c)

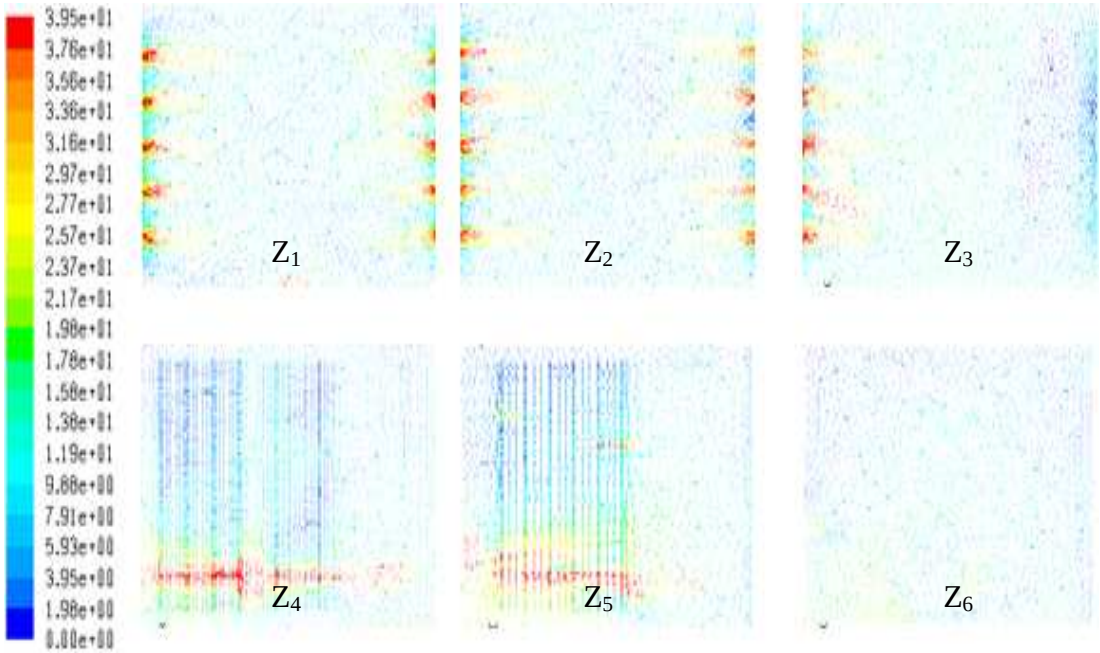

(d)

Figure D.3 Velocity distribution on plane Z_1, Z_2, Z_3, Z_4, Z_5, Z_6 for (c) Case 3 (d) Case 4

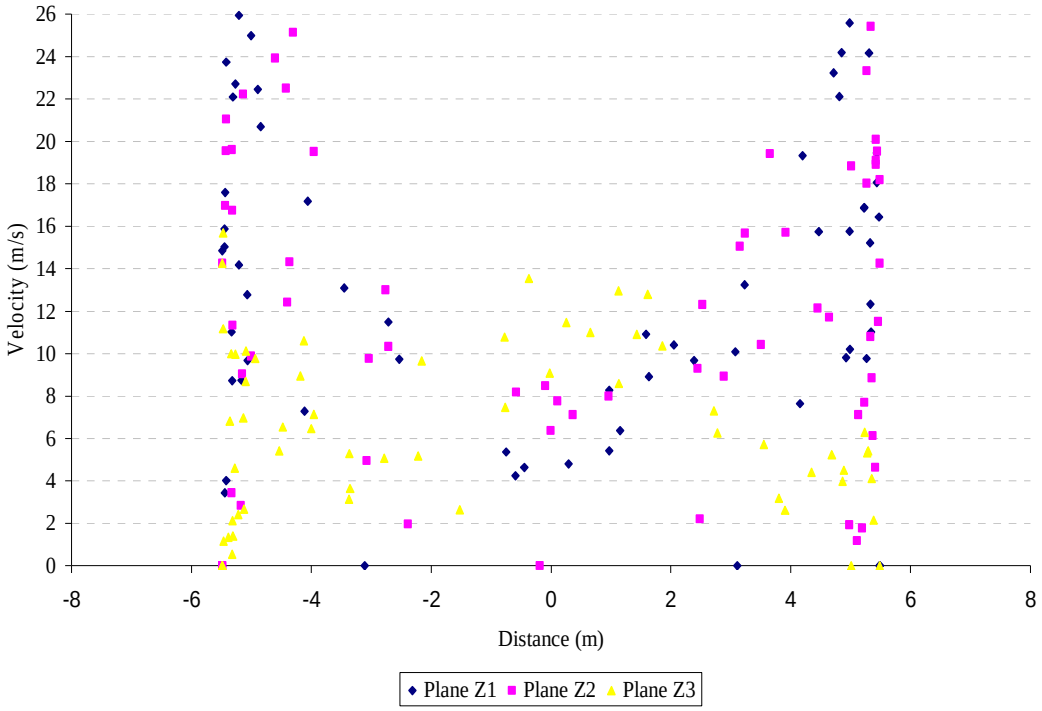

Figure D.4 Velocity distributions in burner zone for case 2

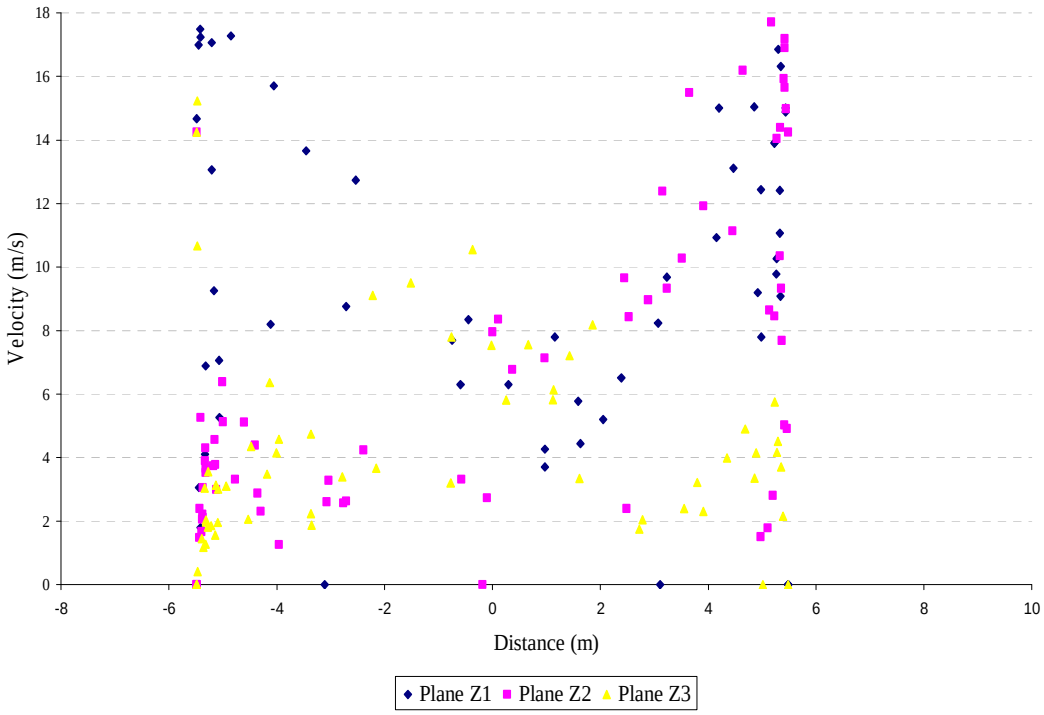

Figure D.5 Velocity distributions in burner zone for case 3

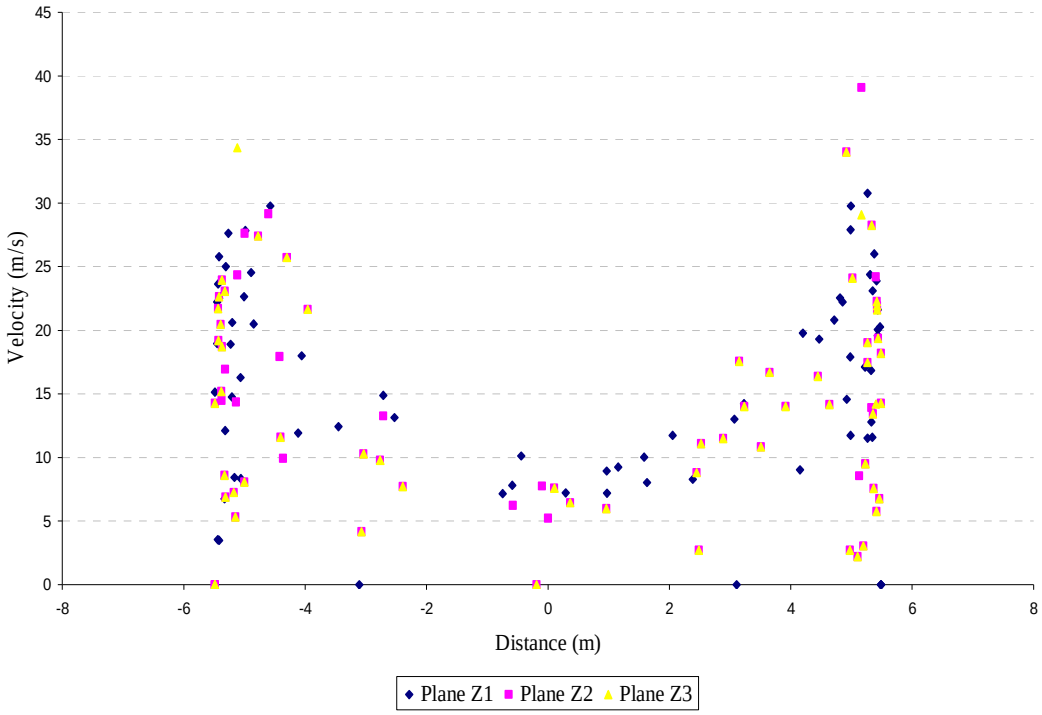

Figure D.6 Velocity distributions in burner zone for case 4

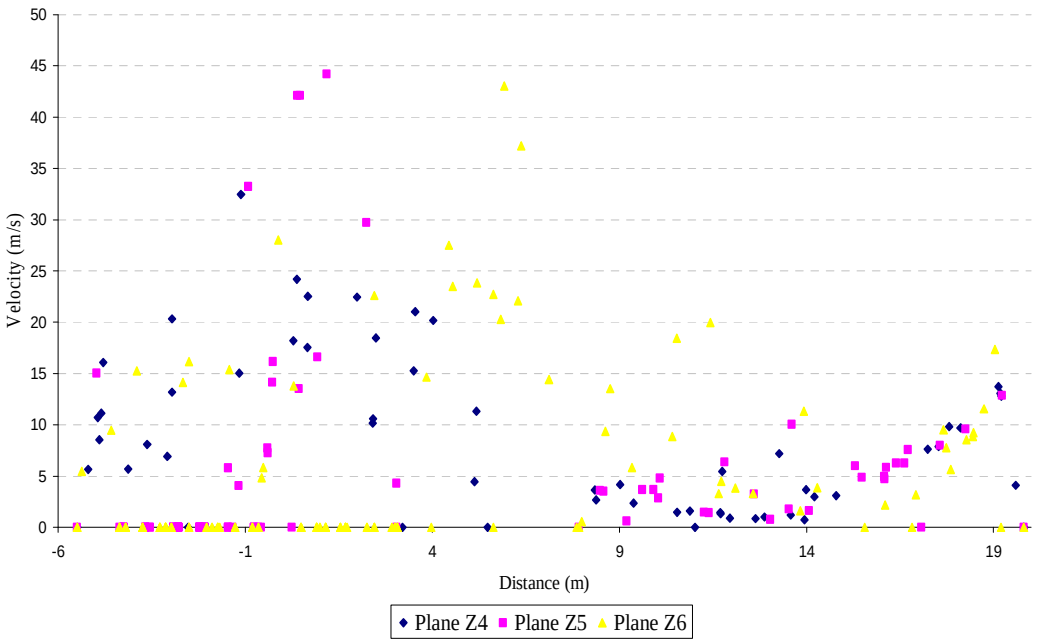

Figure D.7 Velocity distributions along nose for case 1

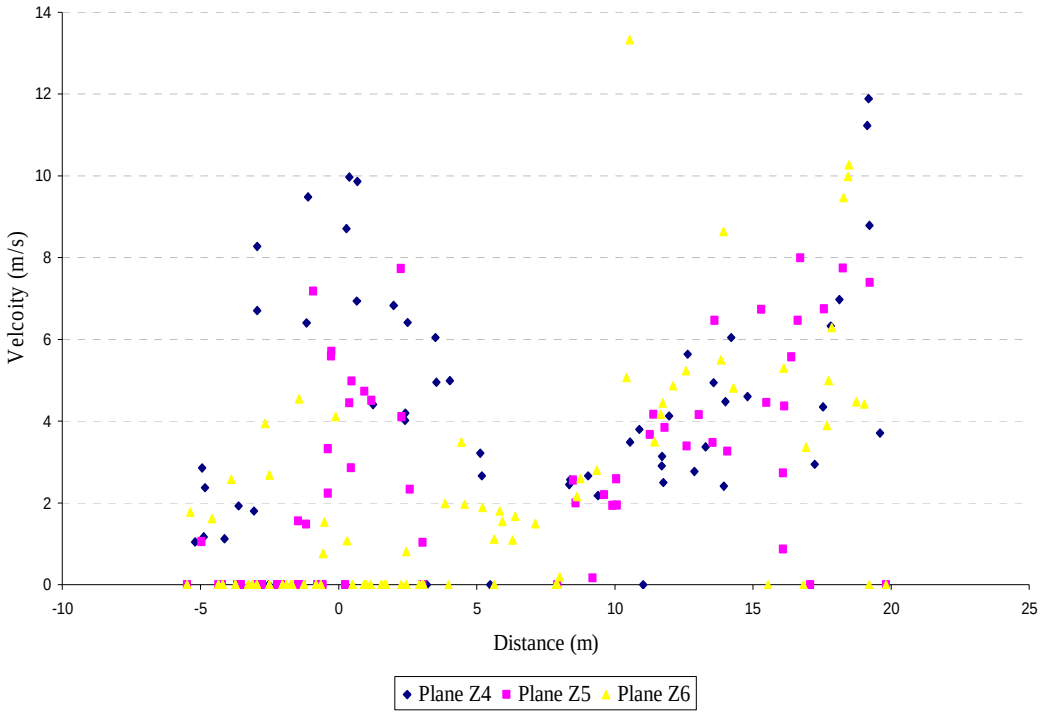

Figure D.8 Velocity distributions along nose for case 2

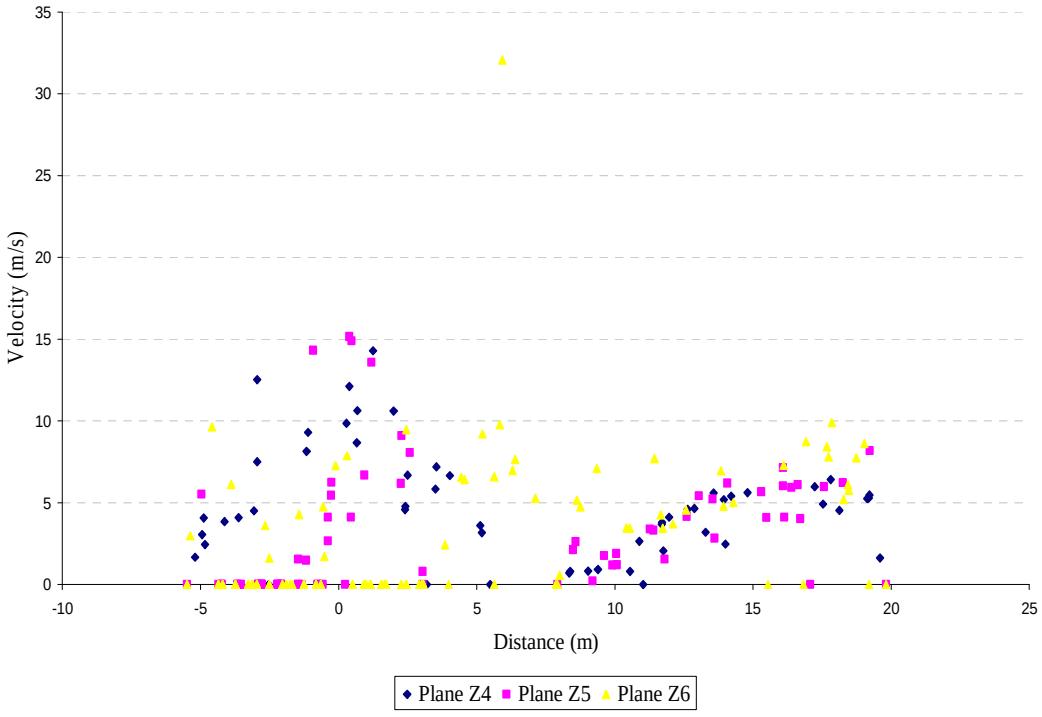

Figure D.9 Velocity distributions along nose for case 3

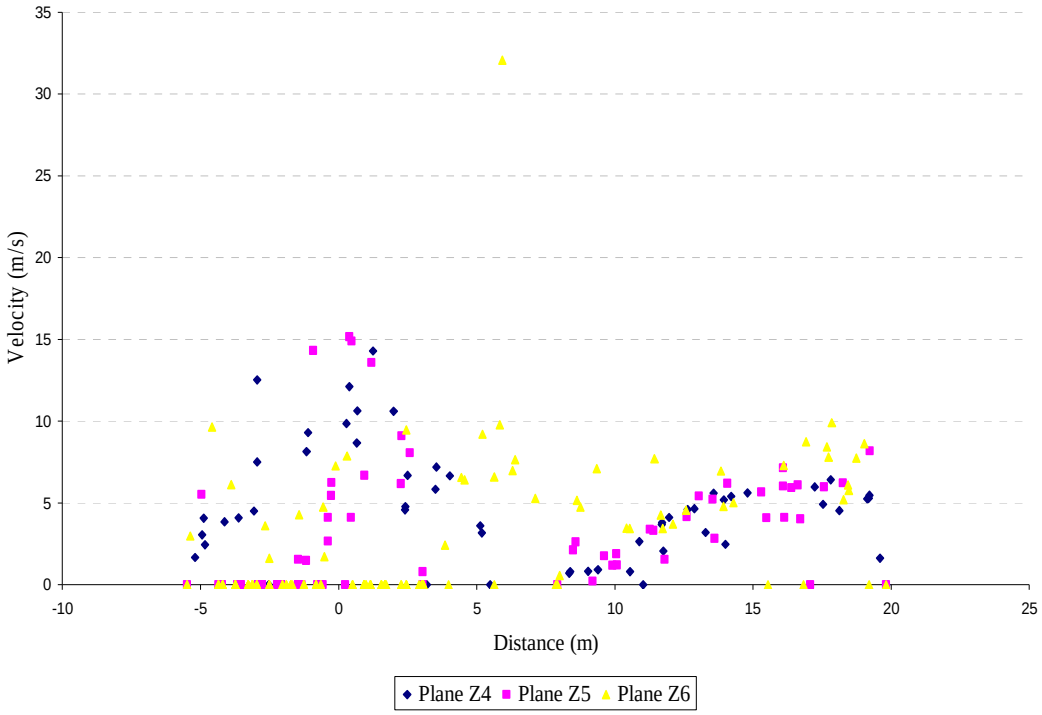

Figure D.10 Velocity distributions along nose for case 4

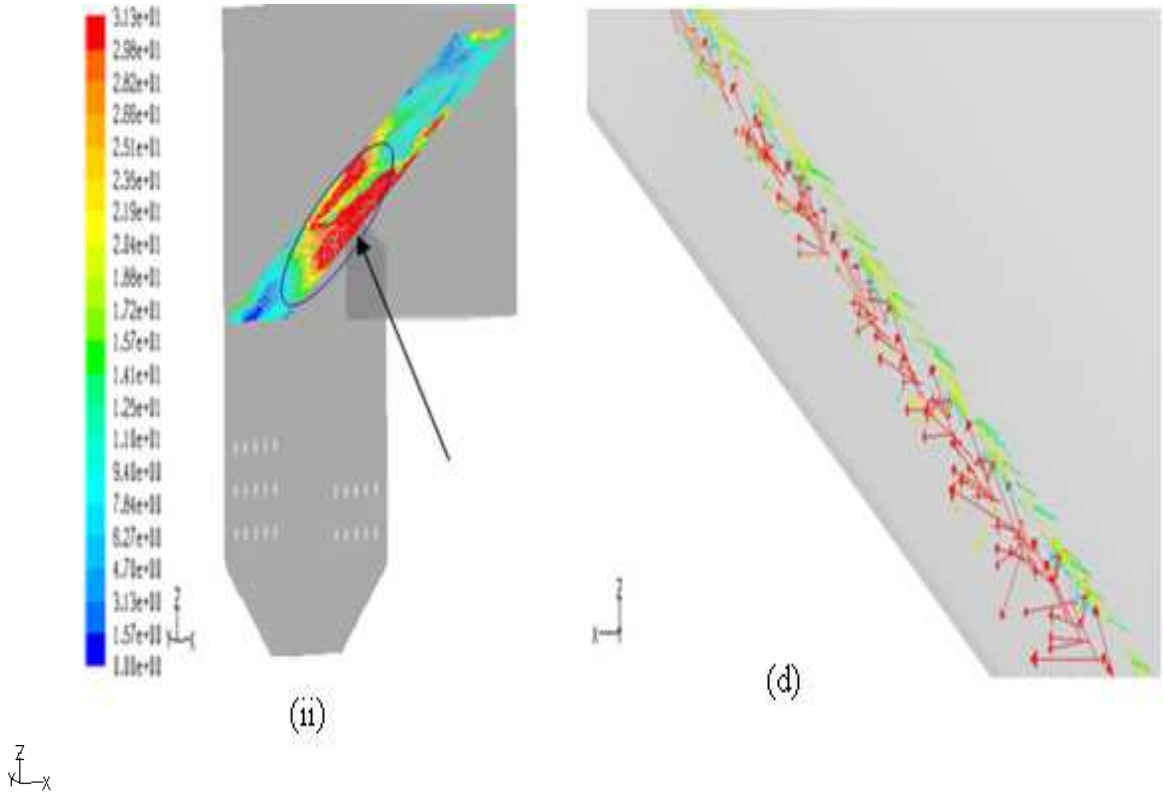

Figure D.11 Schematic of velocity distribution on inclined plane along the nose for Case 1

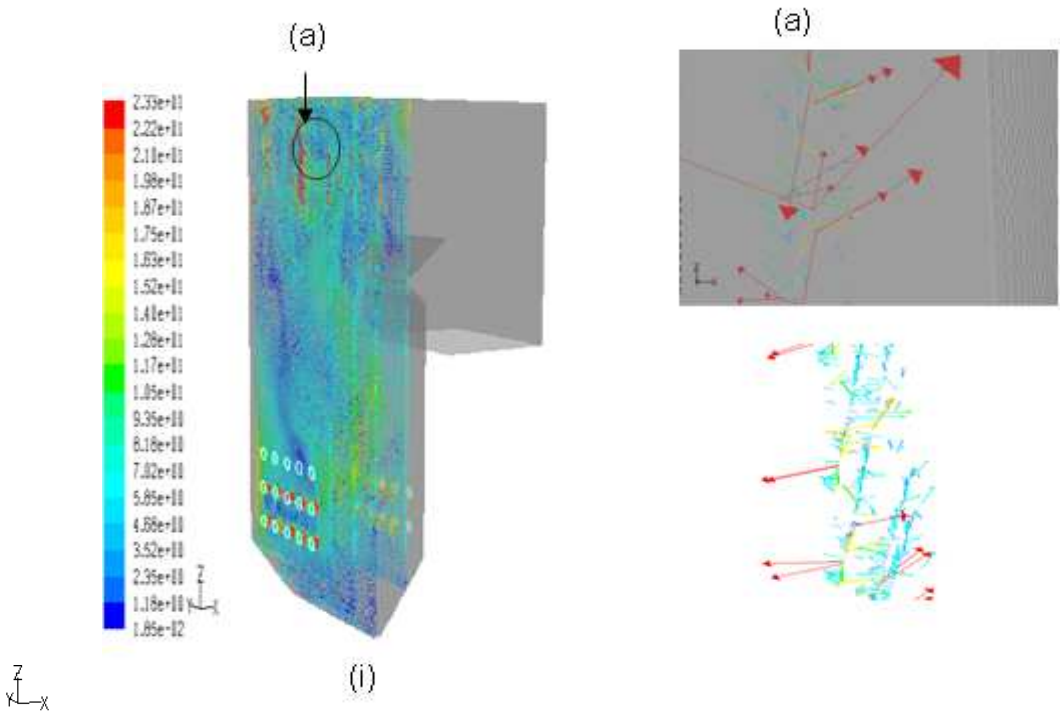

Figure D.12 Diagrams showing velocity distributions on different cross section in x direction for case 2 (i) close view of directional vectors in platen region (a) Close view of flow vectors in between secondary platen heater

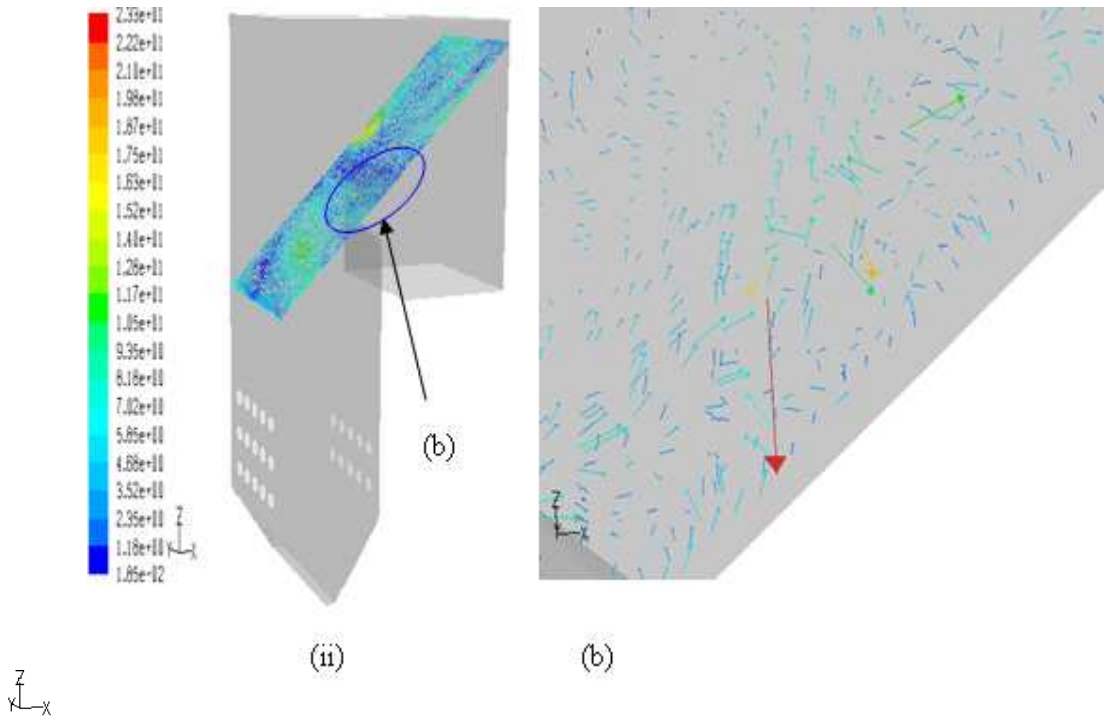

Figure D.13 (ii) Representation of velocity distributions on inclined plane along the nose for case 2 (b) Close view of plane inclined along nose for velocity vector

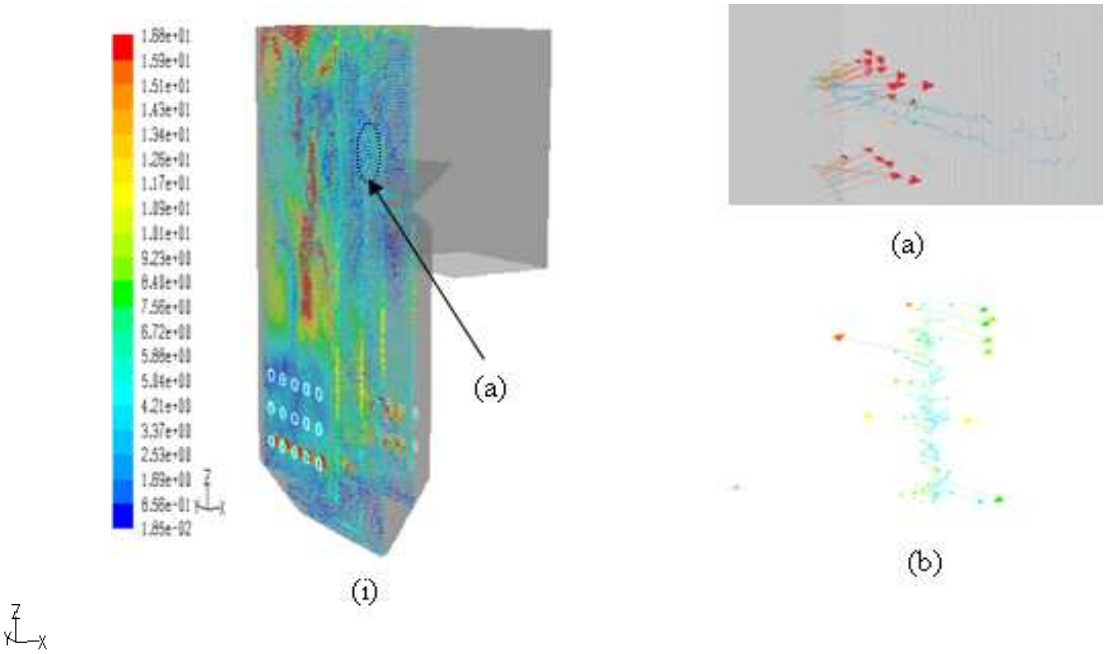

Figure D.14 Velocity distributions on different cross sections in X direction for case 3 (a) Close view of directional vectors on exit of secondary platen heater (b) Close view of flow vectors in between second and tertiary platen heater.

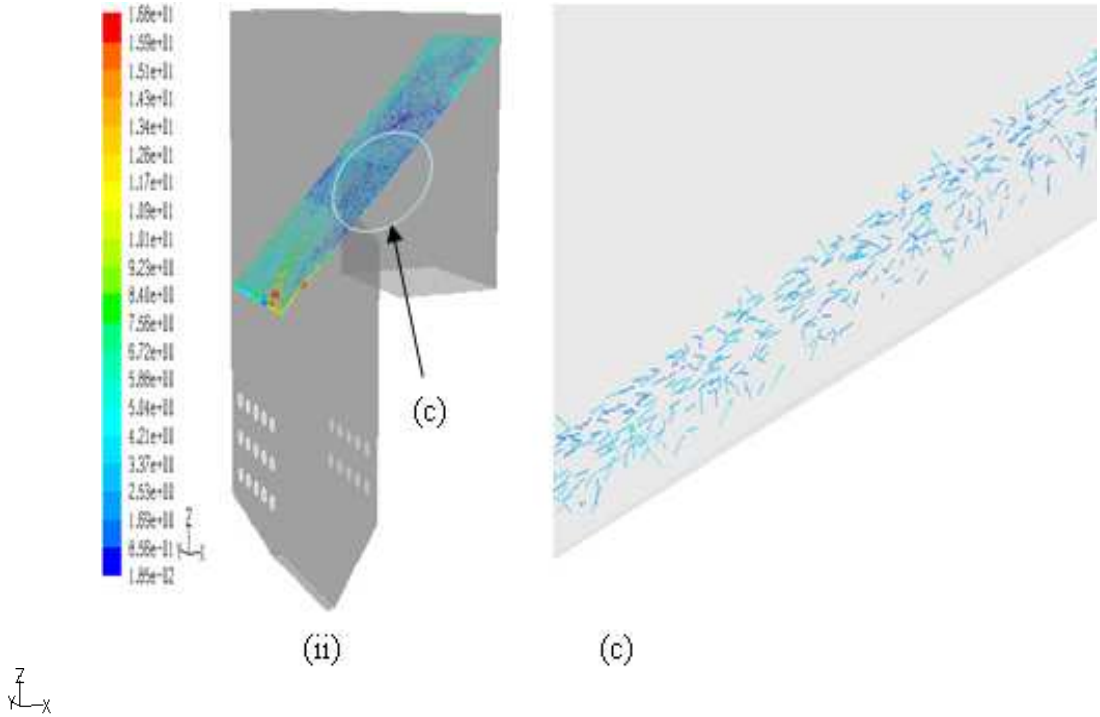

Figure D.15 Velocity distributions on inclined plane along the nose for case 3 (c) Close view of plane inclined along nose for velocity vector

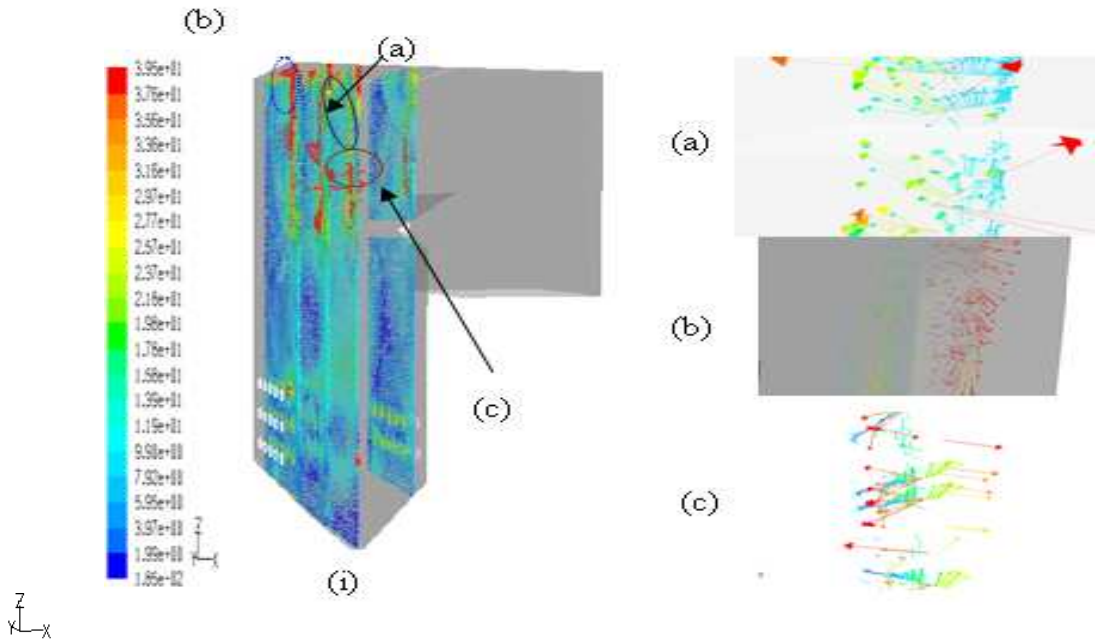

Figure D.16 Velocity distributions on different cross sections in X direction for case 4 (a) Close view of directional vectors plane across secondary platen heater (b) Close view of flow vectors near top corner of furnace wall (c) Close view of directional vectors on the edge of plates

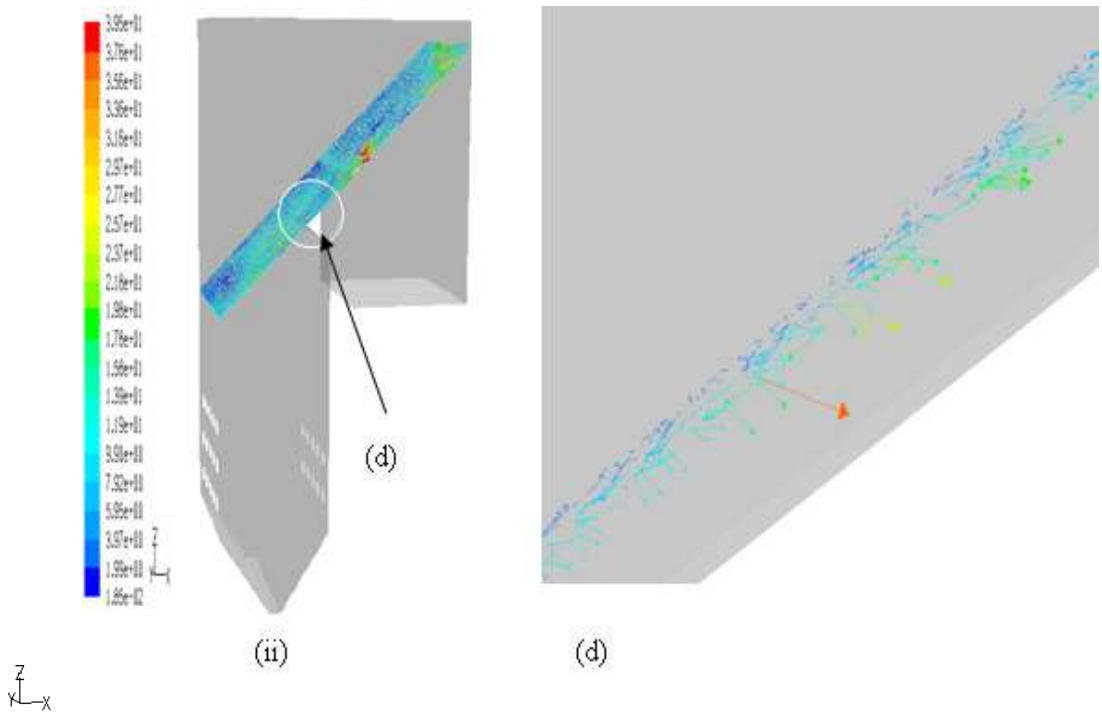

Figure D.17 Diagram showing velocity distribution on inclined plane along the nose for case 4 (d) Close view of plane inclined along nose for velocity vector

Appendix E

E.1 Case 2 (2-2 firing)

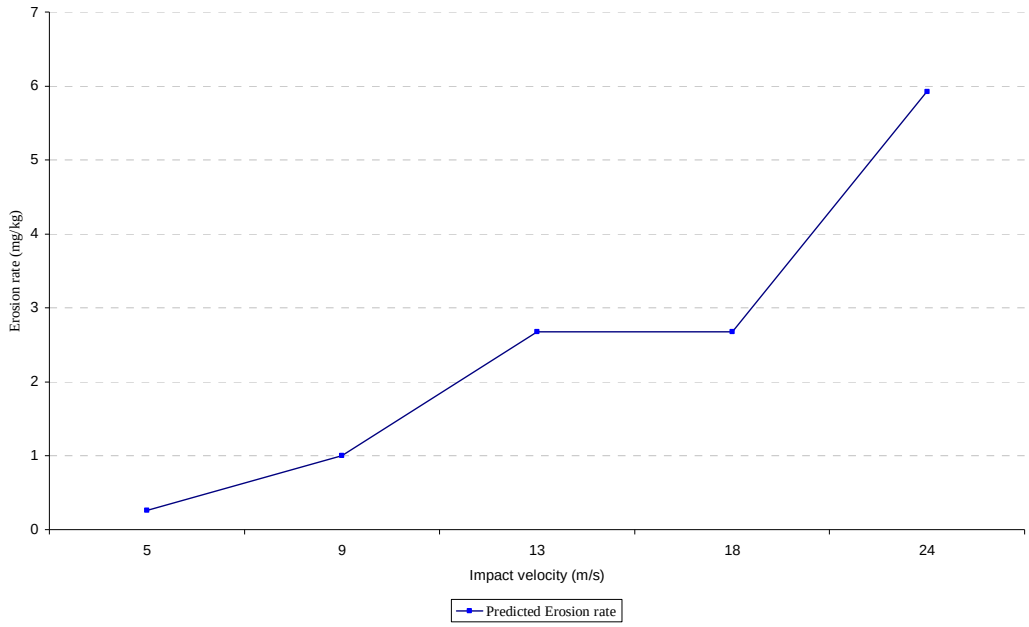

Figure E.1 Predicted erosion rate for different impact velocity at constant impingement angle (30°)

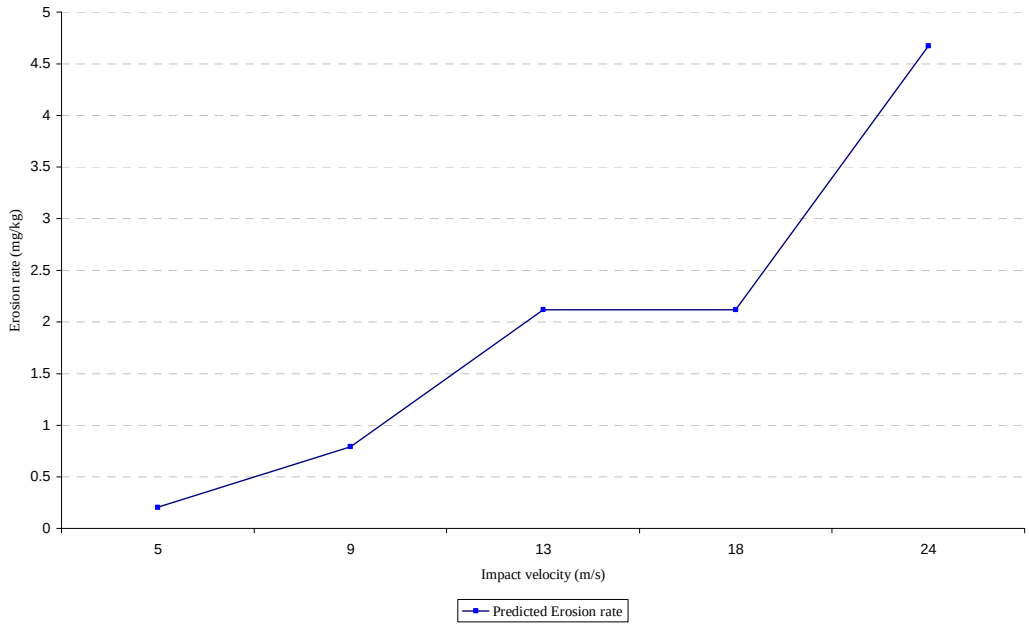

Figure E.2 Predicted erosion rate for different impact velocity at constant impingement angle (20°)

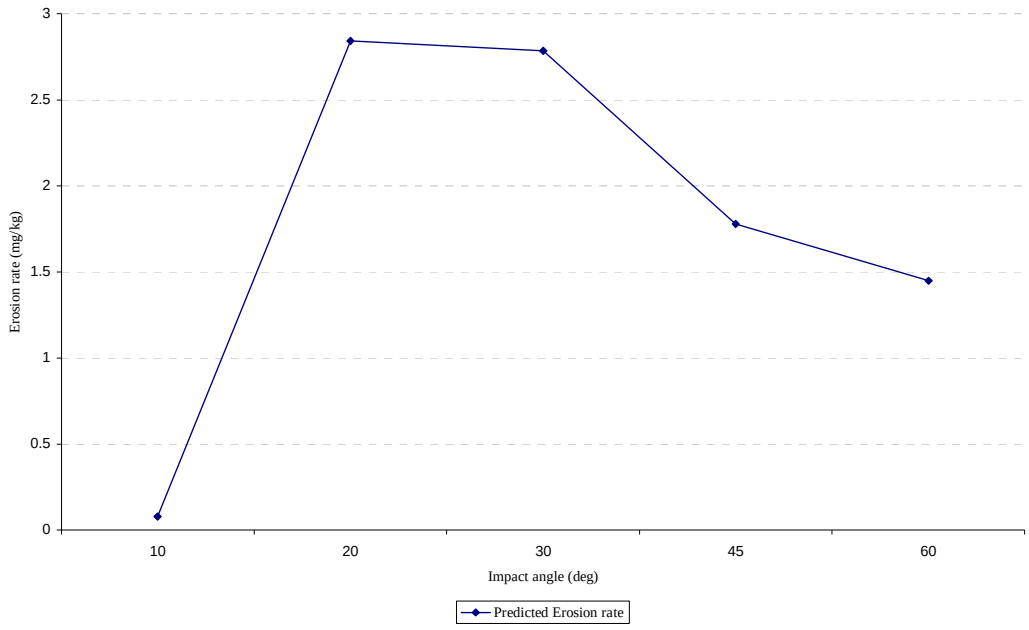

Figure E.3 Predicted erosion rate for different impingement angle at constant impact velocity (18 m/s)

E.2 Case 3 (2-1 firing)

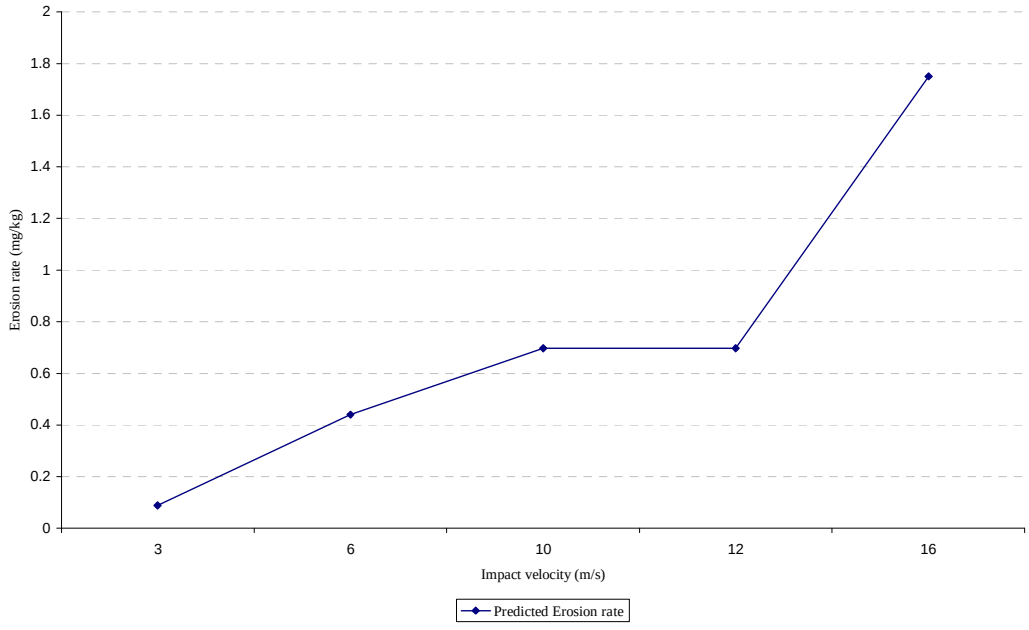

Figure E.4 Predicted erosion rate for different impact velocity at constant impingement angle (30°)

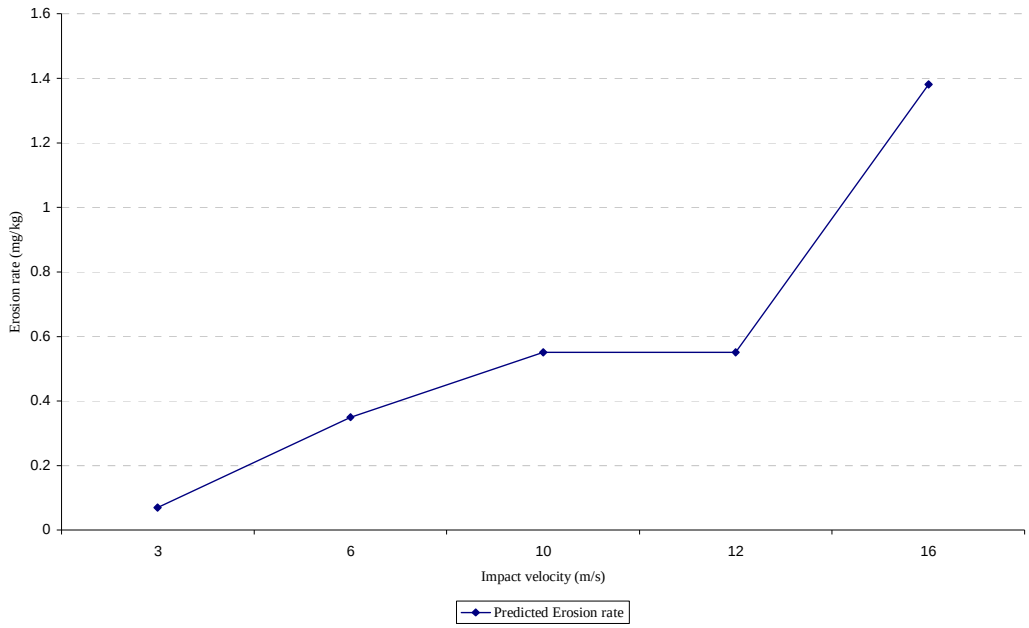

Figure E.5 Predicted erosion rate for different impact velocity at constant impingement angle (20°)

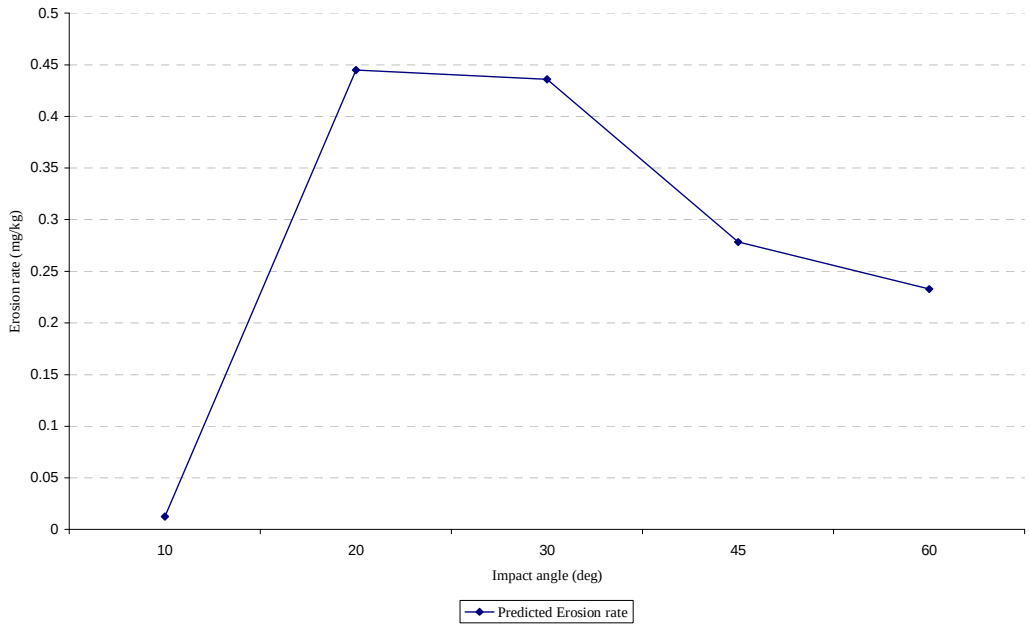

Figure E.6 Predicted erosion rate for different impingement angle at constant impact velocity (9.7 m/s)

E.3 Case 4 (Excess air)

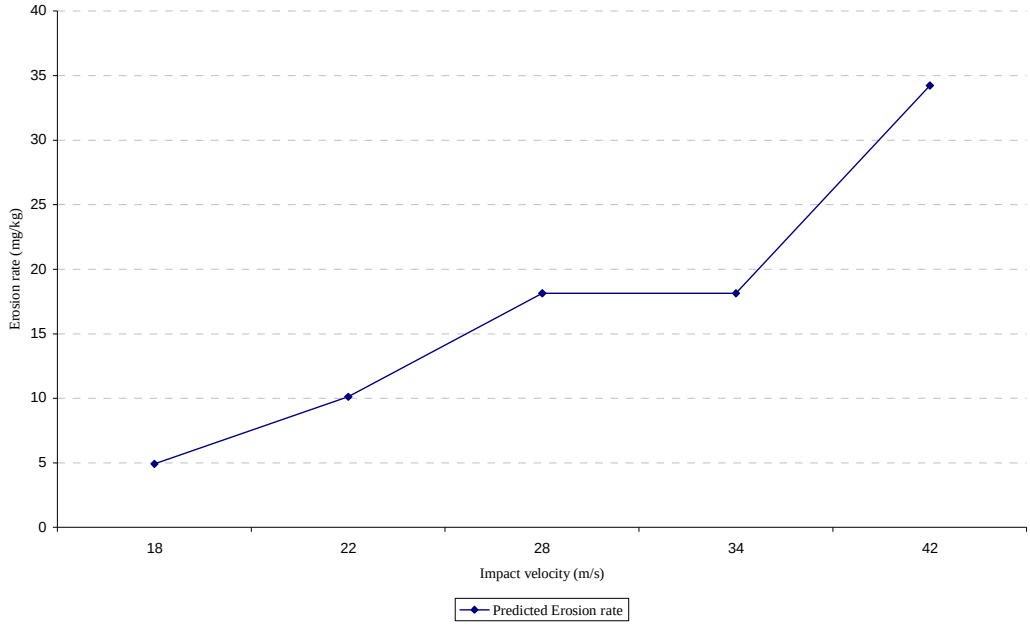

Figure E.7 Predicted erosion rate for different impact velocity at constant impingement angle (30°)

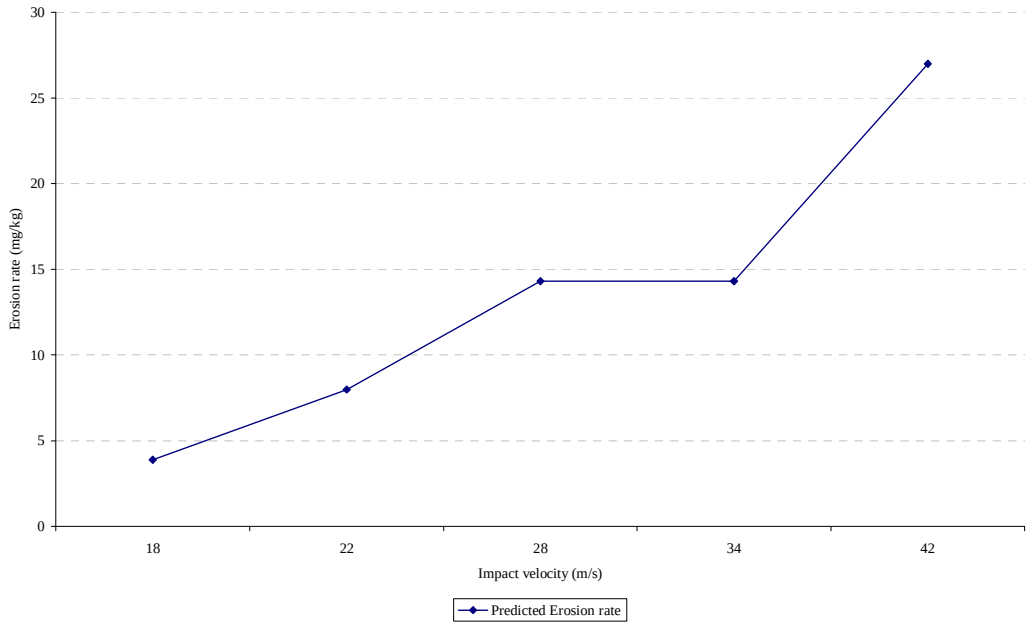

Figure E.8 Predicted erosion rate for different impact velocity at constant impingement angle (20°)

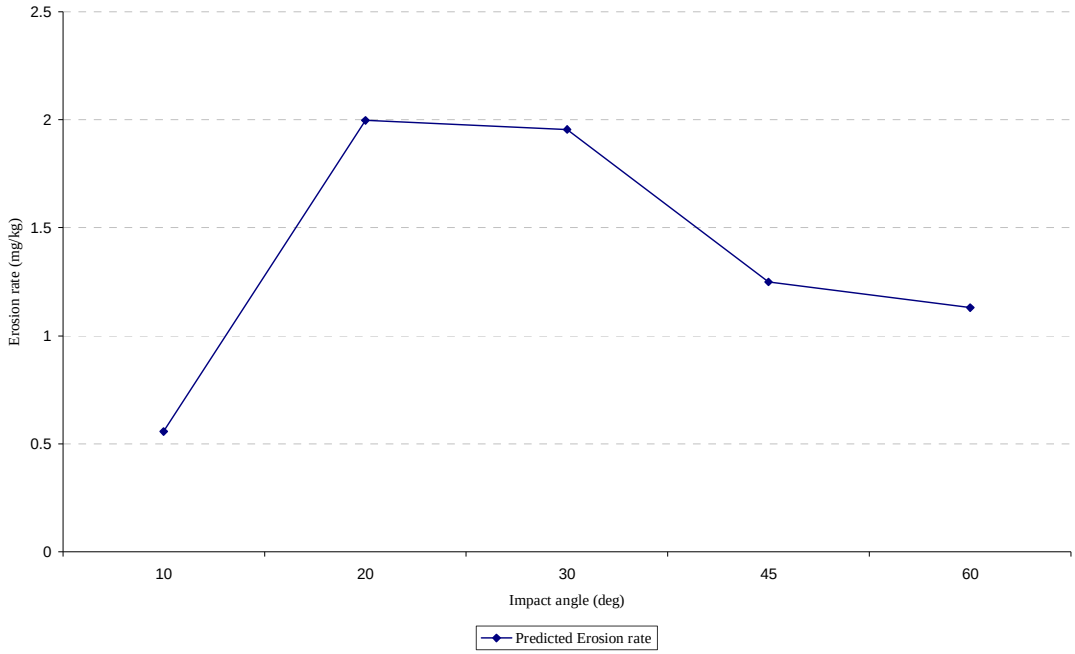

Figure E.9 Predicted erosion rate for different impingement angle at constant impact velocity (16 m/s)

Appendix F

F.1 Case 2 (2-2 firing)

Table F.1 Predicted erosion rate at different impact velocity at constant impingement angle 30°

Velocity (m/s)	Erosion rate (kg/mg)
4.9	0.26
8.18	1
12.82	2.68
17.79	2.68
23.15	5.93

Table F.2 Predicted erosion rate at different impact velocity at constant impingement angle 20°

Velocity (m/s)	Erosion rate (kg/mg)
4.9	0.20
8.18	0.79
12.82	2.12
17.79	2.12
23.15	4.67

Table F.3 Predicted erosion rate at constant velocity (18m/s) with different impingement angle

Angle (deg)	Erosion rate (kg/mg)
12.26	0.07
20.32	2.84
30.01	2.78
45.07	1.77
58.72	1.448

F.2 Case 3 (2-1 firing)

Table F.4 Predicted erosion rate at different impact velocity at constant impingement angle 30°

Velocity (m/s)	Erosion rate (kg/mg)
2.47	0.08
5.71	0.44
9.76	0.70
11.35	0.70
15.42	1.75

Table F.5 Predicted erosion rate at different impact velocity at constant impingement angle 20°

Velocity (m/s)	Erosion rate (kg/mg)
2.47	0.07
5.71	0.35
9.76	0.55
11.35	0.55
15.42	1.38

Table F.6 Predicted erosion rate at constant velocity (9.7m/s) with different impingement angle

Angle (deg)	Erosion rate (kg/mg)
12.26	0.01
20.32	0.44
30.01	0.43
45.01	0.27
58.72	0.23

F.3 Case 4 (excess air)

Table F.7 Predicted erosion rate at different impact velocity at constant impingement angle 30°

Velocity (m/s)	Erosion rate (kg/mg)
17.8	4.9
21.74	10.11
27.67	18.12
33.61	18.12
41.53	34.22

Table F.8 Predicted erosion rate at different impact velocity at constant impingement angle 20°

Velocity (m/s)	Erosion rate (kg/mg)
17.8	3.87
21.74	7.98
27.67	14.30
33.61	14.30
41.53	26.98

Table F.9 Predicted erosion rate at constant velocity (16m/s) with different impingement angle

Angle (deg)	Erosion rate (kg/mg)
12.26	0.55
20.32	1.99
30.01	1.95
45.07	1.24
58.72	1.13

APPENDIX G

Case 2: Partial load (80%)

DATA

Fuel: Sub-bituminous coal

Calorific Value (CV): 5135 Kcal/kg

Type of Furnace: Pulverized coal fired furnace

Power generation (PG): 264 MW

Boiler efficiency (BE): 77 % = 0.77

Turbine efficiency (TE): 38% = 0.38

Excess air (EA): 20%

Primary air distribution: 30%, Secondary air distribution: 70%

Cross sectional area of inner burner (From general arrangement (GA) drawing) = 0.2826 m^2

Cross sectional of outer burner (From general arrangement (GA) drawing) = 0.5024 m^2

Total Number of inner and outer burners in operation = 40

Calculations:

1. Coal flow rate calculations

$$\text{Coal Flow rate} = \frac{\text{PG (KW) / (hour)} * 860 \text{ (Kcal/ KW)}}{\text{CV (Kcal/ kg)} * \text{BE (\%)} * \text{TE (\%)} * 3600 \text{ Sec/ hour}}$$

$$= \frac{264 * 1000 * 860}{5135 * 0.77 * 0.38 * 3600}$$

= 41.97 kg/S

2. Air flow rate calculations

For typical bituminous coal, the air requirement as per stoichiometry comes out as 8 kg per kg of Coal. The calculations are already shown in Case 1.

Excess air was considered 20% for the pulverised coal firing furnace.

Therefore, Total air required

= Theoretical air * Coal flow rate * (1 +EA/100)

= 8 kg of air / kg of coal * 41.97 kg of coal / Sec * (1+20/100)

= 402.95 kg of air /sec

As per plant practice, 30% of the total air was supplied as primary air and rest 70% as secondary air.

Therefore,

Primary air flow rate (from inner burner) = 402.95 * 0.3 = 120.89 kg/s

Secondary air flow rate (from outer burner) = 402.95 * 0.7 = 282.06 kg/s

3. Air velocity calculations (Boundary condition for Fluent)

Flow rate (m^3/s) = cross sectional area (m^2) * velocity (m/s)

Therefore,

Primary air velocity (m/s) (through each burner)

= Flow rate (m^3/s)/(cross sectional area of burner(m^2) *Total number of running burners)

(Density of air = 1.2 kg / m^3)

Primary air velocity (m/s) = (120.89 / 1.2) / (0.2826 * 20) = 17.82 = @18 m/s

Secondary air velocity (m/s) = (282.06 / 1.2) / (0.5024 * 20) = 23.29 = @ 23 m/s

4. Coal injection value (Boundary condition for Fluent)

Total number of inner burners in operation from which coal will be injected = 20

Coal injection from each burner = 41.97/20 = 2.10 kg/s

Case 3: Partial load (60%)

DATA

Fuel: Sub-bituminous coal

Calorific Value (CV): 5135 Kcal/kg

Type of Furnace: Pulverized coal fired furnace

Power generation (PG): 198 MW

Boiler efficiency (BE): 77 % = 0.77

Turbine efficiency (TE): 38% = 0.38

Excess air (EA): 20%

Primary air distribution: 30%, Secondary air distribution: 70%

Cross sectional area of inner burner (From general arrangement GA drawing) = 0.2826 m^2

Cross sectional of outer burner (From general arrangement GA drawing) = 0.5024 m^2

Total Number of inner and outer burners in operation = 30

Calculations:

1. Coal flow rate calculations

$$\text{Coal Flow rate} = \frac{\text{PG (KW) / (hour) * 860 (Kcal/ KW)}}{\text{CV (Kcal/ kg)* BE (\%) *TE (\%) * 3600 Sec/ hour}}$$

$$= \frac{198 * 1000 * 860}{5135 * 0.77 * 0.38 * 3600}$$

= 31.48 kg/S

2. Air flow rate calculations

For typical bituminous coal, the air requirement as per stoichiometry comes out as 8 kg per kg of Coal. The calculations are already shown in Case 1.

Excess air was considered 20% for the pulverised coal firing furnace.

Therefore, Total air required

= Theoretical air * Coal flow rate * (1 +EA/100)

= 8 kg of air / kg of coal * 31.48 kg of coal / Sec * (1+20/100)

= 302.22 kg of air /sec

As per plant practice, 30% of the total air was supplied as primary air and rest 70% as secondary air.

Therefore,

Primary air flow rate (from inner burner) = 302.22 * 0.3 = 90.66 kg/s

Secondary air flow rate (from outer burner) = 302.22 * 0.7 = 211.55 kg/s

3. Air velocity calculations (Boundary condition for Fluent)

Flow rate (m^3/s) = cross sectional area (m^2) * velocity (m/s)

Therefore,

Primary air velocity (m/s) (through each burner)

= Flow rate (m^3/s)/(cross sectional area of burner(m^2) *Total number of running burners)

(Density of air = 1.2 kg / m^3)

Primary air velocity (m/s) = (90.66 / 1.2) / (0.2826 * 15) = 17.82 = @18 m/s

Secondary air velocity (m/s) = (211.55 / 1.2) / (0.5024 * 15) = 23.29 = @ 23 m/s

4. Coal injection value (Boundary condition for Fluent)

Total number of inner burners in operation from which coal will be injected = 15

Coal injection from each burner = 31.47/15 = 2.10 kg/s

Case 4: Full load (100%) – 30% Excess air

DATA

Fuel: Sub-bituminous coal

Calorific Value (CV): 5135 Kcal/kg

Type of Furnace: Pulverized coal fired furnace

Power generation (PG): 330 MW

Boiler efficiency (BE): 77 % = 0.77

Turbine efficiency (TE): 38% = 0.38

Excess air (EA): 30%

Primary air distribution: 30%, Secondary air distribution: 70%

Cross sectional area of inner burner (From general arrangement (GA) drawing) = 0.2826 m^2

Cross sectional of outer burner (From general arrangement (GA) drawing) = 0.5024 m^2

Total Number of inner and outer burners in operation = 50

Calculations:

1. Coal flow rate calculations

$$\text{Coal Flow rate} = \frac{\text{PG (KW) / (hour) * 860 (Kcal/ KW)}}{\text{CV (Kcal/ kg)* BE (\%) *TE (\%) * 3600 Sec/ hour}}$$

$$= \frac{330 * 1000 * 860}{5135 * 0.77 * 0.38 * 3600}$$

= 52.47 kg/S

2. Air flow rate calculations

For typical bituminous coal, the air requirement as per stoichiometry comes out as 8 kg per kg of Coal. The calculations are already shown in Case 1.

Excess air was considered 30% for the pulverised coal firing furnace.

Therefore, Total air required

= Theoretical air * Coal flow rate * (1 +EA/100)

= 8 kg of air / kg of coal * 52.47 kg of coal / Sec * (1+30/100)

= 545.67 kg of air /sec

As per plant practice, 30% of the total air was supplied as primary air and rest 70% as secondary air.

Therefore,

Primary air flow rate (from inner burner) = 545.67 * 0.3 = 163.70 kg/s

Secondary air flow rate (from outer burner) = 545.67 * 0.7 = 381.97 kg/s

3. Air velocity calculations (Boundary condition for Fluent)

Flow rate (m^3/s) = cross sectional area (m^2) * velocity (m/s)

Therefore,

Primary air velocity (m/s) (through each burner)

= Flow rate (m^3/s)/(cross sectional area of burner(m^2) *Total number of running burners)

(Density of air = 1.2 kg / m^3)

Primary air velocity (m/s) = (163.70 / 1.2) / (0.2826 * 25) = 17.82 = @19.31 m/s

Secondary air velocity (m/s) = (381.97 / 1.2) / (0.5024 * 25) = 23.29 = @ 25.34 m/s

4. Coal injection value (Boundary condition for Fluent)

Total number of inner burners in operation from which coal will be injected = 25

Coal injection from each burner = 52.47/25 = 2.10

Reference:

Abbas, T, Costen, PG, Lockwood, FC, (1996), *26th International Symposium on Combustion*, the Combustion Institute, pp.3041

Adler,WF,(Ed), "Erosion : Prevention and Useful Applications, *ASTM STP* 664, pp. 59-76

Arand,JK, Muzio,LJ and Barbour,RL,(1985)" Emission Assessment of Refuse-Derived Fuel Combustion: Suspension Firing", Research and Development EPA 600 52-85 117 December, 1985**.**

Baukal, CE, Gershtein, VY, Li, X, (2000), "Computational fluid Dynamics in Industrial Combustion", Industrial combustion series: CRC press

Belosevic, S, Sijercic, M, Tucakovic, D, Crnomarkovic, N, (2008) "A numerical study of a utility boiler tangentially-fired furnace under different operating conditions" *Fuel* 87(15-16): pp.3331-3338

Belosevic.S, Sijercic,M, Simeon,O, Tucakovic, D,(2006)," Three dimensional modelling of utility boiler pulverised coal tangentially fired furnace" *International Journal Heat and Mass transfer* 49,pp.3371-3378

Benson, SA, Holm, PL, (1985),"Composition of inorganic constituents in three low rank coals", *Industrial and Engineering chemistry, Product Research and Development* 24, pp. 145-149

Bhatt, SM, (2006),"Effect of ash in coal on the performance of coal fired Thermal power plants. Part-II capacity and secondary energy effects", Energy Sources part A, 28, pp.43-58

Bhattacharya,C, Kr. Mitra,A,(2007)," Improving pulverizer output by partial flue gas recirculation", *Proceedings of International Conference on Advances in Energy*

Research 2007: December 12 – 14, 2007, Indian Institute of Technology, Mumbai, India.

Bingley, MS, Deng, T, Bradley, MSA , (2003)," The influence of particle rotation on the solid particle erosion rate of metals", *Wear* 256, pp.1037-1049

Bird, RB, Stewart, WE, Lightfoot, EN, (1960), *Transport phenomena*, New York, Wiley

Boyd, RK, Kent, JH, (1986)," Three dimensional furnace computer modelling", *Twenty first Symposium on combustion*, pp.265-274

Bitter, JGA, (1963)," Study of erosion phenomena part 1" *Wear*, 6, pp.5-21

Bitter, JGA, (1963)," Study of erosion phenomena part 2", *Wear* 6, pp. 169-191

Carpenter, AM, Stephen, N, David, HS, Zhangfa,W,(2005)," Effects of coal ash on combustion system", *IEA clean coal centre*, London,UK

Carpenter, AM, (2002)"Coal quality assessment the validity of empirical tests," *IEA clean coal centre*, clean coal centre, London

Carvalho, MG, Azevedo, JLT, Xu, M, (2001)," Modelling of a front wall fired utility boiler for different operating conditions", *Computer methods in applied mechanics and engineering* 190, pp.3581-3590

Choi, CR, Kim, CN, (2009)," Numerical investigation on the flow, combustion and NOx emission characteristics in a 500 MWe tangentially fired pulverised- coal boiler", *Fuel*, pp.1-12

Das, SK, Godiwalla, KM, Hegde, SS, Mehrotra, SP, Dey, PK (2007), "Mathematical models to characterize effect of silica content in the boiler fly ash on erosion behaviour of boiler grade steel." *Journal of Materials Processing Technology*, pp.239-247

Davis, RM, (1949) *Proc.Roy.Soc*.pp.197

DE Haller, P, (1939),"Erosion and cavitations-erosion", Vol.2, *Springer Verlag*, pp.471-488

Devendra, C, (2005)," Monitoring and controlling the stack gas temperature"

Durst, F, Milojevic, D, Schonung, B, (1984), "Eulerian and Lagrangian predictions of particulate two phase flow – a numerical study", *applied mathematical modelling*, 8, pp. 101

Eaton, M, Smoot, LD, Hill, SC, Eatough, CN, (1999)," Components, formulations, solutions, evaluation, and application of comprehensive combustion models", *Prog. Energy, Combustion science* 25 , pp.387-436

Fan, J, Zhou , D, Cen , K, Jin, J, (1990)," Numerical prediction of tube row erosion by coal ash impaction", *Chem. Eng. Commun*. 95, pp.75-88

Ferziger,JH, Milovan, P, (1999),"Computational methods for fluid dynamics", *Springer publication*

Filkoski, RV, Belosevic, SV, Petrovski, IJ, Oka, SN, Sijercic, MA (2006), "Computational fluid dynamics technique as a tool for description of the phenomena occurring in pulverised coal combustion systems", *Proceeding of the institute of Mechanical Engineers*,pp.221, 399

Finnie, I , (1960)," Erosion of surface by solid particles", *Wear* 3, pp.87-103

Finnie, I, (1972)," Some observations on the erosion of ductile metals", *Wear* 19,pp. 81-89

Finnie, I ,(1962), " Erosion and cavitations", *Am. Soc. Test. Mater. Spec. Tech. Publ. STP* 307, pp.70-82

Finnie, I, Kabil, YH, (1965) ,*wear* 8 pp.60-69

Finnie,I, McFandden ,DH,(1978), *wear* 48 pp.181-190

Finkelman, RB, (1994),” Abundance, source and mode of occurrence of the inorganic constituents in coal”. *Coal Istanbul technical University*, Istanbul, pp.15-125

Field, MA, Gill, DW, Morgan, BB, Hawksley PGW, (1967),” Combustion of pulverised coal”. BCURA

Fluent 6.3.26, (2007) User Guide, Fluent Inc.,

Gee, MG, Gee, RH, McNaught, I, (2003),” Stepwise erosion as a method for determining the mechanisms of wear in gas air borne particulate erosion”, *Wear* 255, pp. 44-55

Given PH, Spackman, W,(1978), “Reporting of analyses of low rank coals on the dry, mineral matter free basis”, *Fuel* 57, pp.319

Glarborg, p, Jensen, AD, Johnson, JE, 2003 “Fuel nitrogen conversion in solid fuel fired systems”, *Process in Energy and Combustion Science*; 29; pp 89-113

Grant,G, Tabakoff,W,(1975),” Erosion prediction in turbo machinery resulting from encironmental solid particles”, *J.Aircraft* 12 pp. 471-478

Gupta, RP, Wall, TF, Kajigaya,I, Miyamae, S, Tsumita, Y, (1998), “Computer-controlled scanning electron microscopy of minerals in coal”, *Progress in energy combustion science* 24, pp.523-545

Gupta, R, Wall, TF, Baxter, LA (Eds), (1999b),”The impact of mineral impurities in solid fuel combustion” Plenum, New York, pp.768

Harvey, RD, Ruch, RR, (1986),” Mineral matter in Illinois and other US coals”, In:Vorres,K,S, (Eds), “Mineral matter in coal ash and coal”, *American chemical society symposium series* ,301,pp.10-40

http://www.iea.org/textbase/nppdf/free/1990/frtrolecoal99.pdf

http://www.rsbweb.nih.gov/ij/download.html

http://www.engineeringtoolbox.com/fuels-combustion-efficiency-d_167.html

Hurley, JP, Schobert, HH (1993), “Ash formation during pulverised sub bituminous coal combustion. 2. Inorganic transformations during middle and late stages of burnout” *Energy and Fuels*, 7, 542-553

Hutchings, IM (1980) "A model for the erosion of metals by spherical particles at normal incidence” *Wear*, 70, pp.269-281

Hutchings, I, Winter, RE, (1974),” Particle erosion of ductile metals: a mechanism of material removal, *Wear* 27, pp.121-128

Hutchings, IM, (1977),” Deformation of metal surfaces by the oblique impact of square plates”, *International Journal of Mechanical Science*, 19, pp.45-52

Hutchings, IM, (1979),” Mechanism of erosion of metal by solid particles”, In: Adler,WF,(Ed), “Erosion : Prevention and Useful Applications, *ASTM STP* 664, pp. 59-76

Ives, LK, Ruff, AW, (1979), *ASTM Spec. Tech. publ.*664, pp.5

Ianzo,I, Domingo,E, Cortes,C, Arauzo, I,(1985)” Combustion characterisation of a pulverised coal utility boiler based on CFD techniques”, *CIRCE*, Spain

Jianren, F, Ping, S, Youqu, Z , Xinyu,Z, Kefa,C,(1999),”A numerical study of a protection technique against tube erosion”, *Wear* 225-229,pp. 458-464

Jones, WP, Wille, M, (1996),” Large eddy simulation of a plane jet in a cross- flow”, International journal of Heat and fluid flow 17(3), pp. 296-306

Jun, YD, Tabakoff, W, (1994),”Numerical simulation of a dilute particulate flow (laminar) over tube banks,” Trans. ASME: *Journal of fluids engineering* 116, pp.770-777

King, JG, Maries, MB, Crossley, HE, (1936), “Formulas for the calculation of coal analyses to a basis of coal substance free from mineral matter”, *Journal of Society of chemical industry* 55, pp.277-281

Kiss, LT, King, TN, (1977)," The expression of results of coal analysis: the case for brown coals", *Fuel* 56, pp.340-341

Kiss, LT, King, TN, (1979)," Reporting of low rank coal analysis – the distinction between minerals and inorganic", *Fuel* 58, pp.547-549

Kjäldman, L,(1993),"Numerical simulation of combustion and nitrogen pollutants in furnaces", VTT Finland

Launder, BE, Spalding, DB,(1972) *Lectures in mathematical models of turbulence*. Academic Press, New York,

Lee, BE, Fletcher, CAJ, Behina, M, (1999)," Computational prediction of tube erosion in coal fired power utility boilers", *Journal of energy gas turbines power* 121, pp. 746-750

Levy, AV,(1986),"The platelet mechanism of erosion of ductile metals", *Wear* 180, pp. 1-21.

Lookwood, FC, Salooja, AP, Syed,SA,(1980),"A prediction method for coal fired furnace", *Department of Mechanical Engineering*, Imperial College of Science and Technology, London.

Magnussen, BF, Hjertager, BH,(1976)," *Sixteenth Symposium (International) onCombustion*, The Combustion Institute, pp. 719

Manickam,M, Schwarz, MP, Mcintosh, MJ,(1999)," CFD analysis of erosion of bifurcation duct walls", *Second International Conferences on CFD in the Minerals and Process Industries*, pp.243-248

Magasiner,N, van Alphen,C, Dr Inkson,M and Misplon,B, "Characterising Fuels For Biomass – Coal Fired Cogeneration", Thermal energy systems.

Mbabazi, JG, Sheer, TJ, Shandu, R, (2004)," A model to predict erosion on mild steel surfaces impacted by boiler fly ash particles", *Wear* 257, pp.612-624

Mbabazi, JG, Sheer, TJ, (2006)," Computational prediction of erosion of air heater elements by fly ash particles", *Wear* 261, pp. 1322-1336

Meng, HC, Ludema, KC, (1995),” Wear models and predictive equations: their form and content”, *Wear*181-183, pp. 443-457

Miller, RN, Given, PH, (1978),” A geochemical study of the inorganic constituents of some low rank coals” *Report, coal research section*, Pennsylvania state university,pp.314

Miller, RN, Given PH, (1986),” The association of major, minor and traces elements with lignite: 1- Experimental approach and study of North Dakota lignite”, Geochimica et cosmochimica Acta 50, pp.2033-2043

Molinari, JF, Ortiz, M, (2002),” A study of solid particle erosion of metallic targets, *Int. J. Impact Eng.* 27, pp. 347-358

Niksa, S (1996), “Coal combustion modelling”, IEAPER/31, *IEA Coal Research*, London

Parr, SW, (1928),“The classification of coal”, University of Illinois Engineering experimental station, Bulletin 180 pp.62

Raask, E, (1969),” Tube erosion by ash impaction”, *Wear* 13, pp.301-315

Raask, E, (1985),” Mineral impurities in coal combustion: Behaviour problems and remedial measures”. *Hemisphere Publishing*, New York, pp.484

Rickerby, DG, Macmillan, NH, (1980) *wear*, 60, pp.369

Rodrigues,CP, Lansarin,MA, Secchi,AR, and Mendes,TF,(2005),” Simulation of pulverized coal fired boiler- Reaction chamber”, Engenharia Térmica *(Thermal Engineering),* Vol. 4 · pp. 61-68.

Saario,A and Oksanen, A,(2007),” Effect of computational grid in industrial-scale boiler modelling”, *International journal of Numerical methods for heat and fluid flow*, Vol.19,pp 93-117

Sahajwalla V, Eghlimi, A, Farrell,K, (1997),” Numerical simulation of pulverised coal combustion”, *International conference CFD in Mineral and Metal processing and power generation,* pp.195-207

Sheldon,GI, Kanhere,A, (1972),” An investigation of impingement erosion using single particles”, *Wear* 21, 195-209

Siegel, R and Howell, JR, (1992),” Thermal Radiation Heat Transfer”, Washington DC, *Hemisphere Publishing Corporation*

Smeltzer, CE, Gulden, ME, Compton, WA, (1970) *J.Basic Eng*., 92,pp. 639

Smith, GD,(1985),”*Numerical solution of partial differential equation: finite difference methods”*, 3rd ed. Oxford: Clarendon Press

Smooth, LD, (1993),” Fundamentals of coal combustion for clean and efficient use” *ElsevierPublication*

Spalding, DB,(1970),” *Thirteenth Symposium (International) on Combustion”*, the Combustion Institute, , pp. 649

Speziale, CG, (1987),”On nonlinear $K-I$ and K - ε ; models of turbulences”, *Journal of Fluid mechanics* 178, pp.459-475

Standards Australia, (1995), “Coal and coke- glossary of terms”, *Australian standard* 2418, pp.180

Stockwell, N, Zhang, C, Ishii,T, Hino,Y,(2001),”Numerical Simulations of Turbulent Non-premixed Combustion in a Regenerative Furnace”, *ISIJ International*, Vol. 41, pp.1272–1281

Sundararajan, G, (1984),”The effect of temperature on solid particle erosion”, *Wear* 98, pp.141-149

Tabakoff, W, Gat, N, (1978), *Wear* 50, pp.85

Tabor, D, (1951),” The hardness of metals”, *Oxford university press*

Taylor, GH, Teichmuller, M, Davis, A, Diessel, CFK, Littke, R, Robert, P, (1998),”Organic Petrology”, Berlin,pp.704

Thompson, JF, Soni, BK, Weatherill, NP, (1999), *Handbook of grid generation* Boca Raton

Tillman, DA, (1991), "The combustion of solid fuels and wastes", London, UK, Academic Press, Inc. pp 378

Tomeczek, J, (1994), "Coal Combustion", *Krieger Publication*

Tu ,JY,Fletcher, CAJ, Behina, M, Reizes, JA, Owens, D, Jones, P,(1997),"Prediction of flow and erosion in power utility boilers and comparison with measurement", *Journal of energy gas turbines power* 119, pp. 709-716

Turner,WC, Doty,S,(2006)," Energy management handbook", *Sixth edition*, Tylors and Francis ltd.

Virtanen,ME, Heikkinen,RE, Patrikainen,HT, Laitinen, RS,(1999)," A novel application of CCSEM for studying agglomeration in fluidised bed combustion", In: Gupta, R, Wall, TF, Baxter, LA (Eds), Impact of mineral impurities in solid fuel combustion. *Plenum*, New York, pp.147-154

Van Riemsdijk , AJ, Bitter, JGA, (1959), *Fifth world petroleum congress*, New York, Section VII, paper 4

Versteeg, HK, Malalasekera, W,(2007),"An introduction to computational fluid dynamics", The finite volume method, second edition

Vuthaluru, R and Vuthaluru, HB (2006) "Modelling of a wall fired furnace for different operating conditions using FLUENT." *Fuel Processing Technology* 87(7): 633-639

Ward,CR, (Ed),(1984),"coal geology and coal technology", *Black well, Oxford*, pp.345

Ward, CR, (1991),"Mineral matter in low rank coals and associated strata of the Mae Moh Basin, northern Thailand, *International journal of coal geology* 17, pp. 69-93

Ward, CR, (1992)," Mineral matter in Triassic and tertiary low rank coals from South Australia", *International journal of coal geology* 20, pp.185-208

Ward.CR (2002)," Analysis and significance of mineral matter in coal seams", *International Journal of Coal Geology* 50, pp.135-168

Warnatz, J, Maas, U, Dibble, RW," Combustion – Physical and Chemical Fundamentals, Modelling and Simulation, Experiments, Pollutant Formation, Springer-Verlag, Berlin, 1993, 2001

Wee, HL (2006),"Collie coal ash deposition and its relation to boiler operation and performance", *Ph.D. Thesis*, pp.145

Wellinger RZ, (1949), Metallk, 40, pp.361

Wigley, F,Williamson, J, (1998)," Modelling of fly ash generation for pulverised coal combustion", *Progress in Energy and Combustion Science* 24, pp.337-343

Wigley, F, Williamson ,J, Gibb, WH, (1997)," The distribution of mineral matter in pulverised coal particle in relation to burnout behaviour", *Fuel* 76, 1286-1288.

William, TR, (1984),"The relation of mineral composition to slagging, fouling and erosion during and after coal combustion", *Progress in Energy and Combustion Science* 10, pp.159-175

Yin, C, Caillat, S, Harion, JL, Bernard, B, Everest, P (2002), "Investigation of the flow, combustion, heat transfer and emissions from a 609 MW utility tangentially fired pulverised coal boiler", *Fuel*, 81, 997-1006

Zienkiewicz, OC, Taylor, RL, (1991) "*The finite element method: Solid and fluid mechanics*," vol. 2. New York: Mcgraw-Hill

Zukas JA, (1990),"High-velocity impact dynamics". New York: Wiley